DETACHMENT FAULTS BETWEEN THE SPECTER RANGE AND NORTHERN SPRING MOUNTAINS: A TRANSPRESSIONAL FAULT ZONE ALONG THE LAS VEGAS VALLEY SHEAR ZONE, SOUTHEASTERN NEVADA

by

Damian Piaschyk

B.S. Geology, SUNY Oswego, 2005

Submitted to the Graduate Faculty of

Arts and Science in partial fulfillment

of the requirements for the degree of

Master of Science

University of Pittsburgh

2007

UNIVERSITY OF PITTSBURGH

ARTS AND SCIENCE

This thesis was presented

by

Damian Piaschyk

It was defended on

August 2, 2007

and approved by

William Harbert, Associate Professor, Faculty

Charles Jones, Lecturer/Advisor for B.S. Programs, Faculty

Thesis Director: Thomas H. Anderson, Professor, Faculty

DETACHMENT FAULTS BETWEEN THE SPECTER RANGE AND NORTHERN SPRING MOUNTAINS: A TRANSPRESSIONAL FAULT ZONE ALONG THE LAS VEGAS VALLEY SHEAR ZONE, SOUTHEASTERN NEVADA

Damian Piaschyk, M.S.

University of Pittsburgh, 2007

Southern Nevada is geologically and structurally complex. Detailed geologic mapping is critical to the understanding of the geologic history and groundwater flow within the region. The Las Vegas Valley shear zone (LVVSZ) is a strike-slips fault along which approximately 50 km of right-lateral movement took place between about 15-10 Ma. The shear zone extends northwestward about 100 km from Las Vegas to Mercury, Nevada. Folded Miocene strata record contraction west of Mercury where the LVVSZ is inferred to bend westward beneath the southern Specter Range creating a positive flower structure in response to transpression. Geologic mapping southwest of Mercury shows that Neoproterozoic and Early Paleozoic carbonate and clastic strata comprise a thick section of rocks deformed by multiple gently dipping faults along which units are detached. The footwalls and hanging walls adjacent to the fault surfaces are generally marked by pebbly cataclastic breccia or less commonly by foliation in fine-grained rocks. The detachments, which commonly crop out in the northernmost Spring Mountains, dip gently north toward the Specter Range. Rare kinematic indicators record south-directed transport.

A principal hanging wall of the fault zone is composed of brecciated Late Cambrian Nopah Formation. Detachment breccias show significant secondary porosity and permeability, which may control groundwater flow between the Spotted Range and Specter Range. Adjacent to the detachment about 1.4 to 3 kilometers of strata are missing between Nopah beds and fault

slices of much lower Early Cambrian Wood Canyon Formation. The footwall of the Nopah detachment comprises two parts: 1) Neoproterozoic and Cambrian strata folded about north-trending hinges and 2) an adjacent basin. Brecciated Nopah Formation and underlying fault rocks rest upon the folded strata of the footwall, and breccia also crops out in an adjacent former lake where they are recorded by crudely tabular masses of breccia intercalated with bodies of carbonate-clast conglomerate. The detachment fault zone is a contractional feature that is compatible with transpression expected along the left-step restraining bend in the LVVSZ.

TABLE OF CONTENTS

LIST OF TABLES

LIST OF FIGURES

LIST OF PLATES

PREFACE

I am grateful for support for fieldwork provided by the Nuclear Waste Repository Project Office. John Klenke, Levi Kryder, Judd Sampson, David Swanson, and Jamison Walker asked important questions and provided other helpful input especially during the field trip.

Sincere thanks to my advisor Dr. Thomas H. Anderson for giving me the opportunity to work on this project and for his intellectual support during fieldwork and conferences. I also appreciate his comments, questions, and suggestions which have improved the content and form of this manuscript. His willingness to help and his interest in my research have been a great motivator.

I am grateful to the members of my committee Dr. William Harbert and Dr. Charles Jones for comments and edits concerning this manuscript. I acknowledge Tamara Misner, Stephen Scheidt, Dr. William Harbert, and Zenon Valin for assistance with ArcGIS. Thanks to Amy Wolfe and Scott Davidson for helping with figures.

Thanks to the members of my family Eric, Olga, Adrian, and Amy Piaschyk for continued support and understanding. Amy Wolfe, Tamara Misner, and Emmett Rafferty provided encouragement and supporting me during completion of my degree.

Lastly and most importantly, I would like to thank my wife Sabrina Piaschyk for her intellectual and emotional support throughout the entire process. Without her love and support none of this would have been possible.

1.0 INTRODUCTION

Southern Nevada is a geologically complex region within which a burgeoning population with growing demand for water abuts the Nevada Test Site, Yucca Mountain nuclear repository, and natural areas at Ash Meadows Wildlife Refuge and Death Valley National Park. Sub-surface nuclear testing on the Nevada Test Site at or near the water table has occurred in Pahute Mesa, Rainier Mesa, Yucca Flat, and Frenchman Flat (Laczniak *et al.*, 1996). To gauge the groundwater effects of weapons testing on the Nevada Test Site combined with withdrawal of groundwater, aquifers and aquitards must be recognized and characterized as well as the impacts of geological history, especially faulting related to the deformational history. This project is part of a broader effort aimed at understand the natural movement of groundwater through the subsurface geology so that the impact of human activities, which may lead to contamination of groundwater followed by migration, may be ascertained and forecast.

The Las Vegas Valley shear zone (LVVSZ) strikes northwest-southeast in southeastern Nevada from Mercury to Frenchman Mountain, a distance of about 130 km, and is one of the principal crustal structures in southeastern Nevada (Longwell, 1960; 1974; Longwell *et al.*, 1965) (Figure 1). The shear zone occupies the broad Las Vegas Valley but shows no surface expression from Mercury to Frenchman Mountain. Apparent oroflexural bending of Paleozoic and Tertiary rocks stops at Mercury or the Spotted Range (Cole and Cashman, 1999). The apparent offset of Mesozoic thrusts and Precambrian and Cambrian isopachs, oroclinal bending of Miocene Basin and Range physiography, and clockwise paleomagnetic rotations indicate that the LVVSZ is a right-lateral strike-slip fault (Albers, 1967; Stewart, 1967; Nelson and Jones, 1987; Wernicke *et al.*, 1988; Sonder *et al.*, 1994). The alignment of the Gass Peak thrust with the Wheeler Pass thrust indicates 48 ± 7 km displacement along the LVVSZ, including bending of the Las Vegas Range (Burchfiel, 1965; Wernicke *et al.*, 1988), and agrees with offset calculated from isopachs of the lower Cambrian Zabriskie Quartzite (Stewart, 1967).

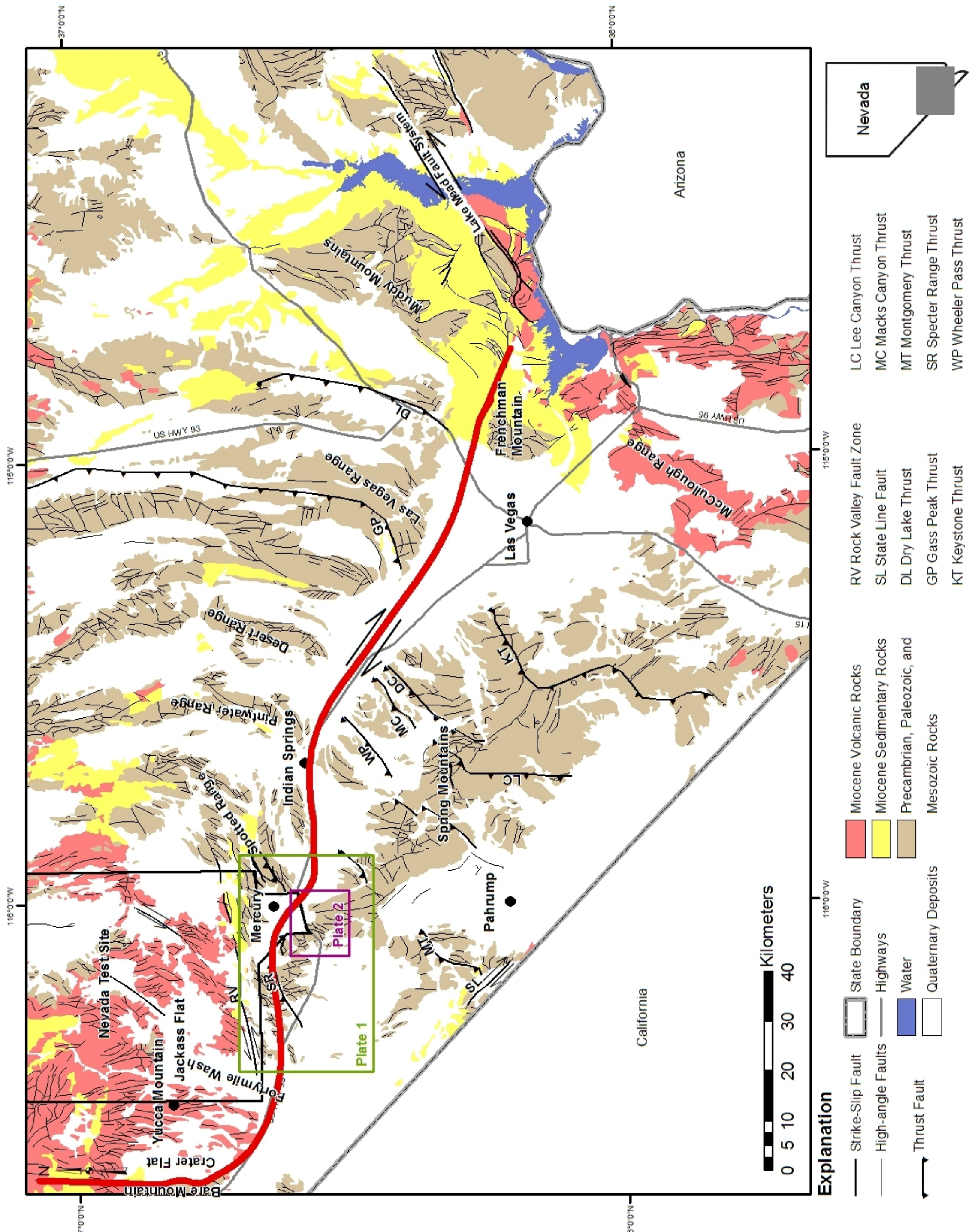

Figure 1. Generalized regional geologic map of southern Nevada data modified from Raines *et al.*, (1996) geology modified from (Stewart and Carlson, 1974). The red line represents the inferred trace of the Las Vegas Valley shear zone.

Thick Tertiary and Quaternary basin-fill deposits conceal the LVVSZ (Plume, 1989). A steep gravity gradient 30 km long may delineate the location of the LVVSZ in the subsurface along the northern margin of Las Vegas Valley (Campagna and Aydin, 1994). Additional geophysical studies including gravity and aeromagnetic surveys of the LVVSZ are interpreted to indicate two non-parallel strike-slip faults creating two sets of pull-apart basins deeper then 4km beneath Las Vegas Valley basins (Langenheim *et al.*, 1997; 1998; 2001; 2005).

Paleomagnetic data indicates a 20 km zone of clockwise rotation as great as 100° in rocks as young as 13.5 Ma adjacent to the LVVSZ (Sonder *et al.*, 1994; Nelson and Jones, 1987). The paleomagnetic data, along with other structural studies, brackets the principal period of movement along the LVVSZ as being between 14 and 8.5 Ma (Duebendorfer and Black, 1992; Duebendorfer and Simpson, 1994). The Lovell Wash Member shows deformation and displacement along the Las Vegas Valley shear zone that indicates motion until at least 13 Ma. (Bohannon, 1984). The Las Vegas Valley shear zone was active concurrently with as the left-lateral Lake Mead fault system. The two fault zones formed a conjugate fault system (Fleck, 1970; Bohannon, 1984). The Las Vegas Valley shear zone accommodates Miocene extension between the Spring Mountains to the south and the ranges to the north (Duebendorfer and Simpson, 1994; Cole and Cashman, 1999).

Previous mapping and structural studies suggest that the Las Vegas Valley shear zone ends or stops at Mercury or even Indian Springs, which seems unlikely along a shear zone with an estimated 48 ± 7 kilometers of displacement (Burchfiel, 1965; Wernicke et al., 1988). Winograd and Thordarson (1975) noted a zone of high transmissibility in the vicinity of the southern Specter Range and northern Spring Mountains. The linear zone extends between Amargosa Valley and Mercury Valley (Figure 2). Winograd (1962) further suggested that faulting and folding within this region controls groundwater flow and contaminate transport between basins and within the bedrock aquifers. Current structural models of the Specter Range and northern Spring Mountains do not adequately explore the diverse structures that may accommodate the movement of groundwater recognized by Winograd and Thordarson (1975). A clear understanding of the fault relationships and fault rocks of the northern Spring Mountains, Mount Schader basin, and Specter Range has implications for both the high level nuclear repository at Yucca Mountain and the movement of contaminates within the Nevada Test Site. This study introduces new structures and an alternative structural hypothesis that should be considered in the regional and local bedrock models and groundwater.

1.1 OVERVIEW

The objective was to characterize the rocks and structures within the zone of high transmissibility noted by Winograd and Thordarson (1975). An additional objective was to further refine the locations of principal groundwater flow paths. In the effort to develop a model of the subsurface, geologic mapping was conducted in order to: 1) characterize fractured rocks within fault zones, 2) document and measure extensional and contractional structures, and 3) determine direction and timing of fault motions based on structural relationships. These data will not only lead to better understanding of local structures, but also constrain the deformational history of the Las Vegas Valley shear zone, which accommodated crustal deformation on the regional scale.

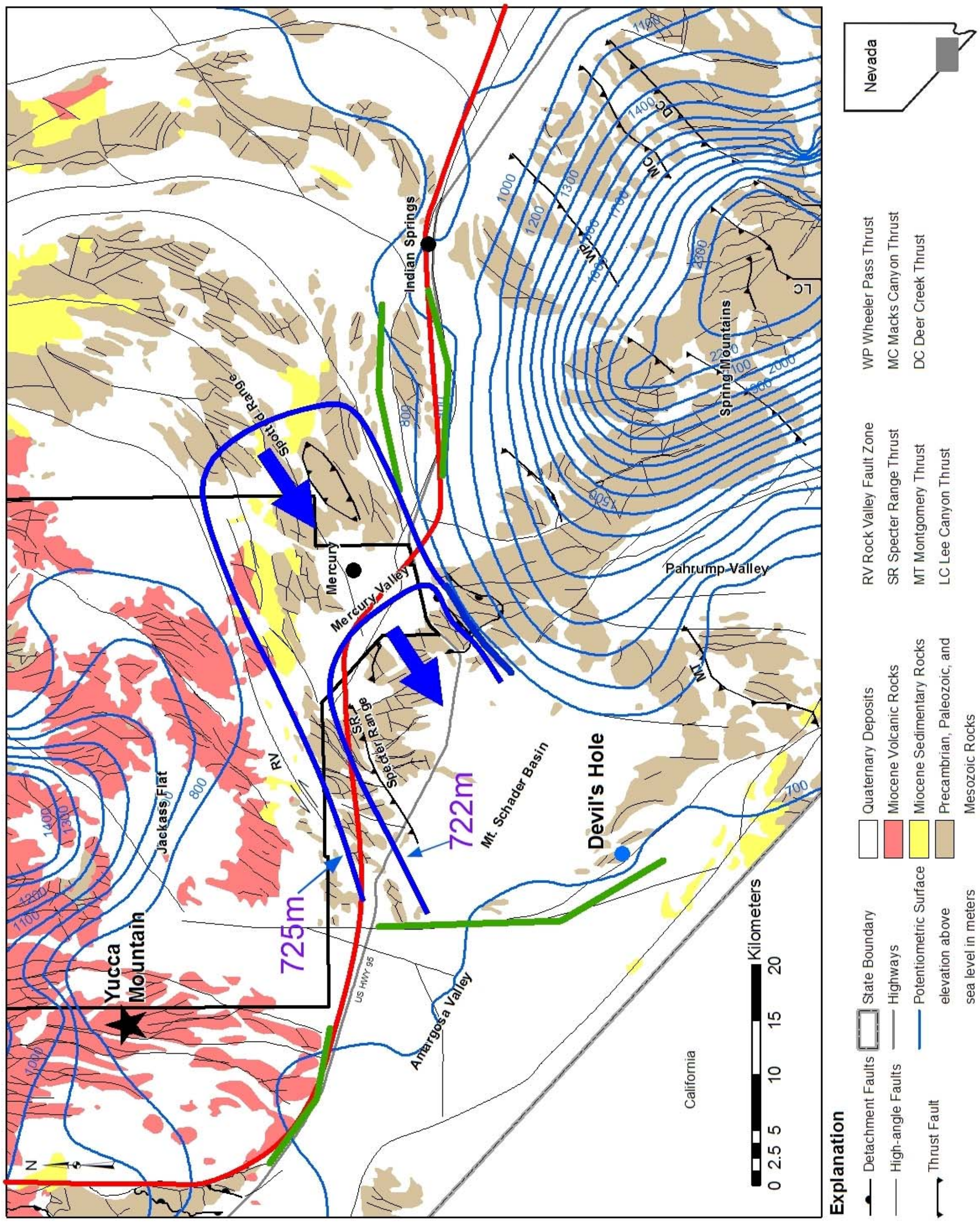

Figure 2. Hydrogeologic map of southern Nevada. Green lines show barriers to groundwater flow, thick blue lines show local potentiometric surface, and blue arrows indicate the direction of groundwater movement from Winograd and Thordarson (1975). Regional potentiometer surface and faults modified from Potter *et al.*, (2002). The red line represents the inferred trace of the Las Vegas Valley shear zone.

1.2 PHYSIOGRAPHY

Southern Nevada is located within the Basin and Range Province, characterized by north-south trending basins and ranges that define the current regional physiography. The Basin and Range covers more than one million square kilometers across western North America (Fenneman and Johnson, 1946; Easton, 1982) (Figure 3). The Basin and Range encompasses a highly extended intracontinental region bound by the Sierra Nevada Province to the west and the Colorado Plateau to the east. The Basin and Range is typically divided into two parts, the northern with an average elevation of 2,000 m above sea level and southern averaging only 1,000 m above sea level. The transition between the northern and southern provinces occurs at approximately 37° N (Wernicke, 1990). Separating the northern and southern sub-provinces is the Walker Lane belt, a 700 km by 200km northwest-trending domain containing a series of right lateral strike-slip faults (Stewart, 1988).

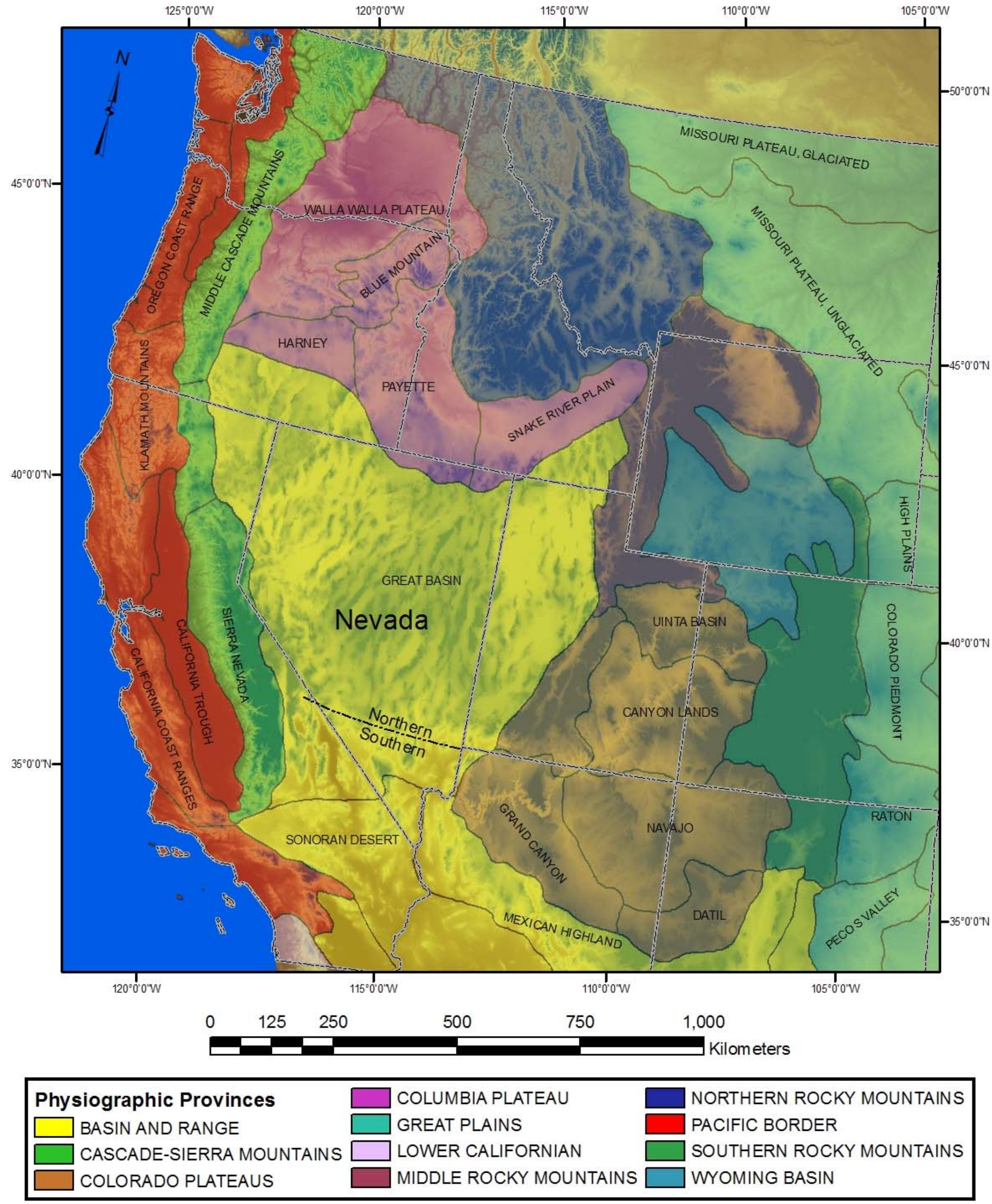

Figure 3. Map showing the physiographic provinces of the United States. (Modified from Fenneman and Johnson, 1946).

2.0 REGIONAL GEOLOGICAL SETTING

2.1 STRATIGRAPHY

More than 13,000 meters of Precambrian and Paleozoic miogeosynclinal rocks crop out in southern Nevada (Stewart, 1970; Burchfiel, 1964; Winograd and Thordarson 1975; Abolins, 1999). The strata are divided into 18 formations within southeastern Nevada (Figure 4). (Nolan, 1929; Burchfiel, 1964; Abolins 1999).

During the Neoproterozoic through Early Cambrian more then 3 km of clastic sedimentary rocks accumulated along the western margin of North America. During the Early Cambrian a shallow sea developed and more then 4.5 km of carbonate rocks formed through the Middle Devonian. Uplift associated with the Antler Orogeny resulted in synorogenic clastic sedimentation through the Middle Mississippian. Shallow marine conditions resumed after the Middle Mississippian and more than 2.5 km of carbonate rocks accumulated through Permian time.

The miogeosynclinal rocks vary in thickness and depositional environments from east to west. The western facies accumulated on a slope in deep water. The eastern facies accumulated on a shallow continental shelf (Trexler and Cashman, 1997; Cole and Cashman, 1999). These cnditions resulted in the thickening of Proterozoic and Cambrian rocks going from east to west (Christian *et. al*, 1966; Stewart, 1980; Trexler *et al.*, 1996; Wahl *et al.*, 1997).

2.1.1 Neoproterozoic

The Neoproterozoic stratigraphy of the region consists of the Johnnie Formation, Stirling Quartzite, and the Wood Canyon Formation (Stewart, 1970). The Johnnie Formation (1375 m thick) is the lowest stratigraphic unit exposed in the northern Spring Mountains and is composed of siltstone and minor sandstone, quartzite, and dolostone (Stewart, 1970; Burchfiel, 1965; and Abolins, 1999). Overlying Stirling Quartzite (1025 m thick) comprises purple pebbly conglomeratic quartzite at the top and bottom and siltstone and shale in the middle. Above the Stirling is the Wood Canyon Formation (600 m thick), which is composed of sandstone and quartzite with interbedded shale. The Neoproterozoic-Cambrian boundary occurs within the middle of this unit. The base and top of the formation contains distinctive 1-3 meter thick marker beds of rusty-red sandy dolomite (Abolins, 1999).

2.1.2 Paleozoic

Paleozoic strata of the region include part of the Wood Canyon Formation through the Bird Springs Formation. However only the Lower Cambrian through Upper Ordovician units are pertinent to this study are described.

The Cambrian Zabriskie Quartzite (85 m thick) conformably overlies the Wood Canyon Formation. The Zabriskie Quartzite is an orthoquartzite with *Scolithus* worm burrows defining the lower part of the formation. The Zabriskie Quartzite is overlain by the Cambrian Carrara Formation (460 m thick) which forms a conspicuous brown slope. The Carrara Formation is composed of shale, which grades to silty limestone with siltstone interbeds at the top. The top of the Carrara Formation records a shift from accumulation of clastic rocks to carbonate rocks that accumulated in a shallow calm intercontinental seaway (Burchfiel, 1964). The contact between the Carrara Formation and Bonanza King is transitional and is defined by the first bed of gray limestone, 0.5 meters thick. The Bonanza King Formation is divided into the upper (560-730 m thick) and lower (360-490 m thick) members. The lower member is dark massive limestone with a 20-30 meter bleached zone that grades into mottled limestone with silty interbeds. The upper member grades from silty mottled limestone to gray or light gray dolostone and limestone. The distinctive Dunderberg Shale (60-90 m thick) crops out at the base of the Nopah Formation. Although it is commonly included within the Nopah it was mapped in this study as a separate unit because of its importance as a structural marker. The Dunderberg Shale is composed of reddish brown coarse-grained limestone at the base, brown fissile shale in the middle, and gray sparry limestone with silty interbeds at the top. The Nopah Formation (325 m thick) is composed of massive gray dolostone which grades to a black dolostone with 20 meter bleached dolostone intercalated within black fenestral dolostone.

The Ordovician Pogonip Group (550 m thick) is composed of silty limestone, siltstone, and dolomite. The base is marked by the Goodwin Limestone, a thin silty limestone with chert lenses. The middle of the group consists of interbedded siltstone and limestone, comprising the Ninemile Formation. The Antelope Valley Limestone which comprises gray limestone with minor silty interbeds. The contact between the Pogonip Group and the overlying Ordovician Eureka Quartzite (145 m thick) is sharp and defined by the first sandstone bed. The Eureka Quartzite is an orthoquartzite composed of 90-95 percent quartz with cross-beds and ripple marks. A regional unconformity separates the Eureka Quartzite from the overlying Ordovician

Ely Springs Dolomite. The Ely Springs Dolomite (130 m thick) is a dark gray to black massive dolostone with crinoid stems and pieces of coral.

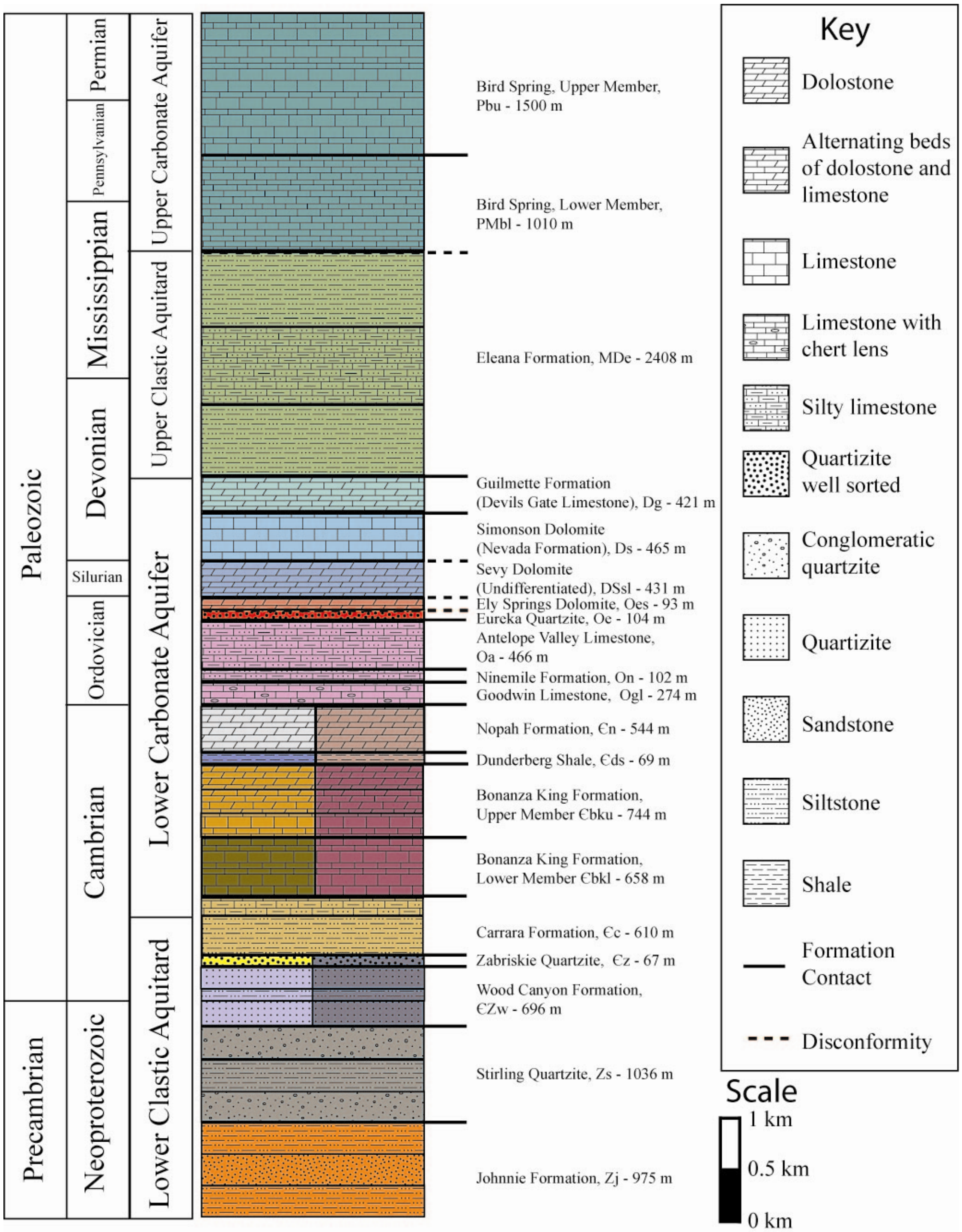

Figure 4. Regional stratigraphic column for Neoproterozoic and Paleozoic rocks in southern Nevada. (modified after Stewart, 1970; Burchfiel, 1964; Winograd and Thordarson 1975; Abolins, 1999). The colors of the units match the geologic bedrock map of the Specter Range and Northern Spring Mountains (Plate 1 and Plate 2).

2.1.3 Tertiary

Tertiary rocks of southern Nevada consist mainly of sedimentary and generally younger volcanic rocks. Tertiary sedimentary rocks in the Specter Range and southern Spring Mountain include units that yield ages between Oligocene (30.2 Ma) to Late Miocene (7.5 Ma) (Marvin *et al.*, 1970; Carr *et al.*, 1996). Volcanic rocks range in age from middle Miocene tuffs (15.05 Ma) to Pleistocene basalt flows (130 Ka) (Turrin *et al.*, 1992; Carr *et al.*, 1996).

Miocene sedimentary units generally formed in a marginal-lacustrine environment above a gently sloping erosion surface on top of bedrock (Bohannon, 1984; Snow and Lux, 1999). Ash fall tuffs are commonly interbedded within the thicker sedimentary section. The contact between the Paleozoic and Tertiary rocks in the Specter Range marks an angular unconformity (Burchfiel, 1965; Sargent and Stewart, 1971).

Miocene sedimentary rocks in the Lake Mead region were studied by Longwell (1963) and Bohannon (1984). Bohannon (1984) defined two main formations, the Horse Spring and Muddy Creek, containing six mappable units. The Horse Spring Formation contains four distinct members: 1) Rainbow Gardens, 2) Thumb Member, 3) Bitter Ridge Limestone Member, and 4) the Lovell Wash Member which yield ages from volcanic ash between 20 and 11.9 Ma (Bohannon, 1984). The Rainbow Gardens Member defines the base of the Horse Spring Formation and is composed of conglomerate, siltstone, dolostone, and limestone at the top. The first clastic bed above the limestone defines the base of Thumb member, which is composed of sandstone and conglomerate with thin altered or weathered tuff beds. The first bed of limestone above the clastic section defines the base of the Bitter Ridge Limestone member. The Bitter Ridge Limestone Member is composed of limestone and sandy limestone, which grades into the

Lovell Wash Member composed of unaltered and or altered tuffs intercalated within limestone beds. Commonly deposited on the Horse Spring Formation is a red sandstone with minor beds of conglomerate. This clastic unit is not included in the Horse Spring Formation or the overlying Muddy Creek Formation because the red sandstone is commonly bound by unconformities. The youngest Tertiary sedimentary unit exposed in the Lake Mead region is the Muddy Creek Formation, composed of sandstone, shale, and thin beds of conglomerate. (Figure 5) (Bohannon, 1984).

In the Specter Range and Spotted Range, the stratigraphic equivalents of the Horse Spring and Muddy Creek are the Horse Spring and Pavits Springs. The Horse Spring Formation is similar to the Lake Mead section, with reworked biotitic tuffs at the base yielding an age of 29.3 Ma (Barnes *et al.*, 1982). Conformably above the tuff is a well-rounded pebble conglomerate with clasts of pebbles and boulders with argillaceous limestone defining the top of the Horse Spring Formation (Barnes *et al.*, 1982). The rocks of the Pavits Spring contain tuffaceous sandstone and mudstone at the base with a clean, well-rounded conglomerate with pebbles, cobbles, and boulders derived from the Stirling Quartzite comprising the middle of the formation (Barnes *et al.*, 1982). Thin bedded argillaceous limestone overlain by zeolitized air fall tuff with interbedded sandstone and shale comprise the top of the Pavits Spring formation (Barnes *et al.*, 1982).

The volcanic rocks exposed in southern Nevada comprise a bimodal assemblage of felsic tuffs / rhyolite and mafic basalts (Table 1). The volcanic products erupted from six major calderas within a multicaldera volcanic field, between 15 and 7.5 Ma (Sawyer *et al.*, 1994). The highest rate of volcanism occurred from 12.8 to 11.4 Ma, depositing the thick sequences of the Timber Mountain and Paintbrush groups (Fridrich, 1999). Volcanism decreased and shifted mainly to rhyolite and basaltic lava flows from 11.4 Ma to 7.5 Ma, followed by minor intermediate and basaltic lavas till 2.5 Ma (Fridrich, 1999). Quaternary volcanic activity has primarily consisted of subalkaline basaltic cinder cones (Fleck *et al.*, 1996). High initial $^{87}Sr/^{86}Sr$ ratios, low SiO_2, and Rb/Sr ratios in Quaternary basalts suggests a lithospheric mantle source (Fleck *et al.*, 1996).

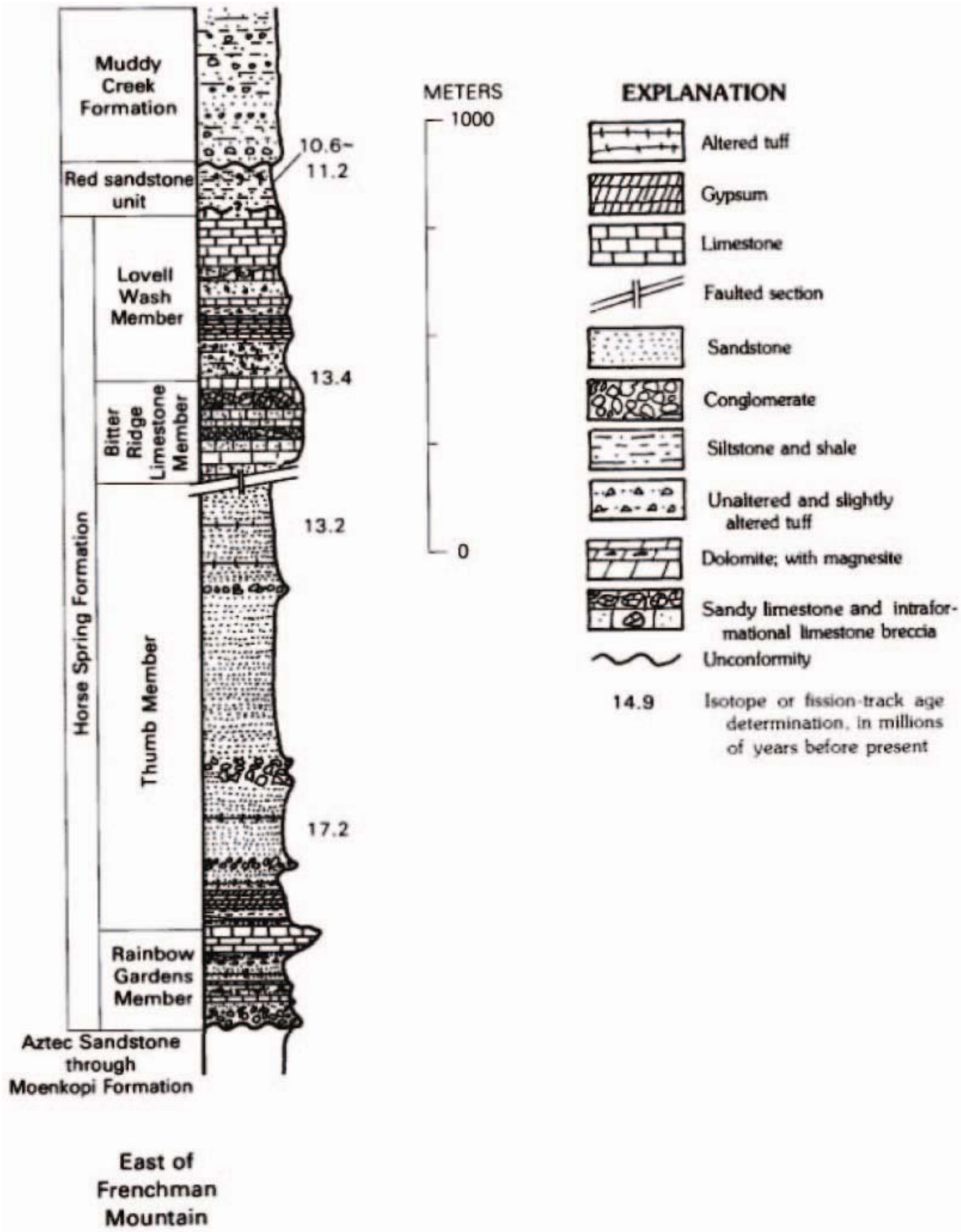

Figure 5. Stratigraphic column for Tertiary sedimentary rocks east of Frenchman Mountain, modified from Bohannon (1984).

Table 1. Major Volcanic units in southeastern Nevada, modified from Sawyer, Carr, Fleck, and Fridrich (1994; 1996; 1996; and 1999).

Volcanic Unit, Assemblage, or Group	Age (Ma)
Late Pliocene and Quaternary volcanics	0.07-3.7
Thirsty Mountain	4.63
Stonewall Flat Tuff	7.6
Miocene basalts	6.3-11.0
Thirsty Canyon Group	9.15-9.4
Timber Mountain Group	11.45-12.5
Paintbrush Group	12.7-12.9
Calico Hills Formation	12.9
Wahmonie Formation	13.0
Crater Flat Group	13.1-13.5
Belted Range Group	13.5-13.85
Lithic Ridge Tuff	14.0
Lava of Tram Ridge	14.0
Tunnel Formation	
Tub Spring Tuff	15.1
Tuff of Yucca Flat	15.1
Redrock Valley Tuff	15.25

2.2 STRUCTURE

2.2.1 Mesozoic Deformation

Mesozoic structures in southern Nevada formed during Cretaceous and older episodes of east-directed shorting and are characterized by low-angle thrust faults along weak bedding planes in the miogeosyncline strata. The deformation resulted in duplication of miogeosynclinal strata and north-trending folds (Burchfiel, 1965; Burchfiel *et al.,* 1974; Abolins, 1999). Preexisting structures may have also influenced the formation of Mesozoic thrusts (Cole and Cashman, 1999). Palinspastic reconstructions suggest west-dipping, north-trending thrusts are part of the Sevier belt and are preserved as far east as the Lake Mead region (Bohannon, 1984). Thrusting in southern Nevada occurred from 75 to 90 Ma. (Fleck, 1970). The same stresses also formed north-plunging folds involving Neoproterozoic and Paleozoic sedimentary rocks (Burchfiel, 1965; Burchfiel *et al.,* 1974; Abolins, 1999).

Folds and thrusts in southern Nevada have variable easterly orientations that do not conform to simple north-south Mesozoic contraction (Figure 6).

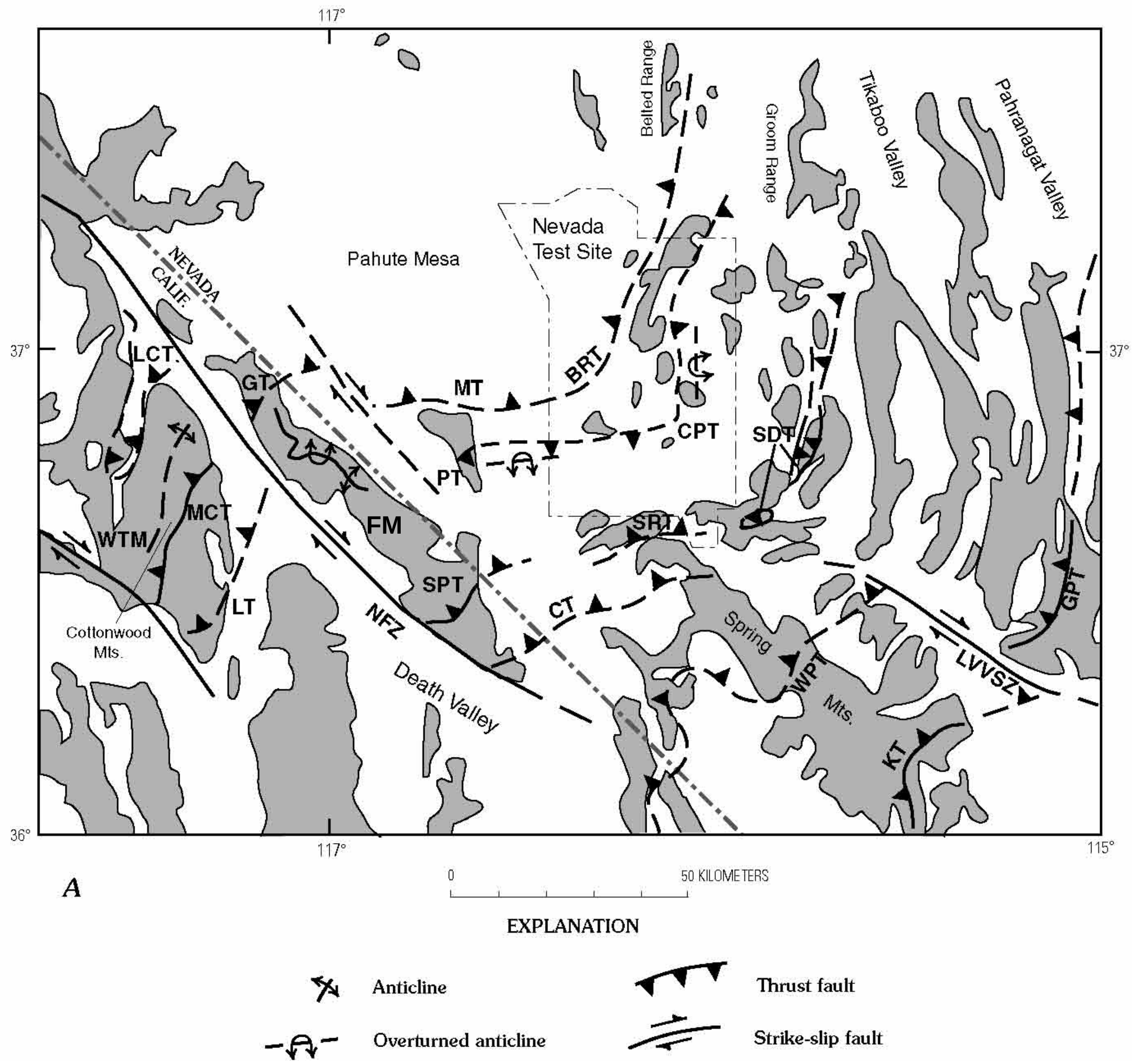

Figure 6. Simplified geologic map of contractional structures in southern Nevada and California; ranges shaded gray. (BRT) Belted Range thrust, (CT) Clery thrust, (CPT) CP thrust, (FM) Funeral Mountains (GPT) Gass Peak thrust, (GT) Grapevine thrust, (KT) Keystone thrust, (LT) Lemoigne thrust, (LCT) Last Chance thrust, (LVVSZ) Las Vegas Valley shear zone, (MT) Meiklejohn thrust, (MCT) Marble Canyon thrust, (NFZ) Northern Furnace Creek fault zone, (PT) Panama thrust, (SDT) Spotted Range thrust, (SPT) Shwaub Peak thrust, (SRT) Specter Range thrust, (WPT) Wheeler Pass thrust, (WTM) Whitetop Mountain fold. Modified from Cole and Cashman (1999).

The differences in orientation of structures make correlations of contractional structures across Miocene basins tentative. Cole and Cashman (1999) recognize two main categories of thrusts and folds: foreland-vergent and hinterland-vergent. Foreland-vergent folds and thrusts and younger hinterland-vergent folds and thrusts deform Neoproterozoic through early Permian miogeoclinal rocks. The main foreland-vergent thrusts are the Belted Range thrust and the Gass Peak thrust, each of which places the Precambrian Wood Canyon Formation on Mississippian or younger rocks (Cole and Cashman, 1999). Hinterland vergent thrusts are not commonly exposed and are inferred from stratigraphy and drill hole data. The CP thrust is hinterland-vergent thrust in which the footwall of the thrust contains overturned units (Carr, 1984; Cole and Cashman, 1999).

Fault blocks in the northern part of the Nevada Test site show apparent left lateral displacements along north striking left-lateral faults (Cole and Cashman, 1999). The Specter Range thrust strikes west-southwest. The maximum throw places Neoproterozoic Stirling Quartzite upon Ordovician and Silurian units. Units in the hanging wall of the Specter Range thrust can be traced to the footwall of Spotted Range klippe, suggesting that the Spotted Range klippe is structurally higher (Buchfiel, 1965; Cole and Cashman, 1999).

2.2.2 Cenozoic Deformation

North-south trending ranges in the Basin and Range formed in response to Cenozoic extension (Fenneman and Johnson, 1946, Hill *et al.,* 1966). At depth the basin bounding normal faults decrease in dip and merge into a system of regional detachment faults (Lister and Davis, 1989). Core complexes and rock mechanics experiments suggest that this occurs below the brittle to ductile transition. As the basement is brought to the surface during extension, detachment faults may cross the brittle ductile transition and deform brittlely (Lister and Davis, 1989). Two types of normal faults are preserved in southern Nevada 1) range bounding or basin bounding and 2) within range (Anderson and Ekren, 1977). Many extensional features are local and domainal in nature (Hamilton, 1988; Jayko, 1990; Cole and Cashman, 1999). Block tilting, basin subsidence, and fault activity on the Nevada Test Site supports extension from 15 to 9 Ma (Carr, 1974; Cole and Cashman 1999). Ekrene et al., (1968) noted a change in stress about 14 Ma creating normal fault oriented more northerly on the Nevada Test Site and Nellis Air Force Range.

Left and right-lateral transfer or strike-slip faults within the Basin and Range separate structural domains (Moores and Twiss, 2000). Southern Nevada contains a series of northwest-striking lateral faults including the Las Vegas Valley shear zone, the Pahrump-State line fault, and the Death Valley-Furnace Creek fault zone. Each shows apparent right-lateral offset. The Las Vegas Valley shear zone shows offset and drag of Mesozoic thrusts, Neoproterozoic isopachs, oroclinal bending of Paleozoic strata, and clockwise paleomagnetic rotations (Albers, 1967; Stewart, 1967; Nelson and Jones, 1987; Wernicke *et al.*, 1988; Sonder *et al.*, 1994). The Pahrump-State Line fault also shows offset of Tertiary and Quaternary basin sediments and drag of Neoproterozoic and Cambrian rock (Stewart, 1988). Offset of modern features such as stream channels, cinder cones, alluvial fans, and fold axis in Tertiary beds indicate that the Furnace Creek fault zone has undergone more recent lateral displacement (Wright and Troxel 1966; Hill and Troxel 1966; Snow and Wernicke, 1989).

Perhaps better studied are left-lateral strike-slip faults have also been recognized northeast of Las Vegas. The Lake Mead fault zone deforms Tertiary rocks and has an estimated displacement of 65 km of left-lateral offset (Bohannon, 1984; Duebendorfer and Black, 1992;

Duebendorfer and Simpson, 1994). A releasing step at the southwest terminus of the fault forms north-south basins adjacent to the Eldorado Mountains and Wilson Ridge (Anderson, 1971; Bohannon, 1979; 1984). In this area south of the Lake Mead region, one hundred percent extension of Tertiary rocks of unknown magnitude occurred in west-southwest direction from about 15 to 10 Ma (Anderson, 1971; Bohannon, 1984).

In the Grand Wash region northeast of Lake Mead, north-south extensional structures were active between 12 and 10 Ma (Bohannon, 1984). Geologic maps of Frenchman Mountain by Longwell *et al.* (1965) show that normal faulting, listric normal faults, and strike-slip faulting were cogenetic during Miocene time. The Rock Valley fault is another left-lateral strike-slip fault, which separates the Striped Hill from the Specter Range. Displacement of Miocene sedimentary and Miocene volcanic deposits indicates offset of less then 4 kilometers (O'Leary, 2000). Seismic activity in 1992 and 1993 suggests that the Rock Valley fault is still active (Smith *et al.*, 2000).

Structures with easterly orientation in southern Nevada have been interpreted as rotated Mesozoic and early Cenozoic faults by Albers (1967). He noted rotation of physiographic features and faults of the Spotted, Desert, and Las Vegas ranges north of the Las Vegas Valley shear zone and inferred oroclinal bending as the main mechanism "absorbing" displacement along the Las Vegas Valley shear zone. The Belted Range, Calico Hills, Halfpint Range, and Yucca Flat north and west of the Spotted Range demonstrate only minor vertical axis rotations (Hudson *et al.*, 1994). Oroflexer deformation may have been in place before Miocene time and may have formed during Mesozoic thrusting (Royse, 1983; and Cole and Cashman, 1999). Folding and bending of thrust faults cannot explain the current orientation of foreland and hinterland thrusts in southern Nevada (Cole and Cashman, 1999).

2.3 SPRING MOUNTAINS

The Spring Mountains are located 15 km west of Las Vegas, trend northwest, and are the highest range in southeastern Nevada (Longwell *et al.*, 1965; Burchfiel *et al.*, 1974). The northern end of the Spring Mountains is defined as the topographic low where US highway 95 passes between the Spring Mountains to the south and the Specter Range to the north. The absence of north-south trending topography suggests the Spring Mountains are a stable block within a highly extended region. The range is composed mainly of Neoproterozoic through upper Jurassic miogeosynclinal rocks and minor Tertiary sedimentary and volcanic rocks (Longwell *et al.*, 1965; Page *et al.*, 2005)

The range shows lithologic and structural similarities to ranges in the western part of the Cordillera (Burchfiel *et al.*, 1974). Western miogeosynclinal sequences are pushed over the thinner eastern sequences along Mesozoic east-directed thrusts (Burchfiel *et al.*, 1974). The Spring Mountains contain three main thrust plates: 1) Keystone in the east, 2) Lee Canyon thrust, and 3) Wheeler Pass in the west. Thrust flats in the Spring Mountains commonly parallel the bedding in the hanging wall and cut across the bedding in the footwall (Burchfiel *et al*, 1974). The hanging wall of the Keystone and Redspring thrust consists of Bonanza King Formation through Bird Springs Formation, which may have moved across an erosional surface (Burchfiel *et al.*, 1974). The dip of the Wheeler Pass thrust is steeper then the bedding cutting units as old as the Stirling Formation in the footwall, with no mylonitization along the fault (Burchfiel *et al.*, 1974). The Wheeler Pass thrust flattens at depth likely along the contact between the Johnnie and the basement. Cross-section reconstructions indicate that the units exposed in the Spring

Mountains have undergone 35 to 75 kilometers of shortening from Jurassic through late Cenozoic (Burchfiel *et al*., 1974).

Cenozoic deformation also has been documented throughout the Spring Mountains. Burchfiel *et al*, (1974) noted a series of normal faults which strike north and northwest; the north striking normal faults cut both the thrust faults and the northwest-striking normal faults. Right lateral drag along the Las Vegas Valley shear zone appears to have rotated bedding and faults Along the northeast flank of the Spring Mountain (Longwell, 1969; Nelson and Jones, 1987).

The northern Spring Mountains contains diverse Cenozoic structures. Previous mapping by Burchfiel (1965,1974) noted low angle discontinuities between the Stirling, Johnnie, and Wood Canyon Formation, but incorrectly called them thrusts likely due to the extent of brittle deformation persevered along the fault planes. Abolins (1999) correctly interpreted these low-angle faults as detachments. A major stratigraphic discontinuity approximately 3 kilometers south of US highway 95 places Upper Cambrian Nopah carbonate on Neoproterozoic quartzite (Burchfiel, 1965; Abolins, 1999). Previous interpretations suggested that these detachments were extensional based on their geographic location and stratigraphic relationships (Burchfiel, 1965; Abolins, 1999).

The Stirling Mine fault, about 1.5 kilometers south of the Stirling Mine, is a major covered structure in the northern Spring Mountains. Burchfiel (1974) and Page (2005) interpreted the Stirling Mine fault as a north-dipping normal fault down dropped to the south. Snow (1992) proposed that the Stirling Mine fault is part of the Mesozoic Kwichup thurst; this proposed geometry places a thrust plate above the Wheeler Pass thrust, and links the Funeral Mountains and northern Spring Mountains. Abolins (1999) linked the Stirling Mine fault with the Wood Canyon-Johnnie detachment and the Montgomery thrust as the same Mesozoic structure which must has been differentially extended during Miocene time due to geographic offset of faults and variation stratigraphy between the faults.

2.4 MT. SCHADER BASIN

The Mount Schader basin is located at the southern end of the Amargosa Desert. Gravity studies first revealed the basin, which shows complex and intersecting gravity highs and low (Healey and Miller, 1965). The basin likely formed in early Miocene time and extends from the gravity fault to the edge of the northern Spring Mountains (Winograd and Thordarson, 1975; Brocher *et al.*, 1993). Paleozoic bedrock horsts are interpreted to separate the Mt. Shader basin into a series of subbasins (Brocher *et al.*, 1993). Holocene, Pleistocene, and Pliocene alluvium unconformably cover the Miocene sedimentary and volcanic deposits within the basin (Brocher *et al.*, 1993; Carr *et al.*, 1996; Workman *et al*., 2002).

Refraction and reflection studies of the Mount Schader basin confirm the complex geometry and history of the basin (Mooney and Schapper, 1995; Brocher *et al.*, 1993). Two seismic lines, oriented east-west across the northern portion of the basin, indicate two shallow subbasins with a maximum depth of 1.5 kilometers. Mooney and Schapper (1995) suggest changes in seismic velocity are not good indicators of the depth of pre-Tertiary rocks because buried Tertiary volcanic rocks within the basin have velocities similar to pre-Tertiary sedimentary rocks. Paleozoic rocks underneath the Mt. Schader basin have lower seismic velocities than similar basins with floors of Paleozoic rocks (Mooney and Schapper, 1995). This difference may be caused by extensive fracturing, secondary cementation, low grade metamorphism, or a higher percentage of clastic material (Mooney and Schapper, 1995).

The seismic reflection study by Brocher (1993) shows complex, dipping, reflectors bounded by faults, unconformities, and nonconformities (Figure 7). Dipping reflectors interpreted to be Miocene sedimentary rocks are as shallow as 200 meters bellow the surface (Brocher *et al.*, 1993). Basalt flows, intercalated within basin deposits, yield ages between 8.5 and 11 Ma (Crowe *et al.*, 1986). Reflectors in the basin that commonly dim and brighten suggest lateral facies change in Miocene sedimentary rocks or the lateral termini of Miocene volcanic rocks (Brocher *et al.*, 1993). Packages of reflectors also show gradual decreases in reflection amplitude laterally and vertically, indicating fining and coarsening of Miocene sedimentary facies (Brocher *et al.*, 1993).

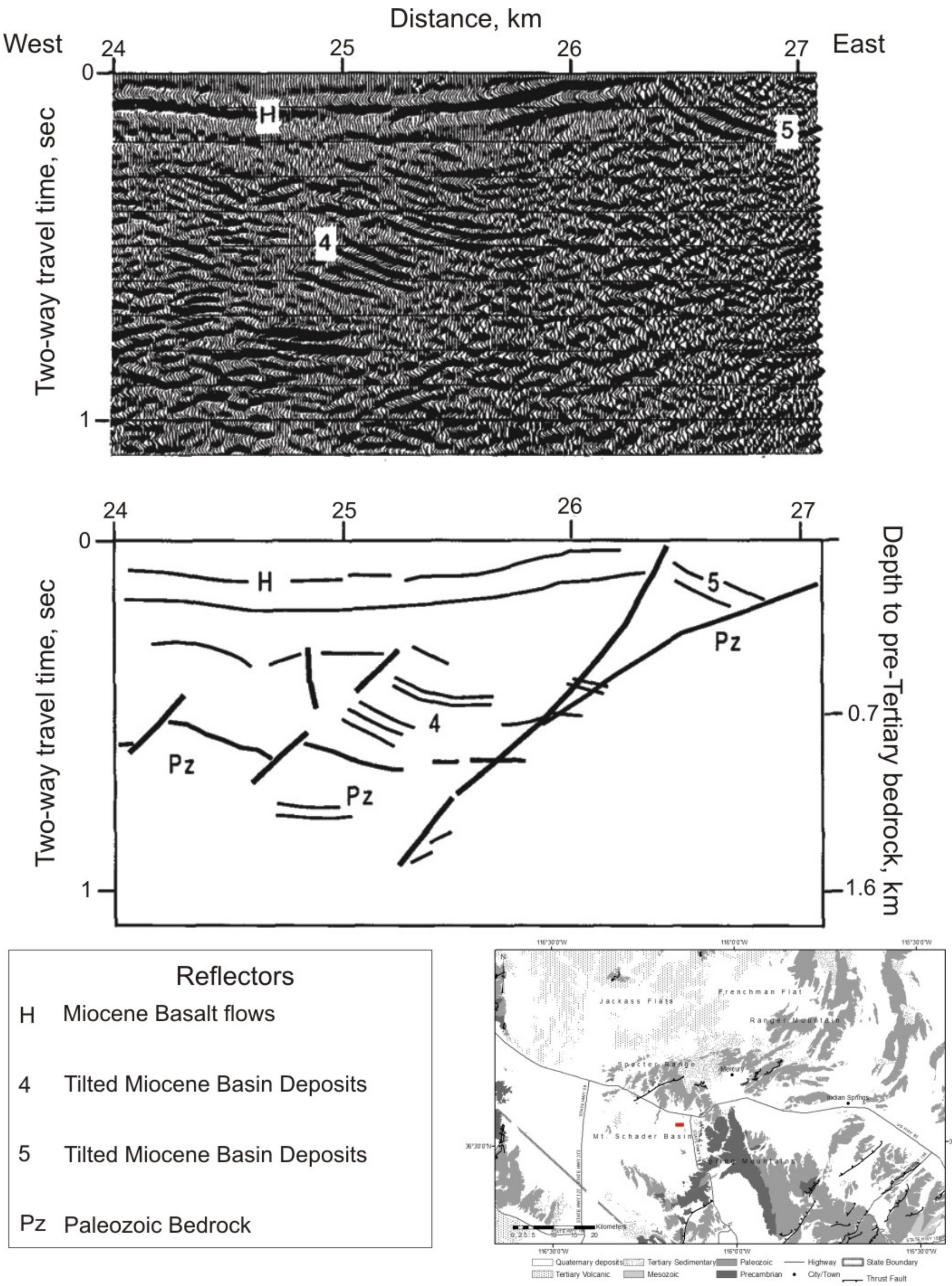

Figure 7. Diagrams showing the uninterpreted (top) and interpreted (middle) detail of the most easterly segment of the USGS seismic line AV-1. The red line on the regional map (lower right) shows the location of USGS seismic line AV-1 Modified from Brocher *et al.*, (1993).

2.5 SPECTER RANGE

The Specter Range is 90 kilometers northwest of Las Vegas. The range is composed of Cambrian to Devonian miogeosynclinal strata and minor Tertiary sedimentary and volcanic rocks (Maldonado, 1985; Carr *et al.*, 1996). The easterly orientation of the range and of structures within the range is distinctly different from nearby ranges to the north and south. Previous geologic mapping in the Specter Range reveals strong faulting, fracturing, and brecciation throughout the range (Burchfiel, 1965; Sargent and Stewart, 1971; Carr *et al.*, 1996).

The principal structure in the Specter Range is the Specter Range thrust, which places Neoproterozoic Wood Canyon Formation on the Ordovician Pogonip Group suggesting more then 3.3 kilometers of stratigraphic throw (Burchfiel, 1965). The Wood Canyon Formation, and Bonanza King Formations in the hanging wall generally strike west-southwest. Detachments along bedding planes are common (Sargent and Stewart, 1971; Carr *et al.*, 1996). The footwall contains Ordovician Pogonip through Devonian Simonson Dolomite. Bedding in the footwall close to the Specter Range thrust is parallel to the strike of hanging wall strata, whereas bedding farther south strikes north-south (Burchfiel, 1964; Carr *et al.*, 1996). The strike and southward transport direction of the Specter Range thrust are different from thrust faults in the Spotted Range and the Funeral Mountains (Cole and Cashman, 1999) (Figure 6).

Previous mapping by Burchfiel (1965) shows high angle faults within the Specter Range that fall into three groups: (1) north-south 330°-035° regional normal faults, (2) northwest 340°-300° right-lateral oblique-slip faults, and (3) northeast 035°-090° left lateral oblique slip faults. Burchfiel (1965) noted that many of the faults within the Specter Range cannot be explained with dip-slip or strike-slip motion alone, the simplest interpretation is that they accommodate oblique motion. Stratigraphy and structures in formations that comprise the low hills that connect the Specter Range to the Spotted Range to the east are continuous and show no evidence of displacement by Las Vegas Valley shear zone (Burchfiel, 1965; Cole and Cashman, 1999). Field studies by Deemer (2003) demonstrated that many of these low hills along Jackass Flats Road show extreme brecciation of the Bonanza King Formation, Nopah Formation, Pogonip Group, and the Eureka Quartzite.

Folds and limbs of folds in units as old as the Neoproterozoic Stirling Quartzite and as young as the Ordovician Ely Springs Dolomite in the Specter Range trend either north-south or east-west. The limbs of north-south folds can be interpreted from map relationships, although high angle faults and transposition of the bedding commonly overprint their geometry. The footwall of the Specter Range thrust contains an east-west trending overturned syncline which appears to overprint or cut north-south bedding and fold limbs.

2.6 TECTONIC HISTORY

The west coast of North America is a geologically complex area that has under gone multiple phases of deposition and deformation. The rifting of Rodinia 750 million years ago resulted in a passive continental margin on the west coast of North America. Deposition along this passive margin continued until mid-Paleozoic, resulting in a thick sequence of clastic and carbonate rocks. The onset of subduction along the west coast of North America began in Devonian time produced eastward dipping subduction of an oceanic plate under North America. During the

Late Devonian and Early Mississippian, the collision of an island arc or microcontinent off the western margin of North America resulted in uplift forming the Antler Highlands (Nilsen and Stewart, 1980). Subduction continued at a more rapid pace in the Mesozoic likely due to the rifting of North America from Africa (DeCelles, 2004).

The Nevadan Orogeny, Sevier Orogeny, and Laramide Orogeny are the main mountain building events in the Mesozoic Era and are collectively called the Cordilleran Orogeny (Figure 8).

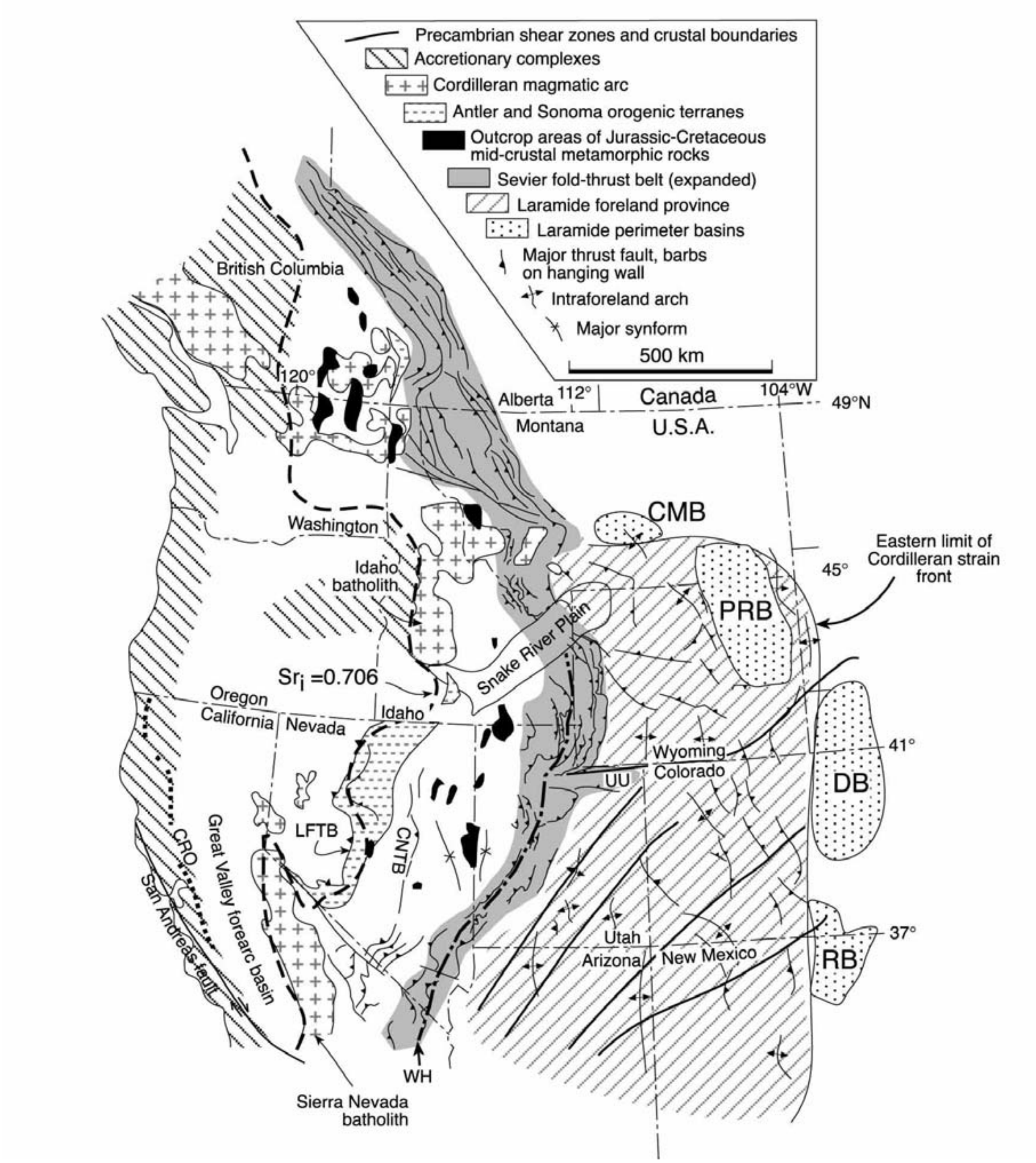

Figure 8. Tectonic map of some Cordilleran orogenic features in the western United States; (CRO) Coast Range ophiolite, (LFTB) Luning-Fencemaker thrust belt, (CNTB) Central Nevada thrust belt, (WH) Wasatch hinge line, (UU) Uinta Mountains uplift, (CMB) Crazy Mountains basin, (PRB) Powder River basin, (DB) Denver basin; and (RB) Raton basin, modified from DeCelles (2004).

The Nevadan Orogeny began during Late Jurassic when subduction created large volumes of magma forming large batholiths in southern California, Sierra Nevada, Idaho, and Coast Range batholiths (Dickinson, 2006). In Cretaceous time, compression increased causing intense back-arc thrusting forming the Sevier fold and thrust belt. The resulting thrusts duplicated strata and created stacks of thrusts, many with tens of kilometers of horizontal displacement (Armstrong, 1968). The Laramide formed east of the Sevier Thrust belt during Late Cretaceous through Early Tertiary. Deformation differed from the Nevadan and Sevier orogenic events, involving large broad fold in the basement creating irregular sized and shaped basins of late Cretaceous to mid Eocene age (Dickinson, *et al.,* 1988). Uplift associated with the Laramide and northeast-southwest shorting formed curvilinear folds and thrust faults along the flanks of the folds (Dickinson, *et al.*, 1988). A decrease in the angle of subduction of the Farallon Plate resulted in greater interaction between the continental and oceanic lithosphere resulting in a shift from thin skinned to basement involved tectonics. This shallow angle also explains the lack of volcanic activity as the oceanic plate would no longer be deep enough to cause partial melting (Dickinson, *et al.*, 1988).

A series of subduction, plate coupling and capture, and continental extensional events defines the Cenozoic Era along the west coast of North America. The Basin and Range has undergone three times the extension when compared to continental rifts settings, such as the Africa rift system (Eaton, 1982). Continental extension has thinned the continental crust to 35 km, significantly thinner then average continental crust (Carr, 1974).

During Eocene time subduction again created widespread volcanism along the west coast, suggesting a steeper subduction angle of the Farallon Plate. In Oligocene time (29 Ma) the

Pacific Farallon spreading ridge begins to be subducted (Bohannon and Parsons, 1995). Buoyancy of the ridge impeded subduction, which stopped around 20 Ma. Coupling of the plates led to the capture of western North Amercia by the Pacific Plate, marking the beginning of continental rotation and extension in the Basin and Range Provence (Nicholson, *et al.*, 1994). Continental extension was fully underway by 15 Ma. Two theories relating Basin and Range extension to plate motions are 1) coupling of the Pacific Plate with the North American Plate, and 2) migration of the Mendocino triple junction (Atwater, 1970; Bohannon and Parsons, 1995). Spreading along Baja California slows around 10 Ma and continental extension continued (Bohannon and Parsons, 1995). The San Andreas Fault system was active by 5 Ma and continental extension has slowed (Bohannon and Parsons, 1995).

3.0 GEOLOGIC AND STRUCTURAL RESULTS

A principal objective of this work is to conduct structural mapping in order to 1) characterize fault zones, 2) document and measure extensional and contractional structures, and 3) determine direction and timing of fault motions based on structural relationships. The collection of field data and observations in southern Nevada spanned more then 10 weeks during three trips (spring 2006, winter 2006, and spring 2007). Fieldwork focused upon three domains in the northern Spring Mountains and Specter Range: 1) the Point of Rocks quadrangle, 2) the hanging wall of the Specter Range thrust, and 3) the area surrounding the Stirling Mine. The areas encompassed approximately 80 km^2, 5 km^2, and 8 km^2 respectively. Geologic maps (Plate 1 and Plate 2) were produced from field observations, structural measurements, and existing geologic maps. A GPS unit was used to record the geographic location of field data, observations, and oriented samples. The orientations of bedding, fractures, fold hinge, and fault surfaces were measured using a Brunton compass. Observations included the description of the mineralogy, texture, and internal structures of outcrops. Sixty oriented rock samples were collected from fault zones and structurally important units.

3.1 FAULTS

Detachment faults, normal faults, tear faults, and thrust are common in the northern most Spring Mountains and Specter Range. The abundance of low and high angle faults is higher than in other ranges in southern Nevada. Samples were collected from high angle and low angle fault zones within the northern Specter Range. The dry conditions in southern Nevada prevent dissolution of fault gouge resulting in relatively unaltered samples (Cladouhos, 1999). Oriented samples were cut perpendicular to the strike of structures. Thin sections of select samples were analysis for ductile structures. None of the samples display any dynamic recrystallization of quartz or calcite and breccia zones are cohesive.

3.1.1 Detachment faults

Detachment is a nongenetic term which means a low-angle normal fault with younger units in the hanging wall and older units in the footwall (Axen, 2007). Low-angle normal faults or detachments in the past were typically interpreted to be odd thrust faults, mega-landslide faults, or unconformities (Axen, 2007). Detachments have recently been recognized in both extensional and contractional settings (Axen, 2007). Detachments are recognized via either stratigraphic discontinues or by breccia and deformation that indicates a fault zone. Burchfiel (1965 and 1974) was the first to recognize stratigraphic discontinues in the northern Spring Mountains between the Johnnie and Stirling Quartzite, Stirling Quartzite and Wood Canyon Formation, and at the base of the Nopah Formation. Abolins (1999) was the first to interpret these structures as detachments. Both Burchfiel (1965) and Abolins (1999) noted that section is missing along these detachments: 750 m along the Johnnie-Stirling detachment, 300 m along the Stirling-Wood Canyon detachment, and 3,000 m along the Nopah-Stirling detachment (Figure 9). Abolins (1999) interpreted the Stirling-Johnnie detachment to be older and folded during Mesozoic east-west contraction. The small “klippe” of Nopah Formation were first noted by Burchfiel (1965 and 1974) who interpreted it as landslide deposits related to the complex structural relationships. Later the “klippe” were grouped into a regional structure by Abolins (1999).

Detail geological mapping within the northern Spring Mountains and southern Specter Range demonstrates common detachments among miogeosynclinal units (Plate 1 and Plate 2). Interformational and interaformational detachments affect the: Johnnie, Stirling Quartzite, Wood Canyon, Zabriskie Quartzite, Cararra, Bonanza King, Dunderberg Shale, and Nopah Formations (Plate 1 and Plate 2). Pebbly cataclastic breccia and gouge is commonly preserved between the hanging wall and footwall of the detachment faults (Figure 10). The most brecciated unit is the Nopah Formation, with tens of meters of breccia located, stratigraphicly and structurally between the Dunderberg Shale and Pogonip group (Figure 10A). Three separate detachments were mapped at different structural levels within the Nopah Formation. Detachments commonly coincide with silty and shaly beds although strong layers are also detached and intensely brecciated (Figure 9). The detachments generally dip north-northwest towards the Specter Range. Most units beneath detachments are thinner than the regional equivalent. The Nopah Formation is 100-325 meters thick in the northern Spring Mountains, 220 meters thinner then Nopah sections measured in the Nopah Range to the south. Generally brittle deformation along detachments increases upwards.

The bedding along detachments also shows systematic variation. Commonly the footwall of a detachment contains beds oriented north-south whereas the hanging wall contains beds that strike east-west. A good example of changes in the orientation of bedding is documented near the boundary between the Specter Range and northern Spring Mountains. The mean strike of the bedding in the footwall of a detachment is 355°/39° (N05°W/39°), near the fault 336°/28° (N24°W/28°), and in the hanging wall 260°/29° (S80°W/29°) (Figure 11).

A major detachment in the northern Spring Mountains can be observed at four localities across the Northern Spring Mountains (Table 2) (Figure 10B).

Table 2. Locations of exposures of the major stratigraphic discontinuity in the northern Spring Mountains, UTM NAD 83 zone 11N

Easting	Northing	Unit in hanging wall	Unit in footwall	Sample number
580859	4045456	Nopah Formation	Wood Canyon Formation	5/06-16
585205	4046790	Nopah Formation	Wood Canyon Formation	No Sample
585320	4045903	Nopah Formation	Wood Canyon Formation	4/06-11
588339	4048749	Nopah Formation	Wood Canyon Formation	5/06-24

The detachment separates the Nopah Formation from underlying Wood Canyon Formation and Stirling Quartzite. About 3,000 meters of section is missing. The hanging wall of the detachment contains a roughly bedded Nopah Formation, composed of breccia with angular fragments ranging from boulders to gouge (Figure 10A). Hand sample and thin section analysis of fault rocks show shear fractures, secondary porosity between breccia fragments, gouge zones with survivor grains, highly rotated clasts, and high density fractures along cleavage planes within dolomite and calcite (Figure 12).

The hanging wall of the Specter Range thrust is composed of Neoproterozoic and Cambrian miogeosyclinal rocks disrupted by many detachments. Detachments are generally parallel to bedding and dip gently to the north-northwest. Detachments were mapped within or along the Zabriski Quartzite, Carrara Formation, Lower Bonanza King Formation, Upper Bonanza King Formation, and the Nopah Formation (Figure 13). Detachments deform both the footwall and hanging wall. Cataclastic breccia is commonly preserved along detachment faults, sheets are commonly a meter thick or more.

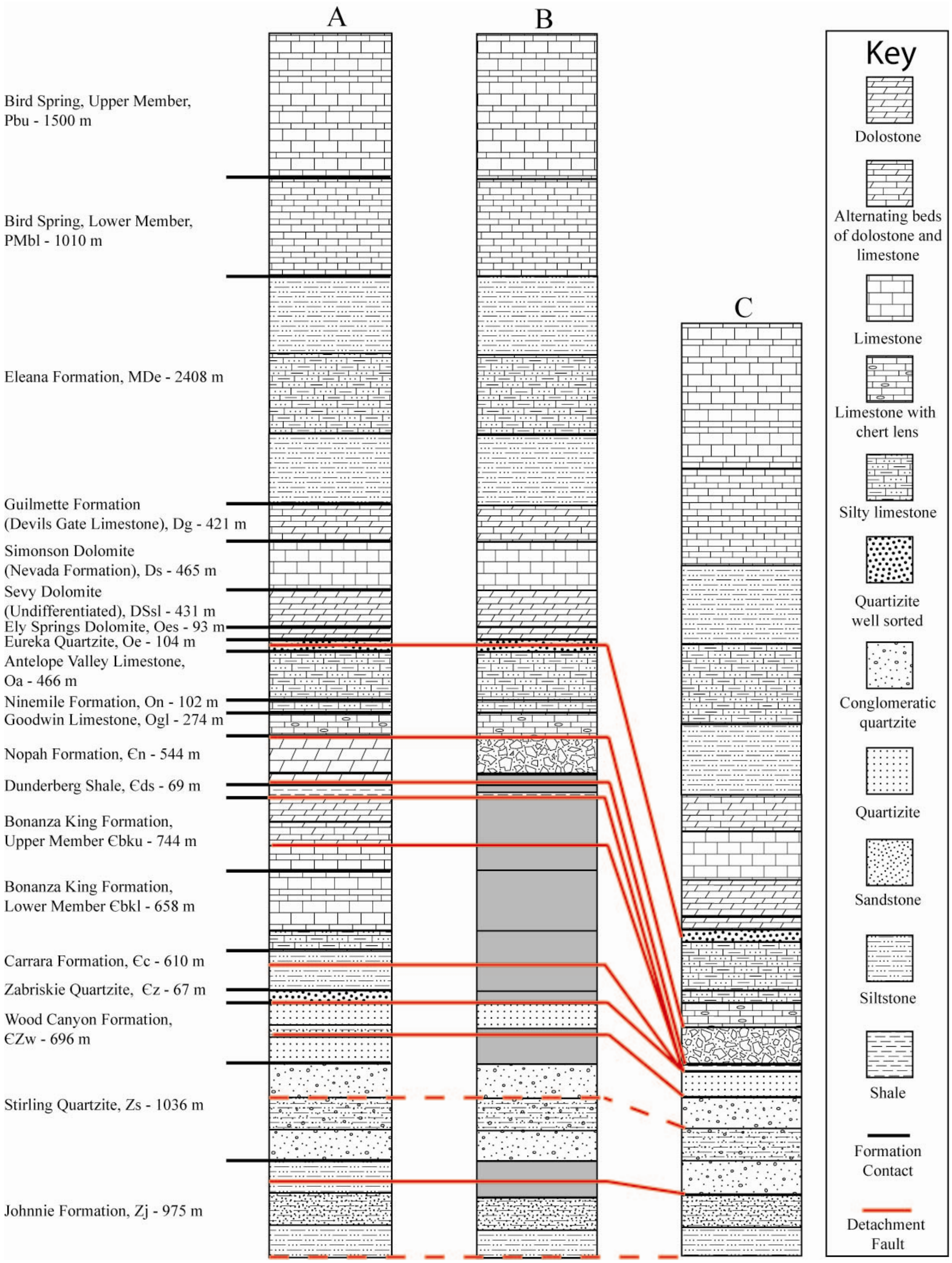

Figure 9. Stratigraphic columns that show: a) stratigraphic units, lithologies, and thicknesses of Paleozoic and Neoproterozoic strata in the Northern Spring Mountains and the Specter Range b) the thicknesses of units missing (shown in gray) among detachments c) stratigraphic column of the showing the detachments within the study area.

The hanging wall of the stratigraphic discontinuity. The Nopah Formation is brecciated, but retains a rough stratigraphy illustrated by the light and dark bands of dolostone.
(585475, 4047381 NAD 83)

A "klippe" of the Nopah Formation resting on the Wood Canyon Formation. The Nopah is extremely brecciated and the underling Wood Canyon Formation is extremely fractured with minor domains of cataclasite. The red line indicates the location of the detachment.
(585330, 4045815, NAD 83)

The footwall of a detachment. Note the extreme faulting, fracturing, and minor brecciation of quartzite beds in the Wood Canyon Formation.
(580802, 4045534, NAD83)

Figure 10. Field photos of the major detachment in the northern Spring Mountains: (A) hanging wall, (B) fault contact, and (C) footwall.

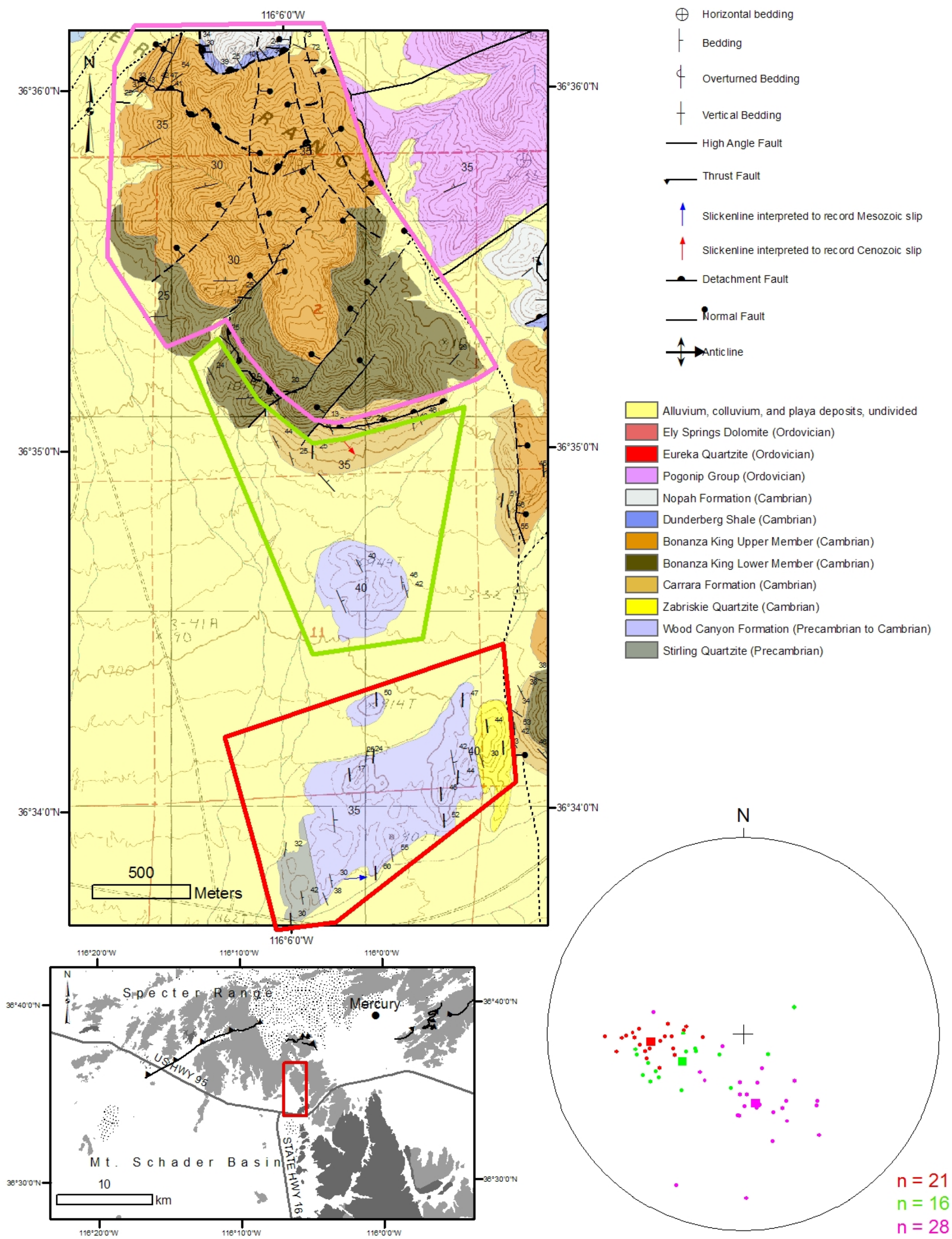

Figure 11. Map and stereogram of poles to bedding in areas in the footwall (red), just below the fault (green), and in the hanging wall of a detachment within the Carrara Formation (hot pink). Small circles represent individual bedding measurements larger squares represent the mean S (bedding) of each domain.

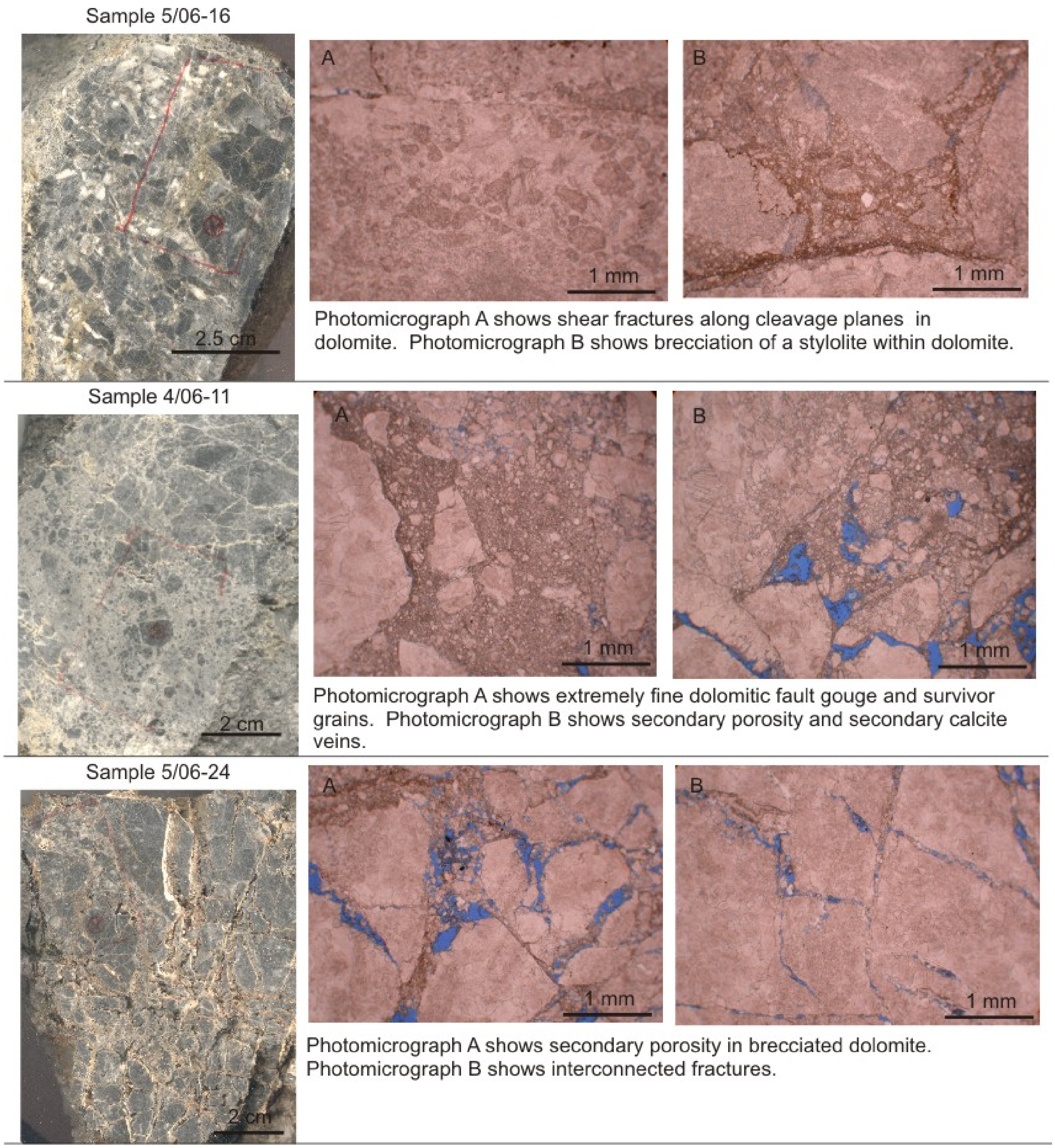

Figure 12. Nopah breccia samples from the hanging wall of the major detachment in the Spring Mountains. Blue domains in photomicrographs represent pore space.

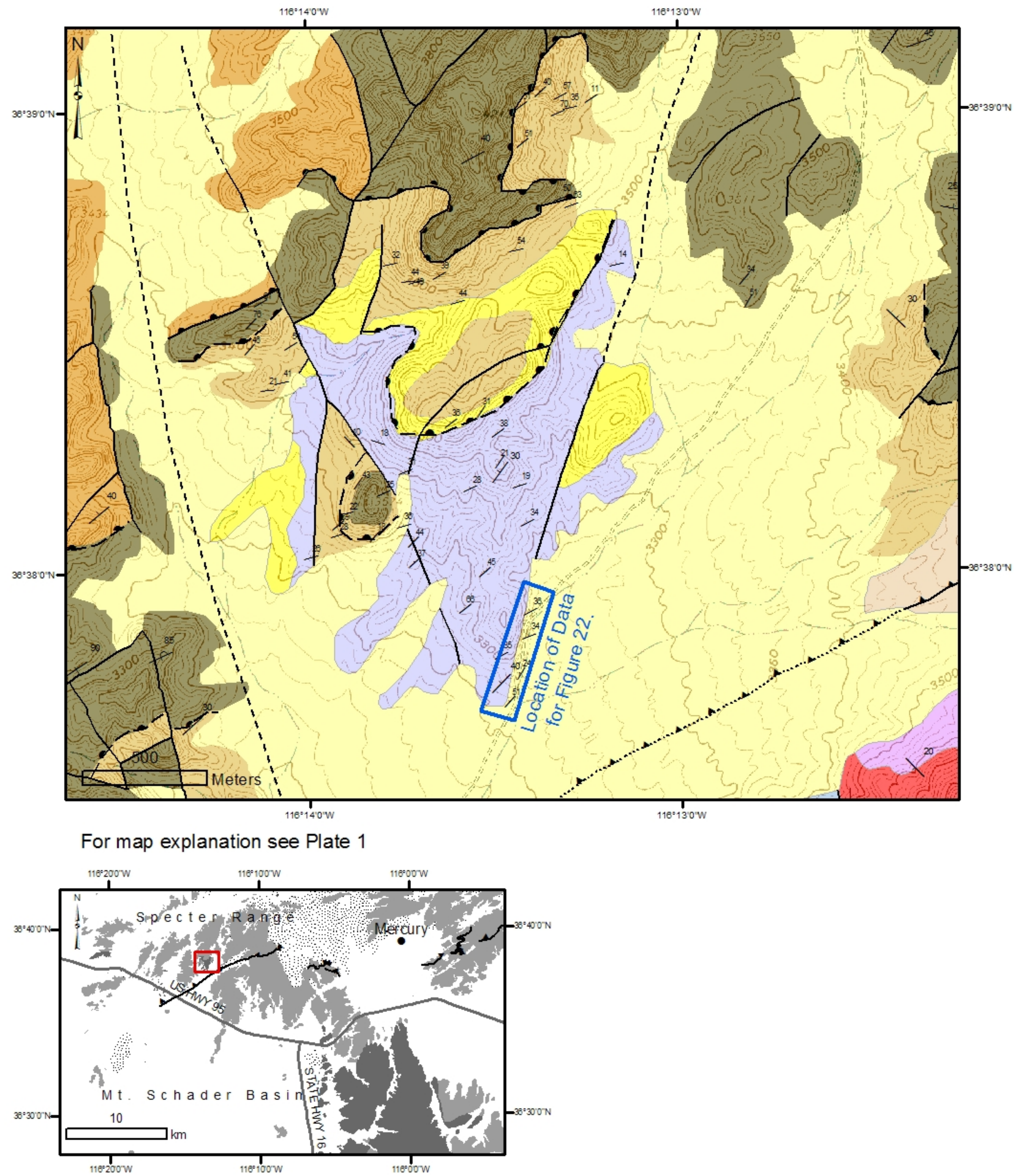

Figure 13. Geologic map of the hanging wall of the Specter Range thrust showing three detachment faults. The blue box shows the location of data plotted on Figure 22.

3.1.2 Normal faults

Normal faults have two general orientations in the northern Spring Mountains: northeast and north. Fracturing in the footwall and hanging wall is generally confined to a few meters (Figure 14) between planar fault surfaces bounding of about 30cm of breccia and fault gouge between the bounding surfaces. Breccia along normal faults is different from breccia along detachment faults. Breccia zones along normal faults are thinner then a meter and contain rotated clasts from both the footwall and hanging wall. The normal faults commonly contain slickenlines within the fault gouge or along the fault planes.

Figure 14. Normal faults. (A) Fault surface (355°/52°) cutting Stirling Quartzite. Slickenlines indicate hanging wall moved down relative to the footwall, pen for scale. (B) Fault surface (038°/76°) cutting Bonanza King carbonate. About 30 cm of breccia is preserved between the footwall and hanging wall, rock hammer for scale.

3.1.3 Thrust faults/tear faults

The Stirling Mine fault is about 1.5 kilometers south of the Stirling Mine in the northern Spring Mountains. A high angle fault to the west and the Las Vegas Valley shear zone to the east isolate the Striling Mine fault which generally strikes east-west (Plate 1 and Plate 2).

Alluvium covers the Stirling Mine fault along its trace, but a measurement from within a mine shaft indicates the fault dips to the north (Page *et al.*, 2005). The hanging wall is composed of brecciated Wood Canyon Formation while the footwall consists of Nopah Formation through Pogonip Group; this suggests a thrust fault. The amount of brecciated Wood Canyon Formation and Zabriskie Quartzite exposed in the hanging wall south of Stirling Mine is thicker than regional stratigraphic thickness. The bedding in the hanging wall along the Stirling Mine fault is generally oriented east-west and the bedding in the footwall is generally orientated north-northwest. The dip of the overlying Carrara Formation and the topographic surface cannot explain the variation in exposed thickness.

Three kilometers east of the Specter Range thrust is a series of thrusts placing the Nopah Formation and Pogonip Group onto the Simonson Dolomite and Guilmettte Formation (Plate 1). These thrusts involve similar units, display similar deformation, and have similar orientations compared to the Specter Range thrust (Plate 1).

3.2 FOLDS

Abolins (1965) and Burchfiel (1999) noted north-plunging hinges in the northern Spring Mountains. Burchfiel also noted northeast plunging folds. Carr (1996) and Abolins (1999) did not recognize northeast plunging folds during later mapping, probably because they both mapped the Dunderberg Shale as a unit of the Nopah Formation.

Detail geological mapping within the northern Spring Mountains and southern Specter Range delineated folds with two general orientations: north plunging and northeast plunging (Plate 1 and Plate 2). Two types of north plunging folds are preserved: large synclines and anticlines and second order parasitic or M-folds. The large open upright synclines and anticlines involve Johnnie Formation through Guilmette Formation. The hanging wall of the Wheeler Pass thrust shows the best example of large open upright synclines with a fold hinge oriented 21°/008° (21°/N08°E) (Figure 15). The parasitic folds or M-folds are preserved in the Johnnie Formation on the west flank of the Spring Mountains. Preliminary field data indicates that these folds are closed upright folds.

The hanging wall of the Nopah Detachment in the northern Spring Mountains also contains open plunging folds. The Nopah breccia sheet is locally folded about northeast plunging hinges. The current orientation of the Nopah Formation in the hanging wall and the bedding in the Dunderberg shale define the fold hinges. Thirty six bedding measurements from both sides of US highway 95 in the Dunderberg Shale indicates that the fold hinge plunges 19° and trends 050° (N50°E) (Figure 16). A parasitic fold within the Dunderberg Shale on the north limb of this fold shows axial planer cleavage (Figure 17).

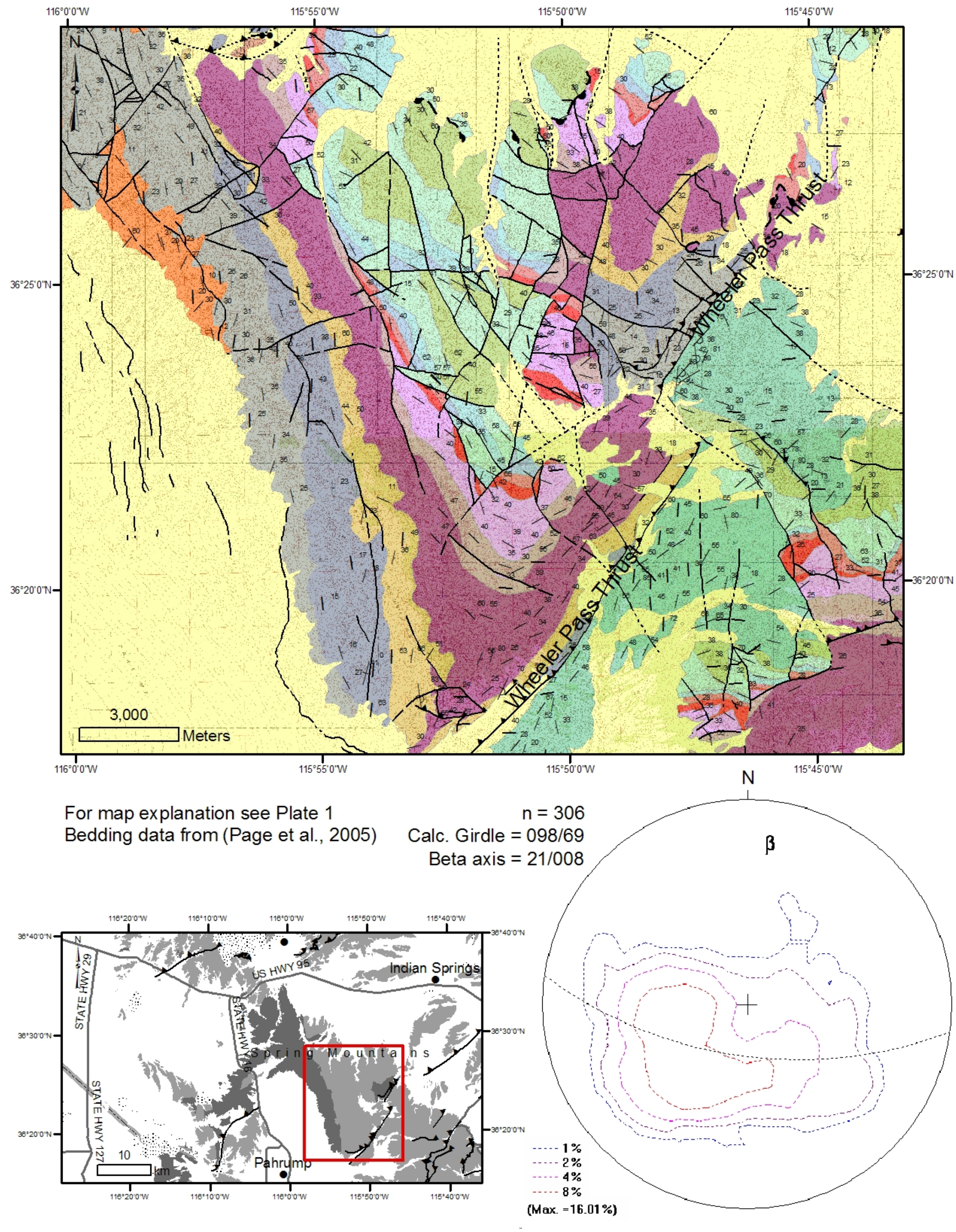

Figure 15. Geologic map that shows a large syncline in the northern Spring Mountains and a stereogram of contoured poles to bedding from the hanging wall of the Wheeler Pass thrust indicating a north plunging syncline

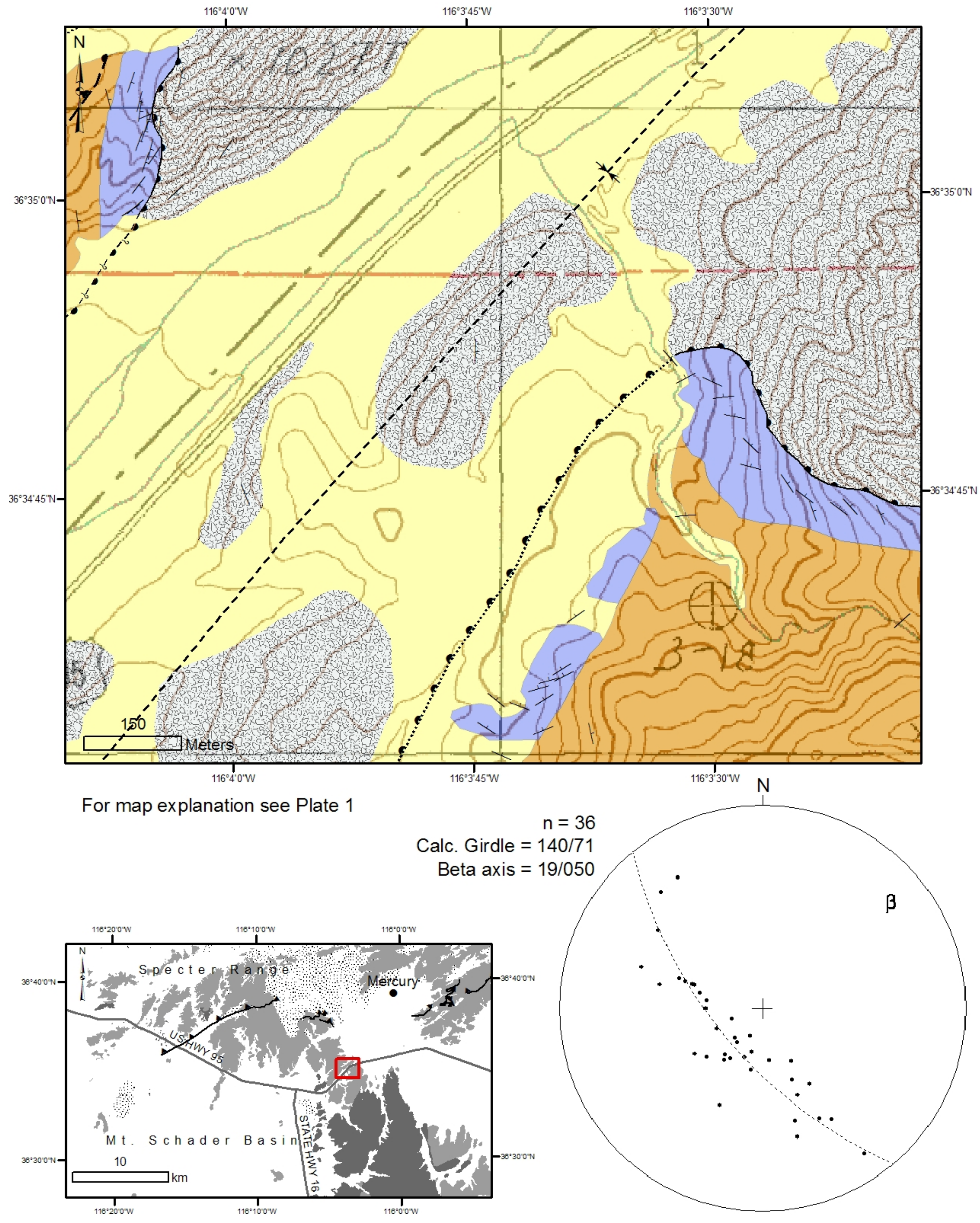

Figure 16. Geologic map and stereogram define a northeast plunging fold hinge. Circles represent poles to bedding from the Dunderberg Shale. The dashed line represents the calculated girdle.

Figure 17. Photograph of an open fold within the Dunderberg Shale (27°/075°). Note the development of cleavage, 15cm ruler for scale.

3.3 BRECCIA IN THE MT. SCHADER BASIN

Rare exposures of Miocene basin deposits crop out on the west flank of the northern Spring Mountains (Plate 1 and Plate 2). These exposures represent the easternmost subbasin of the larger Mt. Schader basin. The exposed Miocene basin deposits comprise two mappable units: masses of breccia and beds of conglomerate (Figure 18). The breccia is composed of angular carbonate fragments in finer-grained cataclastic matrix (Figure 19B,C,C'). The base of the unit commonly contains vertical sedimentary dikes composed of underlying Tertiary basin fill (Figure 19A,F,G). The Tertiary basin fill is poorly lithified, crudely bedded, epiclastic breccia composed of angular to subangular pebbles to boulders of carbonate and minor quartzite. The matrix is composed of silt and sand-sized particles and minor calcite (Figure 19B,E,E').

The oldest units exposed in the basin crop out along an arroyo that cuts into the footwall of a north-south normal fault. The downthrown block is composed of younger Miocene tuffaceous deposits. The Miocene basin deposits dip to the northeast indicating rotation due to faulting either post or contemporaneous with deposition (Plate 1 and Plate 2). The basin-bounding faults are not exposed, but are inferred to be perpendicular to the dip of the Tertiary units. The inferred basin-margin fault may also intersect a paleospring deposit northeast of the Miocene deposits. The paleospring deposits features disturbed bedding and silica precipitates commonly associated with groundwater discharge (Plate 1 and Plate 2).

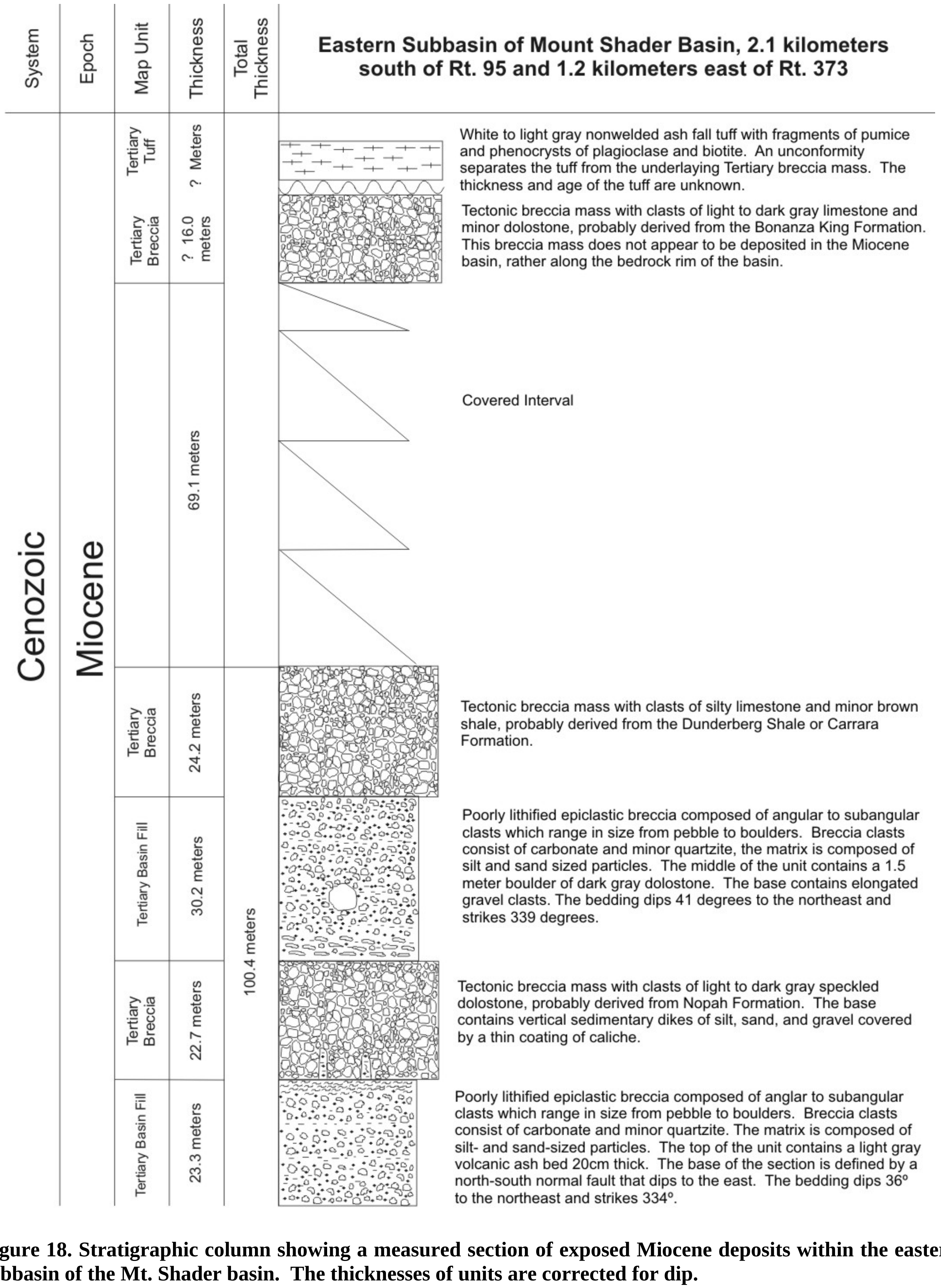

Figure 18. Stratigraphic column showing a measured section of exposed Miocene deposits within the eastern subbasin of the Mt. Shader basin. The thicknesses of units are corrected for dip.

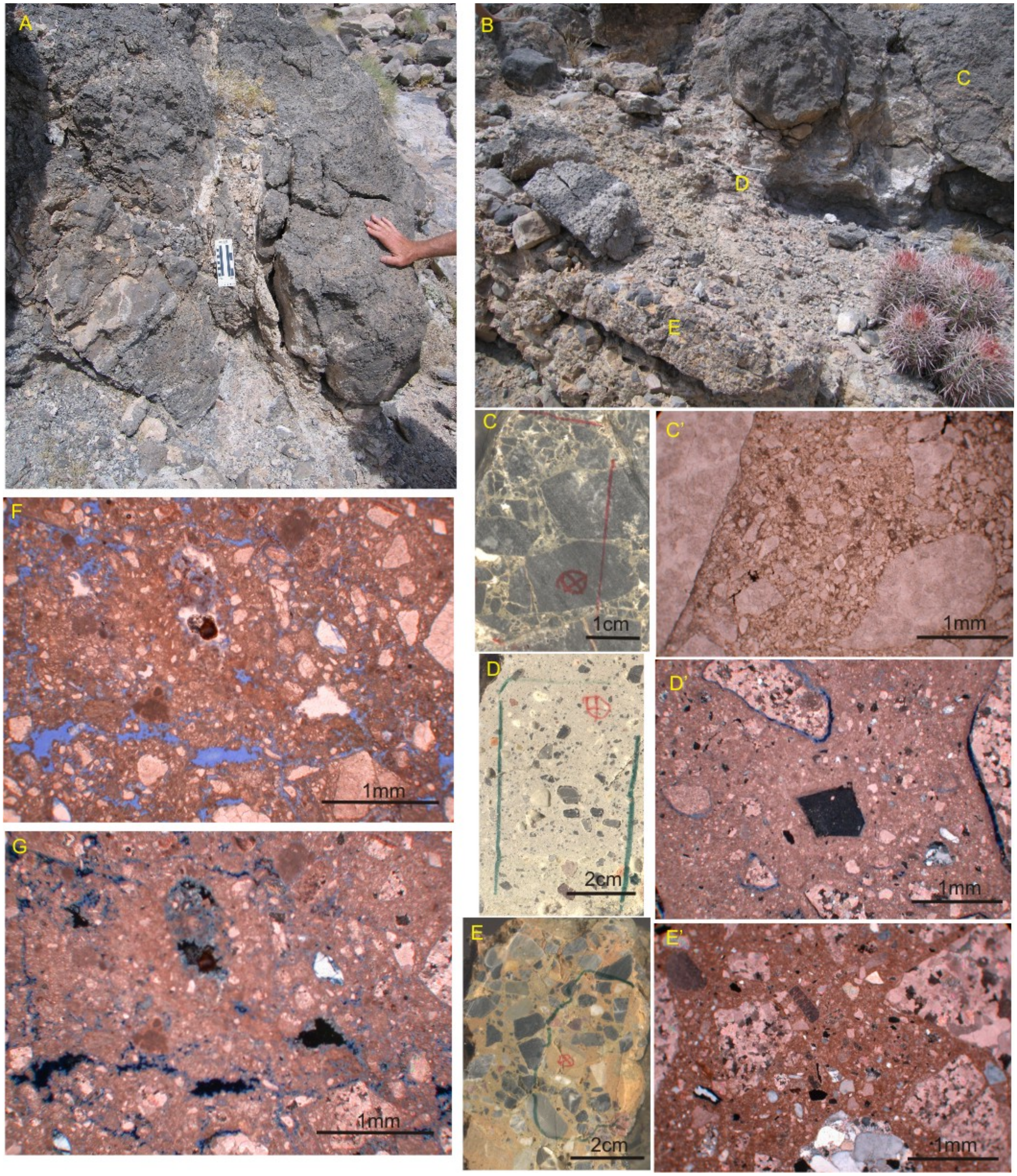

Figure 19. Photographs and Photomicrographs, (A,B) Photographs of outcrops of Miocene basin deposits. (C,D,E) Photographs of rocks sampled form Miocene basin rocks, locations are shown in Photograph B. (C') Photomicrograph (plane light) of the breccia mass with cataclastic texture. (D') Photomicrograph (crossed polars) of volcanicastic ash bed with angular fragments of glass. (E') Photomicrograph (crossed polars) of epiclastic breccia with clasts of quartzite, dolomite, limestone, and volcanic fragments. (F, G) Photomicrographs of sedimentary dike (A) with clasts of glass, dolomite, and calcite note the similarity to D'.

3.4 DIRECTION AND TIMING OF DEFORMATIONS

Cross-cutting relationships and kinematics are critical to understanding the deformational history of the region. The timing of folding and faulting also indicates the past stresses affecting the region. North-plunging folds are the oldest structures as they are cut by all other faults and folds. Northeast-southwest normal faults are cut by detachment faults and north-south normal faults. The detachments are next in age, as they are cut by north-south normal faults and detachment breccias are folded about northeast plunging hinges. Northeast plunging folds are cut by north-south normal faults indicating that north-south normal faults are the youngest structures in the northern Spring Mountains. Cross-cutting relationships also suggest that the detachments are younger as you move up-section because both the Wood Canyon and Stirling detachments cut the Nopah detachment (Plate 1 and Plate 2).

Rare slickenlines along detachment faults show either east-west or southeast trends (Plate 1 and Plate 2). Southeast slickenlines (00°/138°) along the Carrara detachment show step structures and chlorite growths on the lee side of gouges and ploughing structures along the slickensided surface, suggesting southeast transport of the hanging wall (e.g. Petit, 1987) (Figure 20B,D,E,F). The Stirling Johnnie detachment slickenlines (02°/139°) and the slickensided surface show steps and ploughing structures that again suggest southeast transport of the hanging wall of a different detachment fault (Figure 20A). When the orientations of the slickenlines are compared to fold axes, the east-west slickenlines are orthogonal to north plunging folds and southeast slickenlines are orthogonal to northeast plunging folds, which indicates a genetic relationships (Figure 21). Table 3 shows the relationship and timing of observations in the Spring Mountains to pervious studies and other regional and local maps.

An exposure of the Wood Canyon Formation 500 meters north of the inferred trace of the Specter Range thrust contains compressional structures: bedding striking southwest (mean S 235º/42º), fold hinges plunging southwest (mean trend 246º), and reverse faults striking southwest (mean S 246º/74º). Slickenlines along bedding in the Wood Canyon Formation are orthogonal to fold hinges trending northeast-southwest (mean trend 49º, 329º). These slickenlines are generally parallel to slickenlines along detachments in the northern Spring Mountains (Mean trend off by 10.5º). These compressional structures parallel the Specter Range thrust, suggesting a genetic relationship (Figure 22).

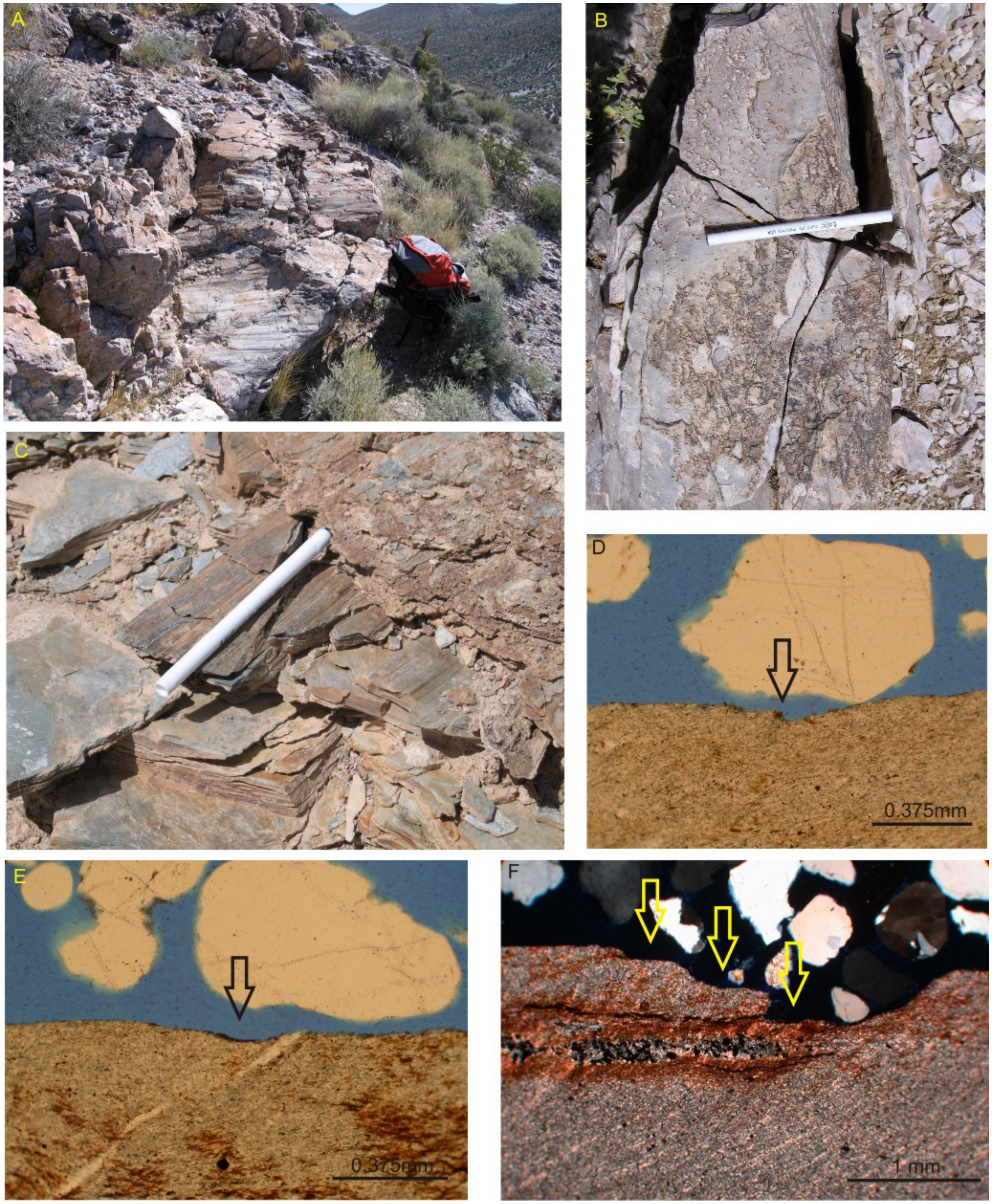

Figure 20. (A,B) Photograph of slickensides along the Stirling Johnnie detachment, backpack for scale. (C) Photograph of a slickensided surface along the Carrara detachment, pen for scale. (D,E) Photomicrograph (plane light) parallel to slickenlines along the Carrara detachment, black arrow pointing to chlorite growth on the lee side ploughing element. (F) Photomicrograph (crossed polars) parallel to slickenlines along the Carrara detachment, yellow arrows pointing to a series of steps along the fault plane.

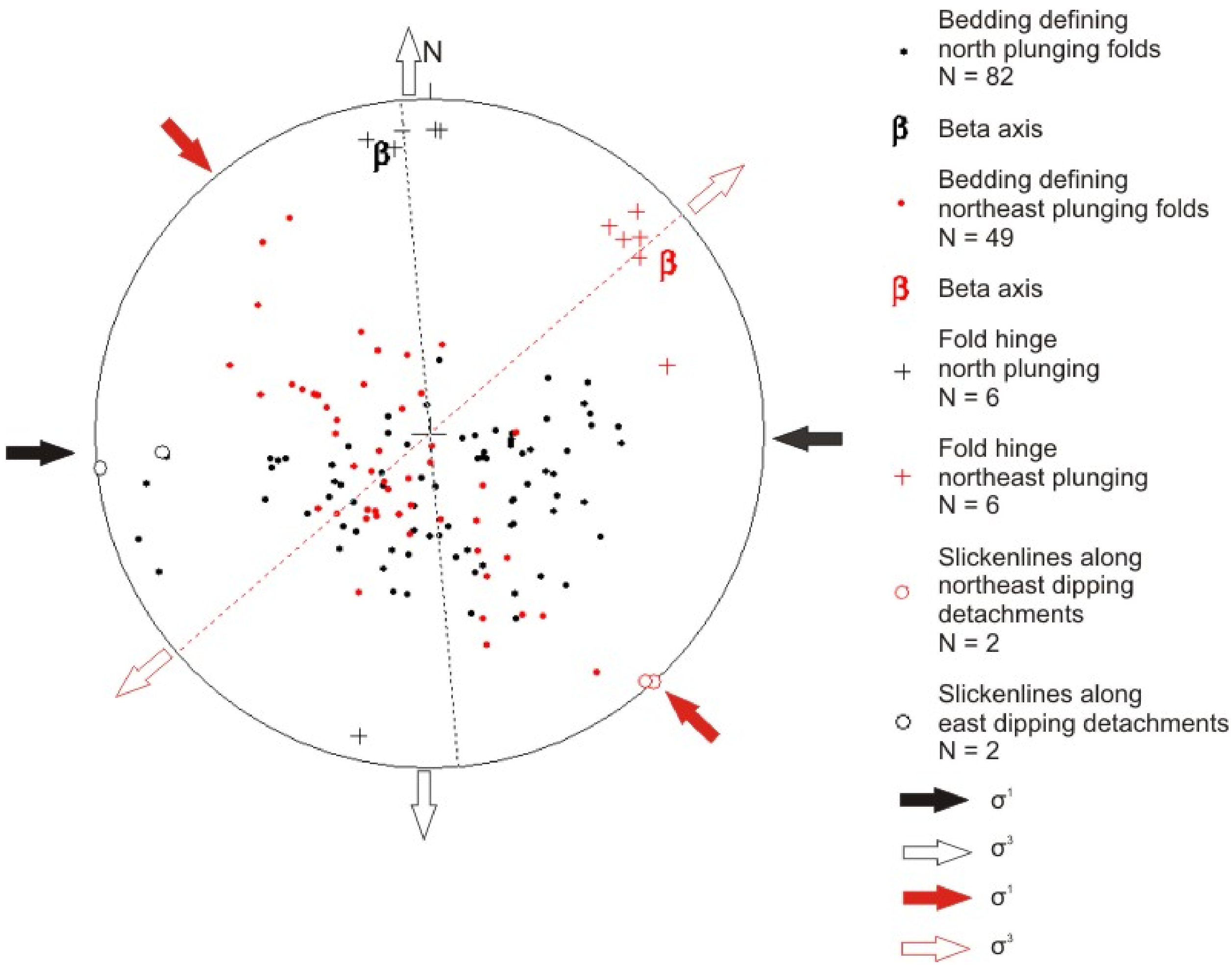

Figure 21. Equal area lower hemisphere stereogram of poles to bedding, folds, and slickenlines from the northern Spring Mountains. Dashed lines represent orthogonal lines to slickenlines, note the association with fold hinges. See text for discussion

Table 3. The timing and order of deformation events based on structural and stratigraphic field studies and map relationships.

Geologic Feature or Structure	Age (Ma)	Source
Thrust faults strike north-south	75-90	1,5,6,7,10,11
Fold, north plunging	75-90	1
East-west slickenlines and west dipping detachments	75-90	5,6,7,9,11,13
Northwest striking normal faults	31-20	4,6,10,11,14
North-south, north-northeast left-lateral strike-slip faults	31-20	11,14
Detachments and some thrusts generally dipping to the north-northwest with rare kinematic indicators recording southeast directed transport of the hanging wall	16-10	1,2,5,15
Adjacent to thrust faults and fold hinges that strike easterly bedding may be rotated easterly to northeasterly	16-10	1,5
Fold hinges recorded by the Paleozoic and Tertiary rocks that trend easterly to northeasterly	16-10	1,12
Some east-northeasterly faults show apparent left lateral offset of geologic contacts	?	5,11,12,14
Normal faults strike north-south	12-10	1,3,5,6,8,10,11

[1](This Study, 2007) [2](Anderson, 1971) [3](Bohannon, 1984) [4](Bohannon and Parsons, 1995) [5](Burhfiel, 1965) [6](Burchfiel *et al.*, 1974) [7](Burchfiel *et al.*, 1983) [8](Carr, 1974) [9](Carr *et al.*, 1984) [10](Carr *et al.*, 1996) [11](Cole and Cashman, 1999) [12](Deemer, 2003) [13](Fleck, 1970) [14](Lauffer-Aho, 2000) [15](Sargent and Stewart, 1971)

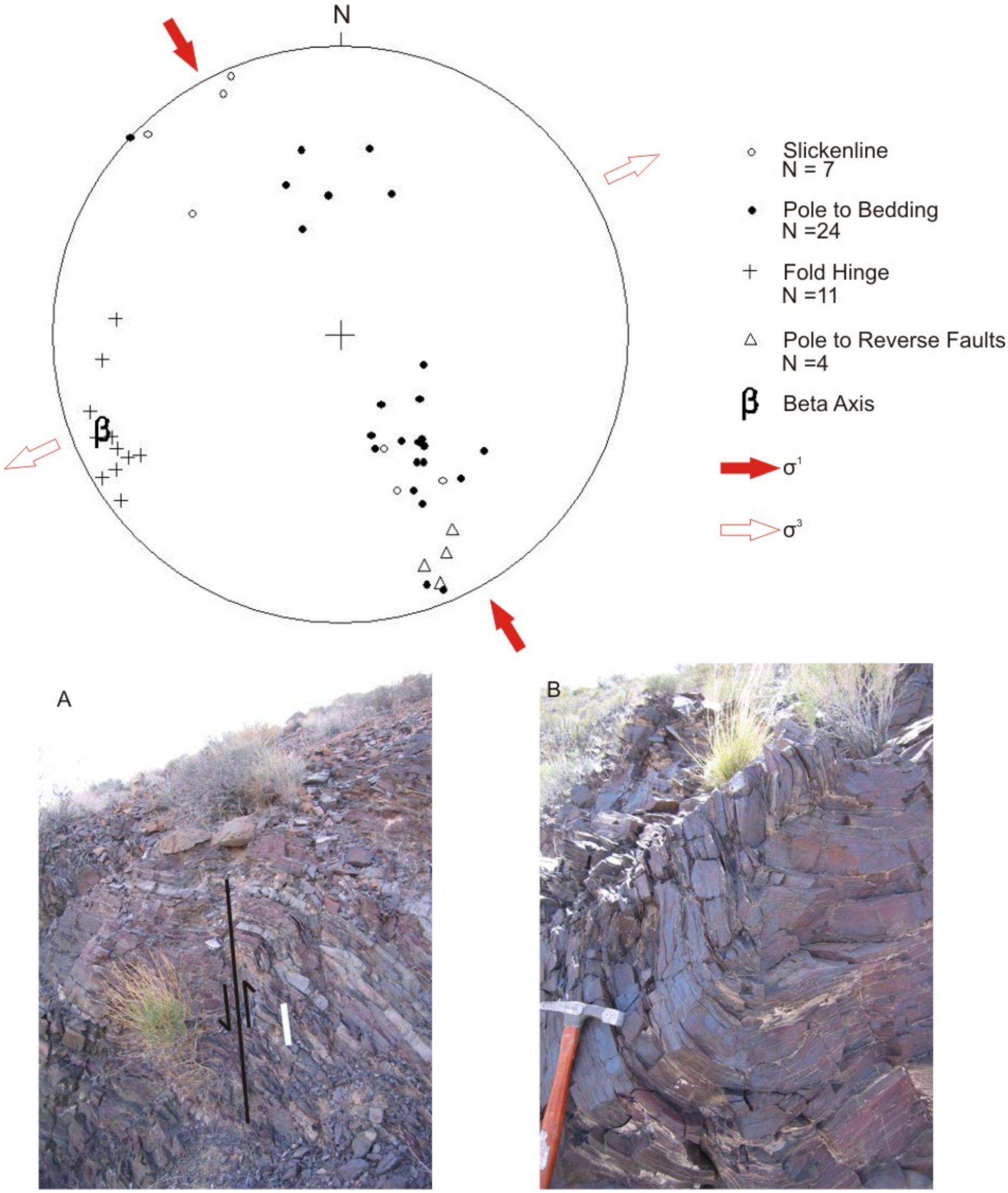

Figure 22. Equal area lower hemisphere stereogram of poles to bedding, pole to reverse faults, slickenlines, and fold hinges. (A) Photograph of a thrust fault, bedding drag indicating fault motion, 15cm ruler for scale. (B) Photograph of a slightly asymmetric steeply inclined syncline, rock hammer for scale. For location of data set see Figure 13.

3.5 FRACTURE DATA

During field mapping and outcrop analysis a total of 338 systematic fractures were measured across the study area using the selection method. In general neither slip nor separation was determined for the fractures. No correction for traverse direction was applied because outcrops were analyzed in three dimensions during data collection.

A rose diagram of the entire fracture dataset shows no statistically significant trends (Figure 23A, B). Because the data were collected across folded sedimentary rocks, fractures with a dip of less than 65º are removed from the dataset and plotted on another rose diagram in an attempt to eliminate fractures that formed pre-folding (Figure 23C, D). Comparison between rose diagrams shows similar trends and a slight reduction in noise after fractures with a dip of less then 65º are removed. Changes in the sector size and start azimuth change the maximum orientation, demonstrating that no unique trend exists within this dataset.

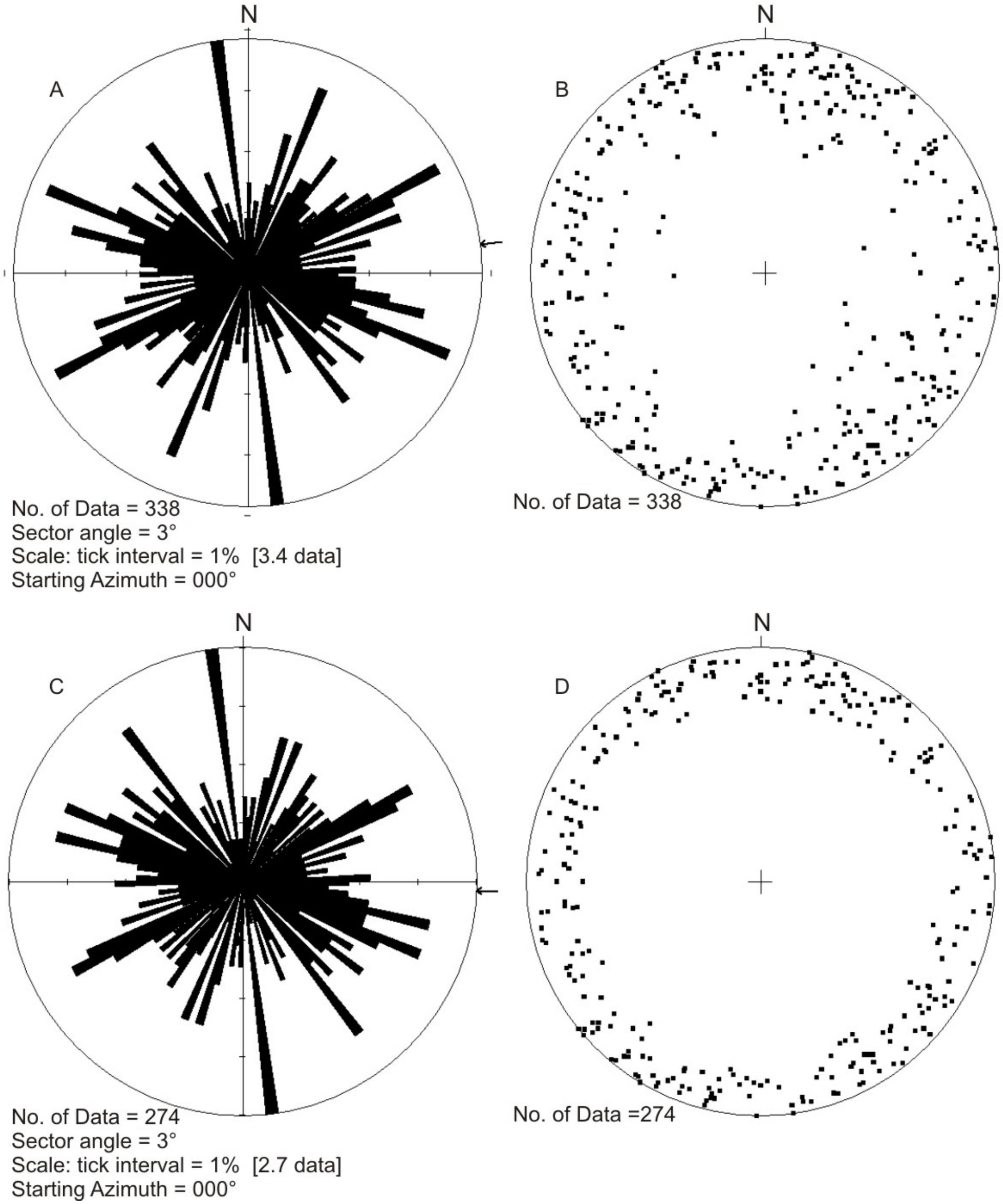

Figure 23. Rose diagrams (A and C) and equal area lower hemisphere stereograms of poles to fractures (B and D) of fracture data collected within the study area. Diagrams A and B plot the entire fracture dataset and diagrams C and D plot fractures with dips greater the 64 degrees.

3.6 DISCUSSION / CONCLUSIONS

3.6.1 Fault rocks and detachments

The lack of dynamic recrystallization of quartz or calcite within fault rocks in the map area indicates that deformation within this domain occurred within 0-7 kilometers of the earth surface between 0-200 C° (Moores and Twiss, 2000). Fault rocks comprised of well lithified gouge and breccia are also compatible with conditions in crust between 2-7 kilometers.

Detachment breccias within the northern Spring Mountains are distinctly different from solution collapse breccias. Solution collapse breccias are typically characterized by inverse grading, sharp and flat bases, breccia pipes, and large V-structures (e.g. Eliassen and Talbot, 2005). Neither gypsum nor salt deposits are known among Precambrian and Cambrian units of the Great Basin, such highly soluble material is generally associated with solution collapse. Thin sections of the Nopah breccia show only minor pressure solution features observed along the boundaries between breccia and gouge. The underlying Dunderberg Shale shows no stylolites or dissolution features commonly associated with pressure solution. These observations lead to the conclusion that tens of meters of Nopah breccia formed tectonically along detachment faults.

Breccia typically associated with extensional detachments tends to contain breccia zones less then 5 meters thick and highly developed gouge zones (e.g. Cowan *et al.*, 2003). Rock mechanics experiments suggest that detachment faults with a dip less then 30° should lock up and form a new fault (Collettini and Sibson, 2001). The Nopah Formation in the northern Spring Mountains contains at least three intraformational detachments. A model in which strain moves up section can explain the observed sequence or series of detachments younging upsection. If a detachment binds weak bedding plane then a bedding plane above accommodates the strain and detaches. This model implies that even more detachments may be present along bedding planes than currently documented, and it explains the thick package of breccia and the pseudostratigraphy within the Nopah breccia. The amount of brecciation and stratigraphic thinning of the Nopah Formation also suggests that the Nopah detachment underwent the largest displacement.

The correlation of detachments with silty units and the vertical axis rotation of bedding in the hanging wall suggests that the detachments are compressional rather then extensional. Stratigraphic control and the rotation of bedding are common along low angle thrusts and compressional detachments (e.g. Holdsworth *et al.,* 2002; Tavarnelli *et al.,* 2004). Silty units allow for significant displacement due to low strength along thin, weak, bedding planes. Detachments within compressional zones commonly produce wide spread rotation of bedding (Van Der Pluijm and Marshak, 2004). Many localities show significant bedding rotation along detachment similar to the 95° rotation along the Carrara detachment. Extensional detachments would passively slide along bedding and would likely not show rotation of north striking beds.

3.6.2 Folds, paleostress, kinematics, and fractures

North-plunging folds formed during Mesozoic contraction (Burchfiel, 1965; Burchfiel *et al.*, 1974; Abolins, 1999; Cole and Cashman, 1999). East-west slickenlines record bedding parallel slip, compatible with Mesozoic folding. Southeast trending slickenlines along detachments suggest south-directed transport of the hanging wall. The geometric relationship between the slickenlines and fold hinges indicates detachments may have formed during the similar stress conditions as the folds. Northeast plunging folds in the Dunderberg Shale contain weak spaced cleavage, common in folds that formed under compressional stress (Van Der Pluijm and Stephen Marshak, 2004)

Although more data is needed to constrain of paleostress orientations within the northern Spring Mountains, preliminary plots indicate two stress orientations in the northern Spring Mountains. These stress orientations can be explained by two different compressional events or 60° or greater rotation of the Specter Range and select blocks in the northern Spring Mountains. The simplest explanation is two different compressional events with the younger event overprinting or reactivating older structures (Figure 24).

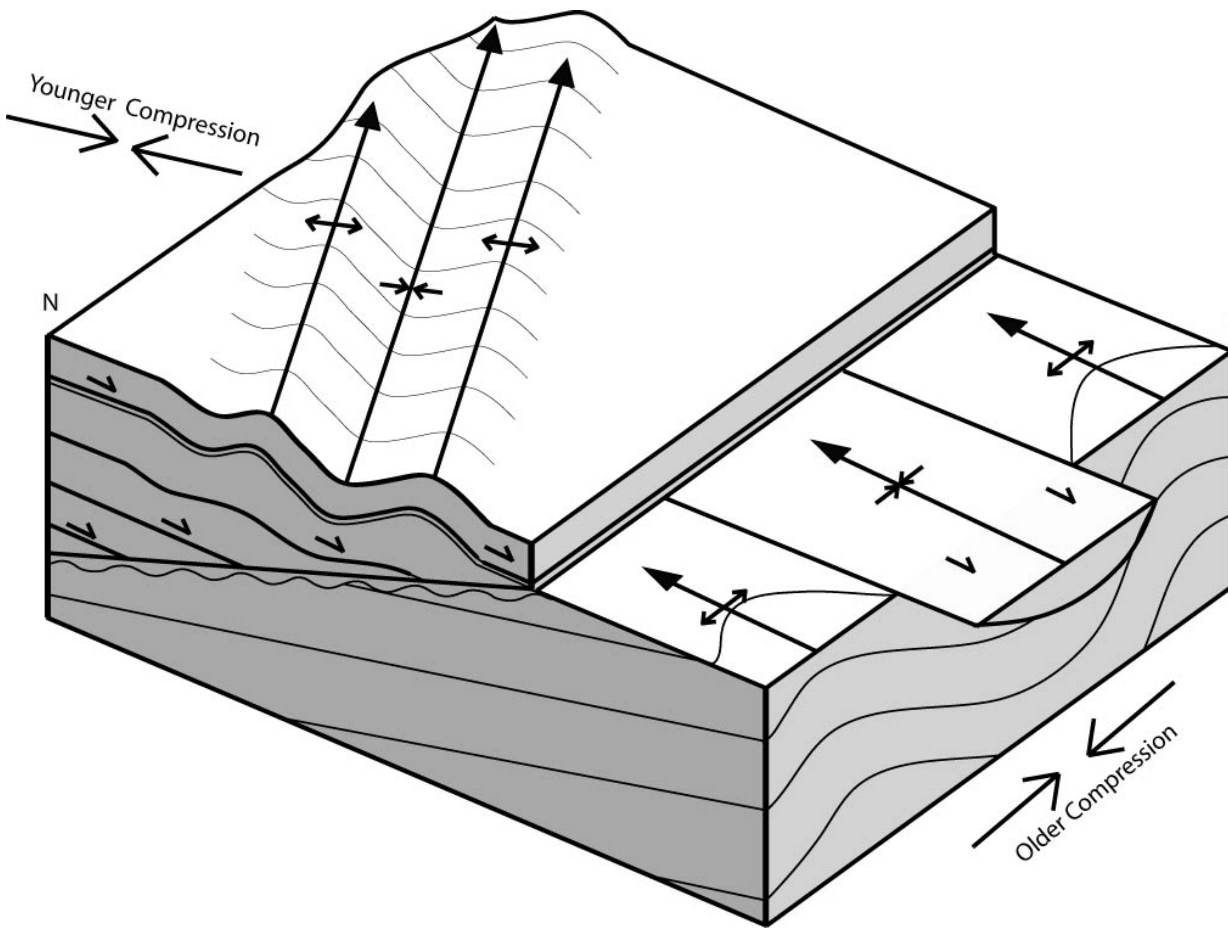

Figure 24. Schematic block diagram of folds and detachments in the northern Spring Mountains.

Similarities between orientations of slickenlines, deformation style, and the orientation of detachments suggest that detachments in the Specter Range may have formed under the same conditions as detachments in the northern Spring Mountains. Reverse faults, thrust faults, and folds in the hanging wall of the Specter Range thrust likely formed under the same stress as the Specter Range thrust. Although more data are necessary to fully constrain paleostress orientations within the Specter Range, initial plots indicate the current orientation of compressional structures in the hanging wall of the Specter Range thrust are incompatible with Mesozoic deformation. Easterly trending folds and thrust faults were formed in Tertiary either as a result of vertical-axis rotation, 70° or more, of pre-existing Mesozoic structures, or in response to north-south-directed shortening (see regional discussion). A covered interval separates thrust faults from the Specter Range thrust three kilometers to the west. However the less prominent faults show the same relationships among units as the Specter Range thrust and must be genetically related and are probably an extension of the main structure.

Multiple episodes of brittle deformation are indicated by rose diagrams of fracture data. Eight maxima may be distinguished, suggesting that the study area has undergone at least two phases of deformation. The fracture data support the field mapping that demonstrates two phases of strain with different orientations within the study area.

3.6.3 Stirling mine fault

Low mountain peaks underlain by Cambrian carbonate strata compose the footwall of the east-striking Stirling Mine fault. The topography in the footwall of the Stirling Mine fault suggests that the hanging wall of the thrust must ramp upward abruptly in order for Wood Canyon beds to have been emplaced onto the northern Spring Mountains and subsequently eroded (Figure 25). The Stirling Mine fault likely flattens at depth between the Wood Canyon Formation and Johnnie Formation along a silty unit, similar to flats in the northern Spring Mountains. The hanging wall of the thrust contains thick breccia at its base. The east-west orientation of the bedding likely results from rotation during fault motion. A detachment between the Bonanza King Formation and Carrara Formation probably cuts out part of the Carrara Formation. . The Stirling Mine fault is bounded by a steep covered fault 1.5 kilometers west of the Stirling Mine. The fault is probably a lateral tear fault along which the Stirling Mine block has moved southward. This block was originally part of the Wheeler Pass syncline before being detached and thrust onto the northern Spring Mountains.

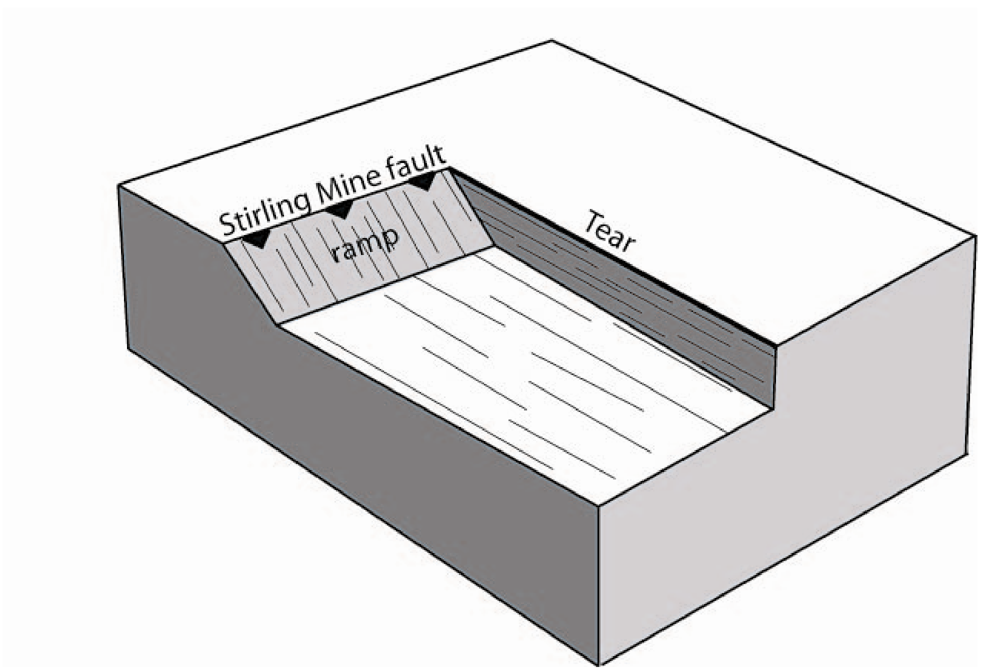

Figure 25. Schematic block diagram illustrating the ramp, flat, tear fault geometry forming the Stirling Mine fault.

3.6.4 Mt. Schader basin

Abolins (1999) recognized Mt. Schader basin deposits as Miocene in age and syntectonic. Breccia masses, systematically intercalated with conglomerate in the basin, suggests that as breccia formed along the Nopah detachment and moved southward across the ground surface, large blocks and slabs calved off into the basin and were covered by conglomerate and epiclastic sedimentary breccia. Soft sediment deformation and sedimentary dikes indicate that these breccia masses were lithified masses before being deposited within the basin.

In the Mt. Schader Basin, normal faults that cut and displace the Miocene deposits have two orientations north-south and northwest. The faults probably record two separate Tertiary extensional events: (1) northwest trending normal faults creating the Miocene Mt. Schader basin and (2) younger north-south normal faulting cutting the Miocene deposits. The relationships observed at the surface of eastern sub-basin of the Mt. Shader basin may also be inferred in subsurface along an east-west seismic reflection profile generated by the USGS (Figure 4). The Mt. Schader basin may have been shortened. The seismic reflection data shows no indication of contraction because the east-west line was parallel to the strike of any transpressional structures, which would only be visible along a north-south line.

4.0 REGIONAL SUMMARY

Transpression in the Specter Range and northern Spring Mountains is compatible with 1) changes of strike along the Las Vegas Valley shear zone and 2) easterly oriented structures in the Specter Range and northern Spring Mountains. Slip along bedding planes within the Wood Canyon Formation, Stirling Quartzite, and Johnnie Formation in the northern Spring Mountains took place during east-directed Mesozoic folding. Bedding planes at other localities record southeast trending slickenlines indicating south- directed transport of the hanging wall of gently north-northwest dipping detachments. Contractional detachments in the northern Spring Mountains within the Nopah Formation, Lower Member of the Bonanza King Formation, Upper Member of the Bonanza King Formation, Carrara Formation, Zabriskie Quartzite, Wood Canyon Formation, Stirling Quartzite, and Johnnie Formation are compatible with Tertiary transpression along the Las Vegas Valley shear zone (Deemer and Anderson, 2002; Deemer, 2003). Extensive brecciation of the Nopah Formation resulted from movement along a major detachment or flat during southeast transport of the hanging wall. Tectonic breccia masses within the Mt. Schader basin were created along the Nopah detachment before being emplaced into the basin. Transpression may also explain the structurally isolated Spotted Range klippe, which previous researches have noted as enigmatic (Cole and Cashman, 1999).

At Indian Springs the Las Vegas Valley shear zone steps to the left or bends southward resulting in a 30 km segment of transpression (Figure 26). After the Spotted Range the LVVSZ steps right, resulting in a domain of simple shear along the Mercury segment. East-west folds in the Miocene strata suggest contraction and uplift associated with another left-step under the Specter Range to Fortymile Wash, linking the LVVSZ with the Highway 95 fault (Deemer and Anderson, 2002; Deemer, 2003) (Figure 27).

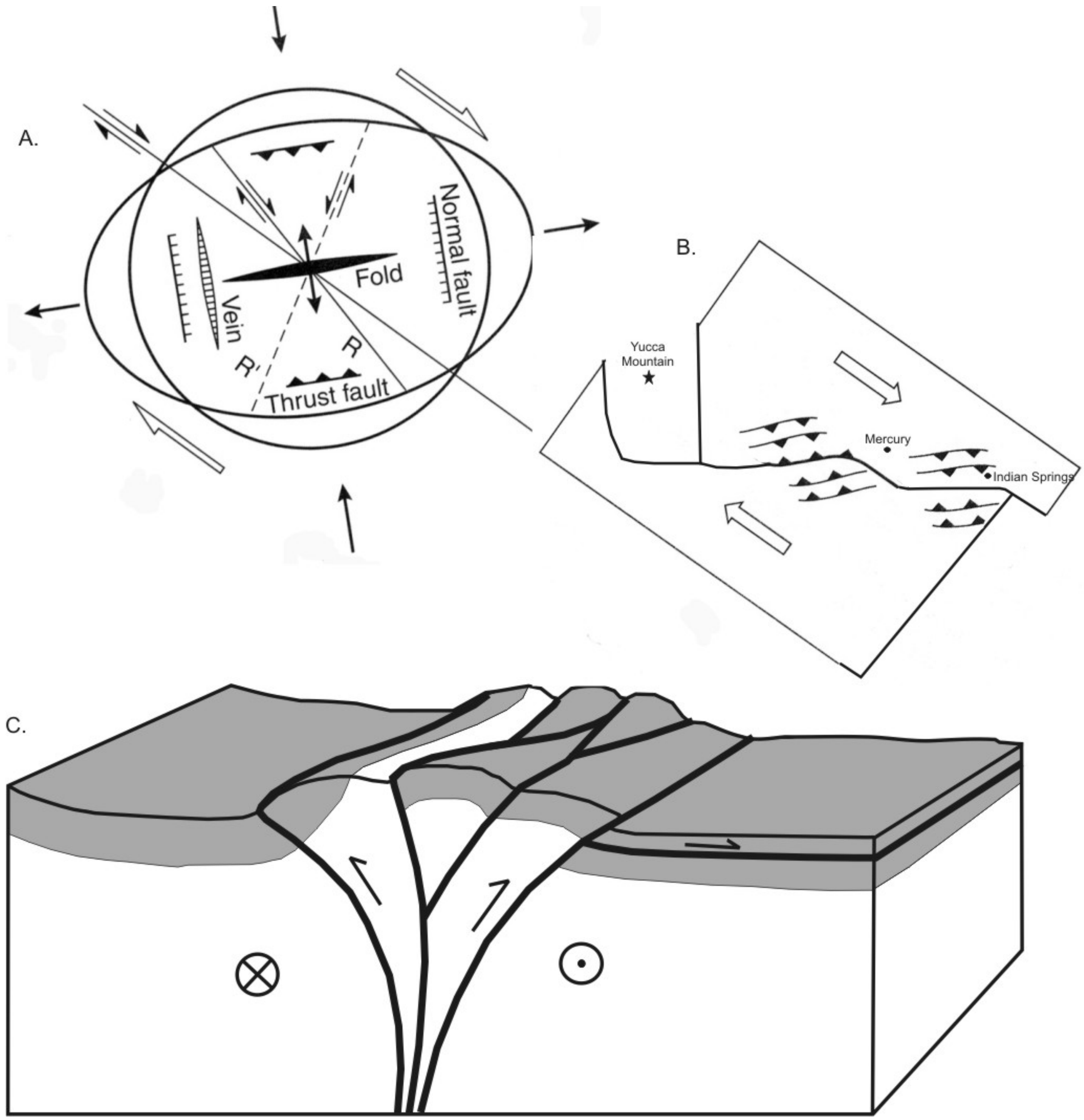

Figure 26. Structures formed at a left-step along a right lateral strike-slip fault. (A) Strain model showing the formation of folds, veins, normal faults, and thrust faults. (B) Map view of thrust formed along a left step. (C) Schematic block diagram showing uplift and the shape of a positive flower structure. Modified from Van Der Pluijm and Marshak (2004)

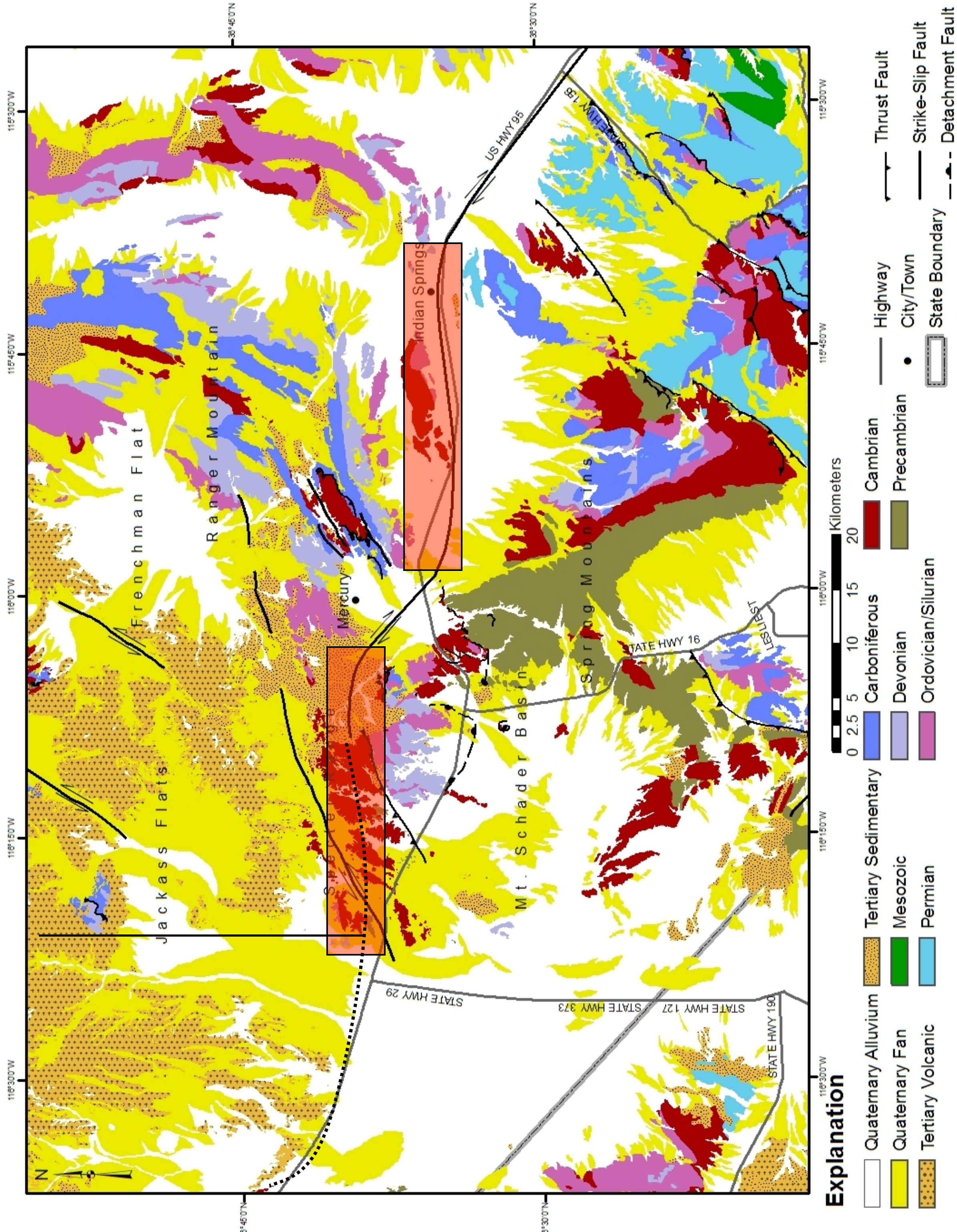

Figure 27. Regional geologic map showing strike-slip and thrust faults. The red boxes illustrate domains of transpression resulting from inferred steps along the Las Vegas Valley shear zone.

5.0 IMPLICATIONS FOR GROUNDWATER PATHWAYS

Carbonate aquifers on the Nevada Site discharge towards Amargosa Desert and Death Valley (Winograd and Thordarson, 1975; Dettinger, 1989; Laczniak et al., 1996). Groundwater flows from Yucca Flat and Frenchman Flat through Mercury Valley then through the Mount Schader basin and emerges at Ash Meadows as springs (Winograd and Thordarson, 1975; McKee et al., 1998). The bedrock aquifers within this region are the main hydrologic units due to storativity and transmissibility. Primary and secondary features control the transmissibility of the aquifers, secondary features having the greatest effect (McKee et al., 1998; Laczniak et al., 1996) (Table 4).

Table 4. Features that affect aquifer transmissibility, modified from (McKee *et al.*, 1998).

Primary Features	Secondary Features
Stratification	Digenetic Minerals
Grain Size	Dissolution
Sorting	Recementation
Cementation	Compaction
-	Brecciation
-	Fracturing

Winograd and Thordarson (1975) divided the Precambrian and Paleozoic stratigraphy into four hydrologic units: 1) the lower clastic aquitard, 2) lower carbonate aquifer, 3) upper clastic aquitard, and 4) the upper carbonate aquifer (Table 5)

Table 5. Hydrologic Units of Bedrock in southern Nevada, modified from Winograd and Thordarson (1975).

Hydrologic Unit	Lithology	Stratigraphic Unit
Upper carbonate aquifer	Limestone	Bird Spring
Upper clastic aquitard	shale, quartzite, and conglomerate	Eleana Formation
Lower carbonate aquifer	limestone and dolostone	Guimette Formation through Upper Carrara Formation
Lower clastic aquitard	shale, siltstone, sandstone, and quartzite	Lower Carrara Formation through Johnnie Formation

The bedrock aquifers within the region are composed mainly of massive limestone and dolostone. In the vicinity of the Nevada Test Site, the primary hydrologic unit is the lower carbonate aquifer. The miogeosynclinal carbonates that make up the lower carbonate aquifer contain extremely low primary intercrystalline porosity (Winograd and Thordarson, 1975). However, faulting and fracturing create secondary porosity and permeability that increases the transmissibility of the units. The lower carbonate aquifer typically contains complex interconnecting fracture patterns and fracture densities resulting in transmissibility between 1,000 to 1,000,000 gpd (Winograd and Thordarson 1975). The lower carbonate aquifer is generally the source of springs throughout southeastern Nevada. The upper carbonate aquifer is similar to the lower carbonate aquifer, with an estimated transmissibility of 1,000 to 100,000 gpd (Winograd and Thordarson 1975).

Bedrock aquitards within the region consists of clastic rocks. Most common are thick shale units; aquitards are important because they block and direct groundwater movement. The lower clastic aquitard comprising Lower Carrara Formation thru Johnnie Formation is nearly impermeable with a transmissibility of less then 1,000 gpd (Winograd and Thordarson, 1975). Faults and fractures are sealed with quartz and calcite, reducing the secondary porosity (Winograd and Thordarson, 1975). The upper clastic aquitard comprising the Eleana Formation is even less transmissible than the lower clastic aquitard, with transmissibility of less then 500 gpd (Winograd and Thordarson, 1975). Although the porosity of the unit is higher then the lower clastic aquitard, the permeability is much lower due to fewer interconnected fractures and pores.

Large structures are important in controlling the regional groundwater flow (McKee et al., 1998). Structures related to faulting, folding, and other deformation within southern Nevada controls groundwater flow and contaminant transport between basins and among bedrock aquifers (Winograd, 1962; Winograd and Thordarson, 1975). Fracturing and brecciation along strike-slip faults in the Spotted Range and oblique slip faults in the Specter Range are significant pathways for groundwater flow (McKee et al., 1998). The regional groundwater flow, which is parallel to the strike of these steep lateral faults, indirectly suggests that they play an important role in transmissibility (McKee et al., 1998). High-angle normal faults striking north-south and northwest-southeast likely have high transmissibility, but are perpendicular to regional groundwater flow in the carbonate aquifer. This suggests that they are not significant in controlling groundwater flow in Specter Range and Spotted Range. Thrusts in the region commonly separate the Cambrian aquitard from underlying lower and upper carbonate aquifers. Thrust commonly acts as a regional aquitard when the thrust is perpendicular to flow and a conduit when parallel to flow (McKee et al., 1998).

5.1 RELATION OF STRUCTURE TO GROUNDWATER FLOW

The age, orientation, and cross-cutting relationships of faults are important factors affecting the transmissibility of a region. Mesozoic and Tertiary structures not only juxtapose clastic aquitards and carbonate aquifers, but also create flow paths and secondary porosity that increases transmissibility (Figure 28).

Detachments, which dip north-northeast under the Specter Range, distinguish a zone that correlates with the domain of high transmissibility noted by Winograd and Thordarson (1975) (Figure 29). The detachments are associated with thick layers of breccia, which affect the porosity and permeability of the rocks (Figure 12). Interconnected fractures and secondary porosity are common within breccia exposed near the surface (Figure 12). Detachments appear to have a stronger effect on transmissibility then previous research estimated (e.g. Winograd and Thordarson, 1975; Mckee et al., 1998) (Figure 28).

The Specter Range thrust may be a structure that strongly influences the flow of groundwater. The southwest strike of the thrust creates pathways for southwest flow of water form Mercury and Frenchman Flat, but the hanging wall composed of the lower aquitard deflects southward flow from Jackass Flats. The intense fracturing, faulting, and brecciation that occur in the footwall are compatible with the extremely high transmissibility of the southern Specter Range and northern Spring Mountains.

The Las Vegas Valley shear zone also influences the regional flow of groundwater. Domains of simple shear along the shear zone oriented northwest are generally more conductive than domains of simple shear and pure shear (transpression) oriented east-west. Where the Las Vegas shear zone juxtaposes an aquitard and an aquifer a barrier to flow is created. In contrast, near Mercury both sides of the Las Vegas Valley shear zone consist of lower carbonate aquifer, and water flows readily across the fault.

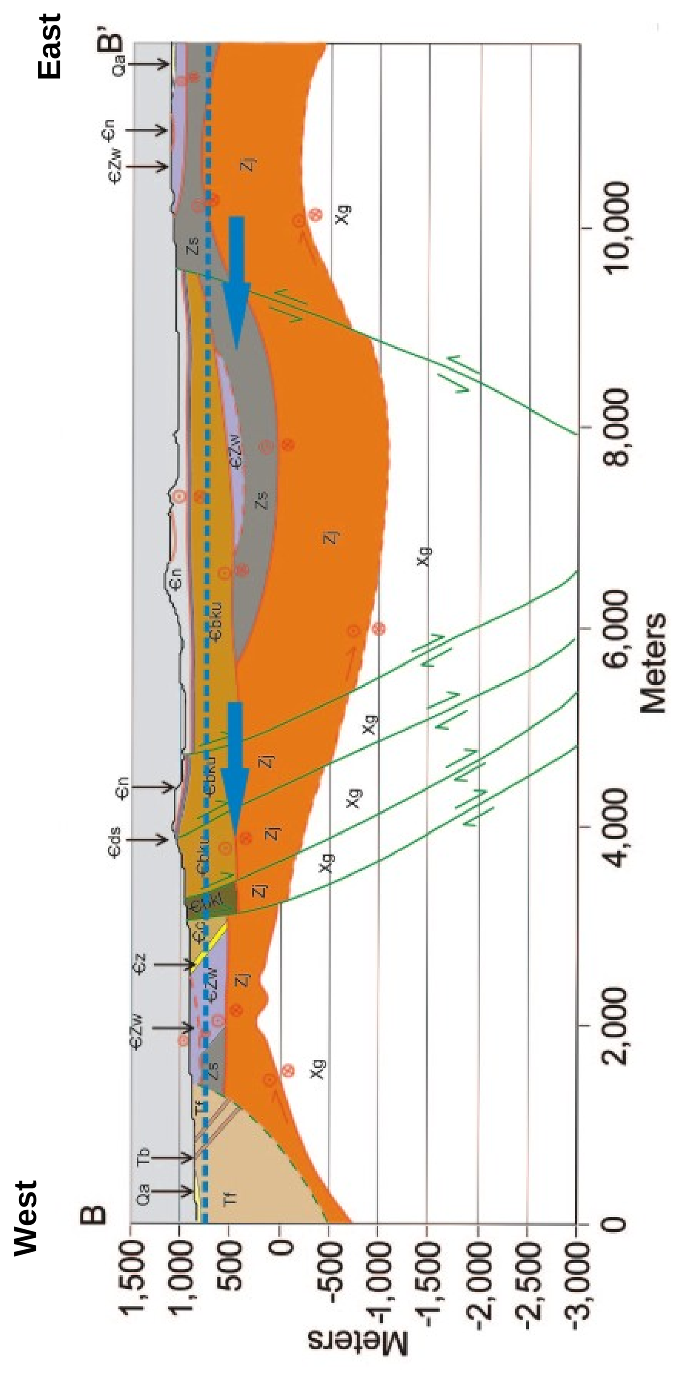

Figure 28. Hydrogeologic cross-section across the northern Spring Mountains, the dashed blue line represents the potentiometric surface and the blue arrows indicate the direction of groundwater flow according to Winograd and Thordarson (1975).

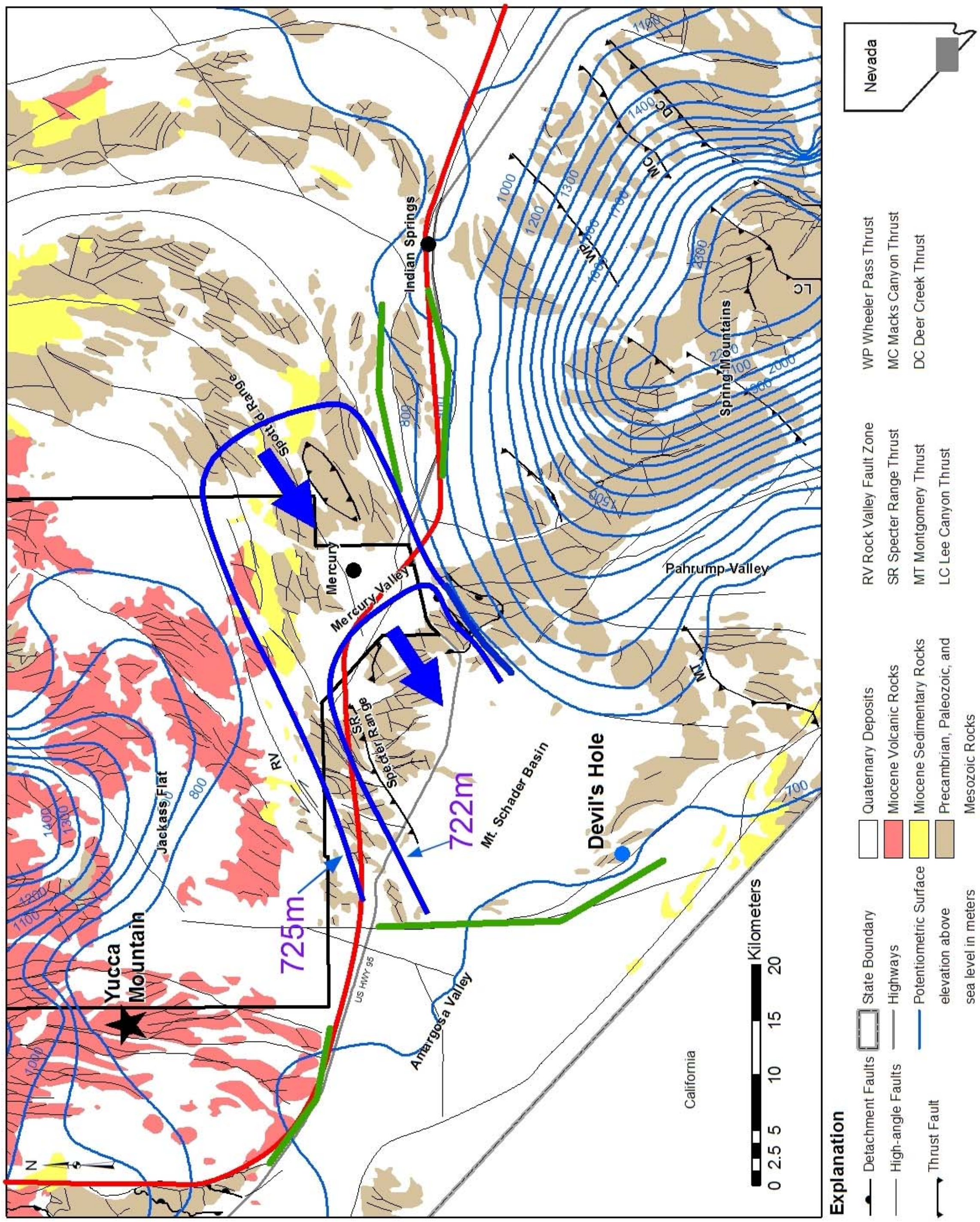

Figure 29. Hydrogeologic map of the bedrock aquifer in southern Nevada. The green lines represent barriers to groundwater flow, thick blue lines represent local potentiometric surface, and blue arrows indicate the direction of groundwater from Winograd and Thordarson (1975). Regional potentiometric surface and faults modified from Potter *et al.*, (2002). The red line represents the interpreted trace of the Las Vegas Valley shear zone.

6.0 FUTURE WORK

Transpression, recorded along the LVVSZ west of Mercury and west of Indian Springs, is compatible with the regional structures. Paleomagnetic studies documenting vertical axis rotation and radiometric dating of the Horse Spring Formation and older Oligocene sedimentary deposits within the Specter Range and Spotted Range could constrain the location of the Las Vegas Valley shear zone and provide a better time constraint on east-west structures in southern Nevada. Further kinematic studies of contractional and extensional structures within the Specter Range and Spring Mountains would better constrain the paleostress orientations. Detailed mapping of diverse structures and landslide deposits in the central Spring Mountains may reveal a tectonic rather then gravity driven system, which may be linked to transpression near Indian Springs. Palinspastic maps of the Indian Springs area suggest significant transpression causing significant uplift and rotation. Well and gravity data near Indian Springs suggest that remains of a Miocene or older basin may have been exhumed during transpression along the LVVSZ. A microgravity study within this area could constrain the size and shape of the exhumed basin (Figure 30).

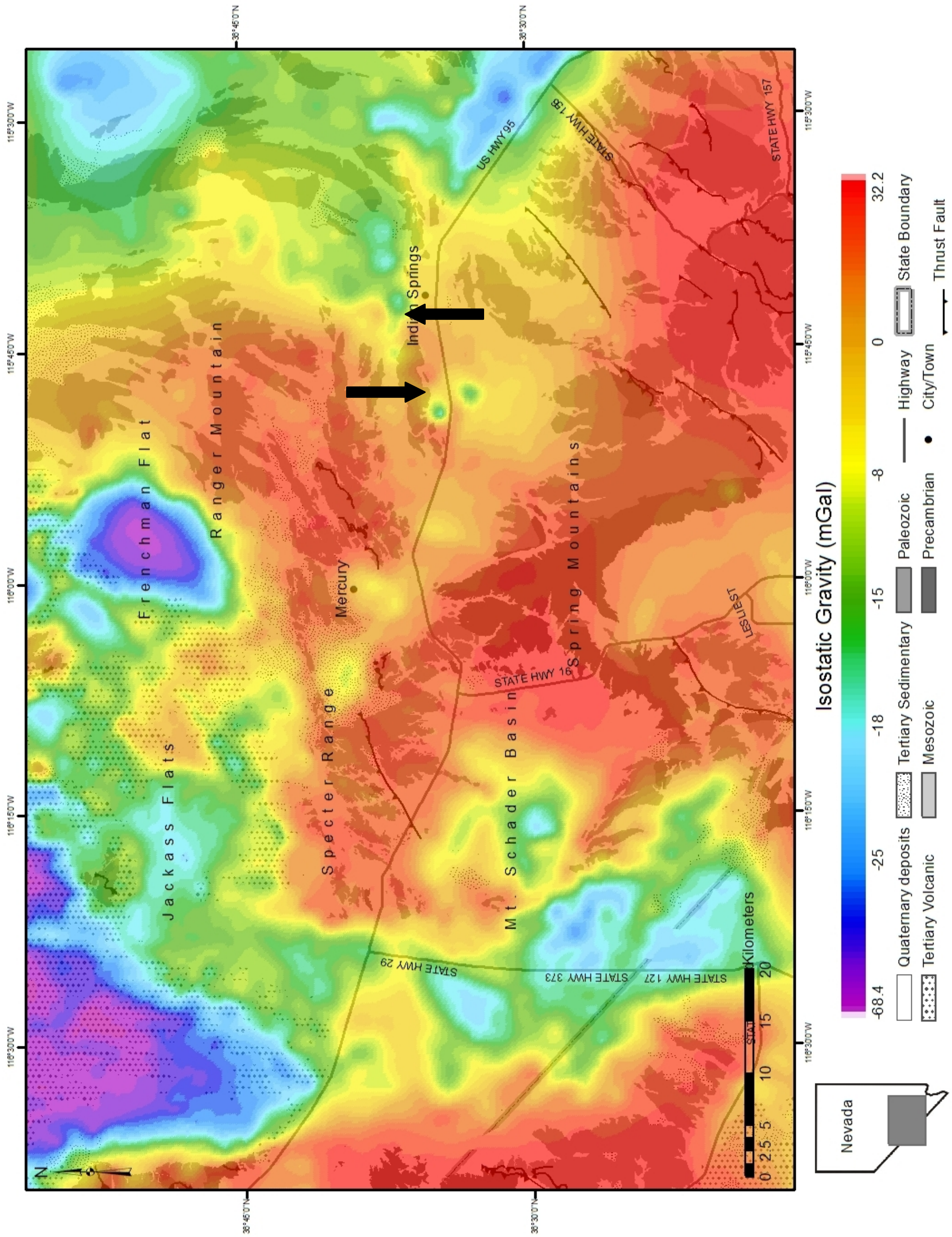

Figure 30. Isostatic gravity map of southern Nevada, black arrows indicate remains of exhumed Miocene basin(s). Gravity data from Ponce *et al.*, (2001).

APPENDIX A

SAMPLE LOCATIONS

Appendix A contains the Waypoint, Location, Zone, Easting, Northing, and Sample Number. The Waypoint is the unique name for each data collection point. The Location is an acronym allowing for quick sorting of the data by geographic location: (POR) Point of Rocks area, (CROC) Crystal Outcrops, (SMMSB) Southern Mount Schader Basin, (SM) Stirling Mine, (SRT) Specter Range Thrust , and (HWSRT) Hanging Wall of the Specter Range Thrust. Zone, Easting, and Northing are the GPS coordinates for each waypoint, projection UTM and Datum NAD 83.

Samples					
Waypoint	**Location**	**Zone**	**Easting**	**Northing**	**Sample Number**
412-14	POR	11	581529	4047430	4/06-2
412-9	POR	11	581319	4047125	4/06-1
415-4	POR	11	580746	4049140	4/06-5
415-8	POR	11	580935	4049148	4/06-4
415-9	POR	11	580935	4049142	4/06-5
417-7	POR	11	582357	4049145	4/06-6
418-11	HWSRT	11	569046	4055096	4/06-7
419-16	HWSRT	11	569502	4056331	4/06-8
421-15	POR	11	585012	4048110	4/06-9
422-24H	POR	11	585358	4045942	4/06-11
422-27F	POR	11	585334	4045766	4/06-10
423-2	HWSRT	11	570437	4057569	4/06-12

Samples					
Waypoint	Location	Zone	Easting	Northing	Sample Number
425-4	POR	11	588181	4049065	4/06-13
425-8	POR	11	588317	4048535	4/06-14
507-24	POR	11	583430	4046929	5/06-1
508-24	POR	11	585147	4047676	5/06-3
508-5B	POR	11	585691	4048041	5/06-2
509-15	POR	11	585244	4047562	5/06-4
509-22	POR	11	585270	4047076	5/06-5,6
512-17	POR	11	585244	4046834	5/06-10
512-4	POR	11	585525	4047472	5/06-7
512-9	POR	11	585379	4047225	5/06-8,9
513-2	POR	11	582148	4045632	5/06-11
514-15B	POR	11	580939	4045470	5/06-16,17
514-2	POR	11	579147	4045783	5/06-12
514-3	POR	11	579560	4045949	5/06-13
514-4	POR	11	579632	4046085	5/06-14
514-6	POR	11	579658	4045981	5/06-19
514-7	POR	11	579770	4045981	5/06-18
514-9	POR	11	580160	4045993	5/06-15
515-3	POR	11	587279	4045803	5/06-20,20A
516-16	POR	11	584257	4046550	5/06-21,21A
518-1	POR	11	587361	4044703	5/06-22
518-4	POR	11	587199	4044436	5/06-23
519-15	POR	11	588761	4047670	5/06-25
519-5	POR	11	588328	4048738	5/06-24
521-8	POR	11	580764	4044738	5/06-26
522-3	POR	11	579575	4044665	5/06-27,28
522-4	POR	11	579549	4044648	5/06-29
523-11	POR	11	588957	4044011	5/06-31
523-3	POR	11	588172	4043364	5/06-30,30A
524-4	POR	11	587409	4042739	5/06-32
524-8	POR	11	586974	4042640	5/06-33,34
525-4	POR	11	586138	4043579	5/06-35
525-5	POR	11	586124	4043576	5/06-36,37
527-1	POR	11	586623	4043441	5/06-38
527-10	POR	11	585500	4042488	5/06-41
527-18	POR	11	585639	4041599	5/06-42
527-21	POR	11	586216	4041372	5/06-43
527-5	POR	11	586117	4043035	5/06-39
527-7	POR	11	585927	4042969	5/06-40
529-11	POR	11	587983	4046983	5/06-44
530-32	POR	11	583523	4048601	5/06-45

Samples					
Waypoint	**Location**	**Zone**	**Easting**	**Northing**	**Sample Number**
530-7	POR	11	583990	4048028	4/06-47
531-1	POR	11	587291	4044988	5/06-48
601-22	HWSRT	11	568903	4054680	6/06-1
602-14	SRT	11	574408	4055408	6/06-2,3
606-20	POR	11	580492	4044728	6/06-5
606-5	CROC	11	576400	4047079	6/06-4
610-4	POR	11	579589	4044671	6/06-6

APPENDIX B

BEDDING DATA

Appendix B contains the Waypoint, Location, Zone, Easting, Northing, Bedding Strike, and Bedding Dip. The Waypoint is the unique name for each data collection point. The Location is an acronym allowing for quick sorting of the data by geographic location: (POR) Point of Rocks area, (CROC) Crystal Outcrops, (SMMSB) Southern Mount Schader Basin, (SM) Stirling Mine, (SRT) Specter Range Thrust , and (HWSRT) Hanging Wall of the Specter Range Thrust. Zone, Easting, and Northing are the GPS coordinates for each waypoint, projection UTM and Datum NAD 83. Bedding Strike and Bedding Dip were recorded using an azimuthal brunton compass. Planes were measured using the right hand rule and 2006 and 2007 average magnetic declination of 13.5°E.

Bedding						
Waypoint	**Location**	**Zone**	**Easting**	**Northing**	**Bedding Strike**	**Bedding Dip**
412-1	POR	11	580532	4046616	358	30
412-10	POR	11	581306	4047264	358	46
412-11	POR	11	581396	4047347	3	44
412-12	POR	11	581455	4047467	346	42
412-13	POR	11	581520	4047431	343	30
412-16	POR	11	581541	4047609	354	44
412-18	POR	11	581415	4047747	1	47
412-19	POR	11	581131	4048302	343	42

Bedding						
Waypoint	Location	Zone	Easting	Northing	Bedding Strike	Bedding Dip
412-2	POR	11	580596	4046732	350	42
412-20	POR	11	581106	4048348	352	46
412-21	POR	11	580891	4048438	333	40
412-22	POR	11	580973	4047749	359	50
412-24	POR	11	580956	4047456	4	25
412-25	POR	11	580927	4047458	8	24
412-26	POR	11	580836	4047359	355	17
412-27	POR	11	580511	4046973	8	32
412-3	POR	11	580717	4046722	338	38
412-4	POR	11	580745	4046820	348	30
412-5	POR	11	580968	4046859	359	60
412-7	POR	11	581057	4046953	352	55
412-9	POR	11	581319	4047125	358	52
413-11	POR	11	580469	4050004	254	21
413-2	POR	11	580113	4049414	152	24
413-3	POR	11	580221	4049531	220	13
413-6	POR	11	580197	4049597	310	25
413-7	POR	11	580212	4049729	242	16
413-9	POR	11	580292	4049812	273	25
414-11	POR	11	581673	4048590	340	55
414-14	POR	11	581822	4048923	176	45
414-15	POR	11	581850	4048933	236	30
414-17	POR	11	582006	4049053	270	20
414-18	POR	11	582094	4049096	343	26
414-19	POR	11	582242	4049160	294	34
414-2	POR	11	581975	4047332	341	64
414-20	POR	11	582286	4049182	8	21
414-22	POR	11	582545	4049185	312	29
414-24	POR	11	582697	4049041	318	5
414-25	POR	11	582721	4049143	348	16
414-28	POR	11	582806	4049105	27	19
414-3	POR	11	581906	4047419	337	63
414-31	POR	11	583313	4049210	346	21
414-5	POR	11	581786	4047860	292	38
414-8	POR	11	581873	4047994	328	59
415-1	POR	11	580393	4049238	178	10
415-10	POR	11	581165	4049161	349	46
415-11	POR	11	581201	4049186	338	46
415-13	POR	11	581363	4049498	222	29
415-2	POR	11	580526	4049326	274	20
415-3	POR	11	580727	4049157	319	13

Bedding						
Waypoint	Location	Zone	Easting	Northing	Bedding Strike	Bedding Dip
415-4	POR	11	580746	4049140	343	21
415-7	POR	11	580888	4049138	283	23
415-8	POR	11	580935	4049148	340	21
417-1	POR	11	581676	4047629	353	55
417-11	POR	11	582352	4049569	247	16
417-12	POR	11	582335	4049693	289	15
417-16A	POR	11	582562	4049755	264	29
417-19	POR	11	583118	4049895	278	22
417-2	POR	11	581691	4047682	304	34
417-20	POR	11	583388	4049748	42	23
417-5	POR	11	582047	4048708	352	16
417-6	POR	11	582278	4048970	352	26
417-8	POR	11	582200	4049329	263	25
418-1	HWSRT	11	569414	4054679	242	34
418-10	HWSRT	11	569101	4055076	233	36
418-15	HWSRT	11	569128	4055560	254	44
418-2	HWSRT	11	569380	4054826	252	19
418-3	HWSRT	11	569300	4054917	214	21
418-4	HWSRT	11	569290	4055037	234	38
418-6	HWSRT	11	569223	4055123	213	31
419-11	HWSRT	11	569659	4056379	237	11
419-12	HWSRT	11	569578	4056344	258	35
419-13	HWSRT	11	569546	4056389	242	57
419-15	HWSRT	11	569535	4056318	247	70
419-18	HWSRT	11	569465	4056402	227	40
419-19	HWSRT	11	569382	4056348	234	51
419-21	HWSRT	11	569393	4056198	231	51
419-3	HWSRT	11	570252	4057088	270	57
419-5	HWSRT	11	570095	4056959	265	43
419-7	HWSRT	11	570035	4056775	262	46
419-8	HWSRT	11	569949	4056691	275	37
420-1	HWSRT	11	569769	4055716	257	14
420-11	HWSRT	11	568859	4055714	258	32
420-16	HWSRT	11	568462	4055383	238	54
420-17	HWSRT	11	568426	4055238	257	41
420-18	HWSRT	11	568924	4054882	248	31
420-19	HWSRT	11	569184	4054812	245	28
420-4	HWSRT	11	569586	4055952	250	63
420-5	HWSRT	11	569546	4055978	249	50
420-6	HWSRT	11	569364	4055770	258	54
420-7	HWSRT	11	569053	4055670	240	39

Bedding						
Waypoint	Location	Zone	Easting	Northing	Bedding Strike	Bedding Dip
420-8	HWSRT	11	568957	4055640	254	49
420-9	HWSRT	11	568936	4055644	264	44
421-1	POR	11	582675	4047503	348	26
421-10	POR	11	583795	4047412	103	25
421-14	POR	11	584794	4048016	53	37
421-16	POR	11	584600	4048067	32	36
421-17	POR	11	584780	4048437	353	26
421-19	POR	11	584537	4048405	228	14
421-2	POR	11	582808	4047327	348	31
421-5	POR	11	583352	4047389	294	49
421-9	POR	11	583598	4047463	302	43
422-10	POR	11	585885	4047009	234	34
422-13	POR	11	585403	4046546	283	28
422-17	POR	11	585089	4046594	238	36
422-18	POR	11	585164	4046685	243	12
422-19	POR	11	584998	4046642	212	32
422-2	POR	11	587140	4047380	147	15
422-21	POR	11	584984	4046456	222	22
422-22	POR	11	585165	4046288	182	6
422-3	POR	11	586926	4047042	238	39
422-30	POR	11	585677	4046379	204	22
422-31	POR	11	585960	4046547	204	50
423-1	HWSRT	11	570426	4057453	253	23
423-2	HWSRT	11	570437	4057569	242	41
423-4	HWSRT	11	569428	4054322	242	36
423-5	HWSRT	11	569420	4054225	249	34
423-6	HWSRT	11	569384	4054073	211	24
423-7	HWSRT	11	569341	4053959	222	51
425-10	POR	11	580541	4048978	343	25
425-11	POR	11	580643	4049018	1	25
425-12	POR	11	583524	4048600	339	44
425-3	POR	11	588116	4048699	297	38
425-8	POR	11	588317	4048535	218	26
425-9	POR	11	580464	4049074	333	44
429-1	HWSRT	11	570293	4055560	210	51
429-2	HWSRT	11	570282	4055653	220	34
430-12	POR	11	582257	4047929	344	43
430-13	POR	11	582315	4048010	353	46
430-15	POR	11	582527	4048208	18	20
430-16	POR	11	582528	4048308	342	41
430-18	POR	11	582495	4048548	34	39

Bedding						
Waypoint	Location	Zone	Easting	Northing	Bedding Strike	Bedding Dip
430-2	POR	11	582083	4047417	183	87
430-3	POR	11	582068	4047444	332	80
430-4	POR	11	582052	4047531	169	76
430-6	POR	11	582014	4047626	337	70
430-7	POR	11	582016	4047671	322	49
430-8	POR	11	582102	4047650	343	68
430-9	POR	11	582152	4047741	303	30
502-1	POR	11	582211	4047437	343	84
502-10	POR	11	582474	4047991	11	56
502-13	POR	11	582620	4048443	10	26
502-14	POR	11	582684	4048486	9	41
502-16	POR	11	582812	4048465	349	56
502-17	POR	11	582757	4048620	47	41
502-18	POR	11	582753	4048669	34	29
502-2	POR	11	582233	4047547	358	86
502-20	POR	11	582714	4048754	343	15
502-21	POR	11	582784	4048799	17	11
502-22	POR	11	582756	4048893	18	13
502-23	POR	11	582719	4048984	152	1
502-24	POR	11	582892	4049016	24	20
502-25	POR	11	583059	4049040	42	12
502-26	POR	11	583116	4048855	54	36
502-3	POR	11	582209	4047679	351	63
502-4	POR	11	582237	4047668	357	63
502-6	POR	11	582366	4047681	351	43
502-7	POR	11	582397	4047764	7	59
502-8	POR	11	582437	4047830	2	56
504-10	POR	11	583391	4049169	7	28
504-11	POR	11	583370	4049189	248	31
504-12	POR	11	583424	4049243	13	40
504-14	POR	11	583541	4049338	7	38
504-15	POR	11	583683	4049474	24	43
504-16	POR	11	584185	4049910	4	26
504-17	POR	11	584267	4050137	134	8
504-18	POR	11	584326	4050185	314	5
504-19	POR	11	584577	4049874	44	26
504-20	POR	11	584352	4049746	52	4
504-22	POR	11	583759	4049339	24	51
504-23	POR	11	583494	4049132	34	56
504-25	POR	11	583415	4049064	47	34
504-5	POR	11	583161	4048839	28	76

Bedding						
Waypoint	Location	Zone	Easting	Northing	Bedding Strike	Bedding Dip
504-6	POR	11	583265	4049024	352	16
504-8	POR	11	583351	4049042	49	65
505-1	POR	11	582592	4047514	354	31
505-10	POR	11	582607	4046724	351	46
505-11	POR	11	582641	4046729	332	38
505-12	POR	11	582745	4046779	325	36
505-16	POR	11	582618	4046594	18	9
505-19	POR	11	582529	4046632	284	36
505-2	POR	11	582551	4047357	343	24
505-20	POR	11	582473	4046580	337	28
505-21	POR	11	582396	4046554	328	10
505-23	POR	11	582381	4046638	2	44
505-25	POR	11	582337	4046780	102	26
505-3	POR	11	582518	4047094	335	12
505-4	POR	11	582503	4046964	338	9
505-5	POR	11	582464	4046844	348	19
505-9	POR	11	582544	4046879	3	21
506-1	POR	11	582134	4047198	12	74
506-10	POR	11	582254	4046412	328	33
506-10A	POR	11	582317	4046328	154	16
506-11	POR	11	582390	4046380	27	18
506-12	POR	11	582427	4046410	24	34
506-13	POR	11	582417	4046344	344	49
506-15	POR	11	582435	4046290	263	16
506-16	POR	11	582517	4046305	87	14
506-17	POR	11	582587	4046303	33	16
506-19	POR	11	582409	4046055	304	8
506-2	POR	11	582178	4047085	359	39
506-21	POR	11	582186	4045904	314	14
506-23	POR	11	582062	4046037	11	43
506-25	POR	11	582124	4046089	355	21
506-27	POR	11	581688	4046162	344	43
506-27B	POR	11	581665	4046372	341	40
506-4	POR	11	582102	4046680	16	48
506-5	POR	11	582241	4046676	298	11
506-7	POR	11	582094	4046546	24	11
506-8	POR	11	582151	4046469	272	61
506-8A	POR	11	582158	4046421	324	21
506-9	POR	11	582201	4046411	7	22
507-10	POR	11	583125	4046822	200	6
507-14	POR	11	583264	4046650	355	39

Bedding						
Waypoint	Location	Zone	Easting	Northing	Bedding Strike	Bedding Dip
507-15	POR	11	583317	4046611	18	18
507-16	POR	11	583377	4046531	38	27
507-19	POR	11	583016	4046528	34	25
507-19A	POR	11	583137	4046620	24	11
507-20	POR	11	583280	4046782	342	13
507-26	POR	11	583298	4046997	248	9
507-3	POR	11	582855	4046778	311	30
507-4	POR	11	582803	4046634	28	25
507-5	POR	11	582769	4046568	358	18
507-6	POR	11	582789	4046546	14	6
507-6A	POR	11	582856	4046519	25	33
507-9	POR	11	582934	4046681	17	8
508-12	POR	11	585172	4047987	158	11
508-13	POR	11	585154	4047938	196	21
508-15	POR	11	585173	4047886	183	10
508-18	POR	11	585244	4047823	99	8
508-2	POR	11	585878	4048154	123	18
508-20	POR	11	585220	4047779	57	18
508-21	POR	11	585164	4047744	148	17
508-22	POR	11	585209	4047706	140	40
508-24	POR	11	585147	4047676	96	36
508-26	POR	11	585009	4047615	98	23
508-30	POR	11	585007	4047810	187	15
508-31	POR	11	585010	4047859	126	6
508-33	POR	11	584979	4047936	194	17
508-4	POR	11	585797	4048117	104	34
508-6	POR	11	585586	4048092	70	8
508-9	POR	11	585275	4048008	26	11
509-12	POR	11	585253	4047643	163	36
509-14	POR	11	585241	4047574	102	32
509-22	POR	11	585270	4047076	339	40
509-24	POR	11	585250	4046944	188	10
509-26	POR	11	585185	4046963	246	31
509-29	POR	11	585232	4046847	264	41
509-3	POR	11	585548	4048062	125	31
509-6	POR	11	585672	4047921	152	38
509-7	POR	11	585621	4047723	168	70
512-1	POR	11	585779	4047820	118	22
512-19	POR	11	585167	4046793	234	40
512-21	POR	11	585063	4047271	218	38
512-4	POR	11	585525	4047472	169	31

Bedding						
Waypoint	Location	Zone	Easting	Northing	Bedding Strike	Bedding Dip
512-5	POR	11	585468	4047430	194	41
512-7	POR	11	585424	4047235	216	11
513-1	POR	11	581987	4045540	34	34
513-10	POR	11	582642	4045911	348	24
513-13	POR	11	582723	4045834	44	15
S-425-11	POR	11	579752	4051608	341	29
S-425-12	POR	11	579694	4051582	334	28
S-425-2	POR	11	579214	4051404	314	28
S-425-3	POR	11	579341	4051593	305	35
S-425-4	POR	11	579402	4051843	314	41
S-425-7	POR	11	579736	4051998	342	22
S-426-10	POR	11	580910	4051726	210	68
S-426-16	POR	11	580635	4051028	269	72
S-426-17	POR	11	580576	4051096	294	73
S-426-19	POR	11	580437	4051090	274	34
S-426-20	POR	11	580398	4051068	319	24
S-426-22	POR	11	580279	4051006	329	10
S-426-24	POR	11	580225	4050981	267	25
S-426-25	POR	11	580134	4050980	14	39
S-426-26	POR	11	580092	4051072	269	30
S-426-27	POR	11	580073	4051105	273	34
S-426-3	POR	11	580025	4051542	179	60
S-426-4	POR	11	580031	4051560	324	35
S-427-1	SM	11	589926	4049233	358	33
S-427-2	SM	11	591056	4042775	339	82
S-427-3	SM	11	591063	4042706	284	55
S-427-4	SM	11	591014	4042768	324	45
S-427-5	SM	11	591004	4042750	295	40
S-427-6	SM	11	590854	4043028	233	58
S-428-1	POR	11	583345	4049037	57	66
S-428-11	POR	11	583362	4049191	8	23
S-428-12	POR	11	583362	4049206	14	26
S-428-13	POR	11	583347	4049236	19	29
S-428-14	POR	11	582967	4049294	282	23
S-428-15	POR	11	582744	4049397	245	27
S-428-16	POR	11	582718	4049428	247	23
S-428-17	POR	11	582807	4049589	243	21
S-428-18	POR	11	582794	4049689	253	34
S-428-19	POR	11	583064	4049875	298	23
S-428-2	POR	11	583360	4049077	37	54
S-428-20	POR	11	583054	4049946	259	38

Bedding						
Waypoint	Location	Zone	Easting	Northing	Bedding Strike	Bedding Dip
S-428-21	POR	11	582971	4049982	245	23
S-428-3	POR	11	583369	4049112	19	53
S-428-4	POR	11	583383	4049121	34	31
S-428-5	POR	11	583377	4049132	13	43
S-428-6	POR	11	583361	4049145	20	36
S-428-7	POR	11	583368	4049160	19	33
S-428-8	POR	11	583374	4049175	19	30
S-428-9	POR	11	583372	4049179	0	23
S-429-1	POR	11	583918	4048198	294	43
S-429-10	POR	11	584202	4048781	242	24
S-429-11	POR	11	584246	4048776	295	12
S-429-12	POR	11	584260	4048752	263	21
S-429-13	POR	11	584280	4048722	281	25
S-429-14	POR	11	584305	4048676	314	16
S-429-15	POR	11	584362	4048617	326	33
S-429-17	POR	11	584387	4048598	307	17
S-429-18	POR	11	584404	4048575	341	13
S-429-19	POR	11	584440	4048579	307	26
S-429-2	POR	11	583910	4048283	309	24
S-429-20	POR	11	584507	4048569	337	20
S-429-3	POR	11	583946	4048274	291	21
S-429-4	POR	11	583974	4048301	254	48
S-429-5	POR	11	583992	4048314	255	55
S-429-6	POR	11	584012	4048319	243	51
S-429-7	POR	11	584010	4048329	238	54
S-429-8	POR	11	584030	4048412	235	76
S-429-9	POR	11	584181	4048810	319	30
S-430-3	SM	11	590850	4043053	320	31
S-430-5	SM	11	590854	4043013	289	30
S-430-6	SM	11	590876	4042963	42	81
S-430-8	SM	11	590959	4042962	257	76
S-501-1	POR	11	579670	4050812	273	25
S-501-11	POR	11	579914	4050901	243	41
S-501-16	POR	11	579944	4050944	233	54
S-501-17	POR	11	579857	4051449	308	45
S-501-2	POR	11	579703	4050870	260	31
S-501-3	POR	11	579737	4050889	237	33
S-501-4	POR	11	579763	4050871	224	43
S-501-6	POR	11	579845	4050893	222	42
S-501-9	POR	11	579895	4050886	255	47
513-16	POR	11	582785	4045709	333	28

Bedding						
Waypoint	Location	Zone	Easting	Northing	Bedding Strike	Bedding Dip
513-19	POR	11	582669	4045570	323	30
513-2	POR	11	582148	4045632	301	41
513-20	POR	11	582425	4045830	333	37
513-21	POR	11	582137	4046367	16	20
513-23	POR	11	581982	4046422	342	11
513-24	POR	11	581962	4046582	22	10
513-3	POR	11	582267	4045620	304	15
513-4	POR	11	582387	4045653	336	27
513-5	POR	11	582511	4045767	342	36
514-14	POR	11	580971	4045276	288	47
514-3	POR	11	579560	4045949	312	8
514-4	POR	11	579632	4046085	118	4
514-6	POR	11	579658	4045981	223	35
514-7	POR	11	579770	4045981	271	10
514-8	POR	11	579820	4046012	332	14
515-1	POR	11	587292	4045532	192	12
515-10	POR	11	586575	4045537	284	12
515-11	POR	11	586339	4045567	214	45
515-13	POR	11	586193	4045527	214	20
515-16	POR	11	586056	4045269	307	6
515-17	POR	11	586197	4045225	228	25
515-18	POR	11	586297	4045219	249	18
515-19	POR	11	586423	4045187	194	14
515-21	POR	11	586565	4045114	214	46
515-22	POR	11	586661	4045066	263	9
515-23	POR	11	586784	4045035	105	12
515-4	POR	11	587154	4045842	256	15
515-5	POR	11	587073	4045789	272	14
515-8	POR	11	586701	4045450	267	19
515-9	POR	11	586653	4045473	302	17
516-10	POR	11	583418	4046672	3	10
516-17	POR	11	584206	4046334	78	10
516-19	POR	11	584129	4046260	98	22
516-22	POR	11	584135	4046013	263	3
516-23	POR	11	584180	4045974	179	21
516-24	POR	11	584254	4045913	224	18
516-26	POR	11	584323	4045815	327	17
516-28	POR	11	584339	4045595	292	32
516-30	POR	11	584139	4045524	298	20
516-4	POR	11	583394	4046857	352	30
516-6	POR	11	583326	4046814	357	26

Bedding						
Waypoint	Location	Zone	Easting	Northing	Bedding Strike	Bedding Dip
516-8	POR	11	583318	4046712	313	10
518-1	POR	11	587361	4044703	347	18
518-10	POR	11	586641	4043944	316	20
518-13	POR	11	585974	4043884	177	16
518-15	POR	11	585856	4044162	204	15
518-19	POR	11	586175	4044586	203	42
518-2	POR	11	587203	4044553	349	28
518-20	POR	11	586206	4044609	34	90
518-21	POR	11	586493	4044506	322	10
518-22	POR	11	586861	4044537	273	16
518-3	POR	11	587215	4044456	235	24
518-6	POR	11	586983	4043919	232	12
518-7	POR	11	586957	4043907	224	55
519-10	POR	11	588964	4048437	307	30
519-11	POR	11	588962	4048025	283	40
519-12	POR	11	588880	4047977	318	25
519-14	POR	11	588732	4048198	257	46
519-16	POR	11	588842	4047684	259	23
519-17	POR	11	588741	4047680	282	18
519-18	POR	11	588526	4047874	342	25
519-20	POR	11	588192	4048429	279	24
519-22	POR	11	586682	4046612	338	17
519-3	POR	11	588147	4048741	249	29
519-3A	POR	11	588187	4048777	278	36
519-6	POR	11	588338	4048790	290	69
519-7	POR	11	588362	4048821	268	43
519-8	POR	11	588795	4048974	312	55
521-10	POR	11	580893	4044638	288	30
521-11	POR	11	580996	4044658	333	80
521-12	POR	11	581307	4044599	278	40
521-13	POR	11	582614	4044451	333	27
521-14	POR	11	583038	4044313	13	23
521-15	POR	11	583402	4044140	342	45
521-16	POR	11	583543	4043777	328	35
521-17	POR	11	583743	4043225	341	39
521-5	POR	11	580421	4044988	209	85
521-8	POR	11	580764	4044738	242	22
521-9	POR	11	580773	4044665	228	51
523-11	POR	11	588957	4044011	204	81
523-16	POR	11	590108	4044141	264	61
523-17	POR	11	590077	4043943	330	28

Bedding						
Waypoint	Location	Zone	Easting	Northing	Bedding Strike	Bedding Dip
523-19	POR	11	589954	4044500	303	34
523-20	POR	11	589919	4044608	293	28
523-21	POR	11	589523	4044632	27	38
523-22	POR	11	589394	4044872	314	46
523-23	POR	11	588620	4044778	302	28
523-5	POR	11	588220	4043376	208	24
524-1	POR	11	587461	4042753	223	64
524-12	POR	11	586660	4043002	217	21
524-14	POR	11	586343	4043070	265	25
524-15	POR	11	586338	4042858	248	34
524-16	POR	11	586187	4042533	289	22
524-19	POR	11	586712	4042204	282	16
524-4	POR	11	587409	4042739	161	21
524-8	POR	11	586974	4042640	129	20
525-1	POR	11	586507	4043600	229	15
525-10	POR	11	585974	4043332	207	13
525-11	POR	11	585910	4043331	335	6
525-13	POR	11	585781	4043386	333	26
525-15	POR	11	585705	4043488	258	31
525-16	POR	11	585391	4043639	22	11
525-17	POR	11	585225	4043651	344	24
525-18	POR	11	585118	4043629	19	16
525-19	POR	11	584953	4043369	290	30
525-20	POR	11	584576	4043113	179	16
525-22	POR	11	583944	4042709	330	48
525-23	POR	11	584100	4042489	339	29
525-24	POR	11	584265	4042502	23	21
525-25	POR	11	584618	4042521	282	12
525-28	POR	11	585068	4042944	325	16
525-29	POR	11	585318	4042950	124	2
525-3	POR	11	586231	4043563	178	47
525-30	POR	11	585395	4042976	6	25
525-4	POR	11	586138	4043579	188	8
525-5	POR	11	586124	4043576	169	39
525-7	POR	11	585935	4043564	199	14
525-8	POR	11	585909	4043539	204	14
525-9	POR	11	586004	4043376	183	11
527-1	POR	11	586623	4043441	219	33
527-10	POR	11	585500	4042488	1	29
527-11	POR	11	585420	4042402	27	24
527-12	POR	11	585328	4042199	353	23

Bedding						
Waypoint	Location	Zone	Easting	Northing	Bedding Strike	Bedding Dip
527-13	POR	11	585324	4042110	332	49
527-14	POR	11	585367	4042010	322	46
527-17	POR	11	585689	4041676	329	36
527-18	POR	11	585639	4041599	335	36
527-19	POR	11	585860	4041336	352	24
527-2	POR	11	586525	4043353	202	27
527-20	POR	11	586071	4041315	303	26
527-21	POR	11	586216	4041372	230	4
527-22	POR	11	586140	4041830	118	17
527-24	POR	11	585718	4042351	256	4
527-3	POR	11	586260	4043228	328	29
527-4	POR	11	586214	4043103	219	26
527-5	POR	11	586117	4043035	207	27
527-6	POR	11	586054	4042972	308	36
527-7	POR	11	585927	4042969	85	7
527-9	POR	11	585533	4042551	73	6
528-12	POR	11	584659	4046572	142	55
528-14	POR	11	584867	4046355	217	25
528-15	POR	11	584906	4046110	74	20
528-16	POR	11	585101	4045781	348	8
528-19	POR	11	585274	4045331	73	6
528-2	POR	11	583591	4047466	307	46
528-21	POR	11	584928	4044782	12	12
528-22	POR	11	584821	4044615	319	20
528-23	POR	11	584351	4045124	237	26
528-3	POR	11	583965	4047339	124	3
528-4	POR	11	584043	4047007	42	9
528-6	POR	11	584366	4046976	58	24
528-9	POR	11	584367	4046852	74	20
529-1	POR	11	587997	4048309	313	31
529-15	POR	11	588077	4046469	155	32
529-17	POR	11	588253	4046254	187	34
529-18	POR	11	588599	4045658	245	51
529-19	POR	11	588342	4045086	233	33
529-2	POR	11	588030	4048195	252	36
529-21	POR	11	587592	4047503	252	30
529-4	POR	11	587898	4048076	97	18
529-5	POR	11	587973	4047939	227	30
529-7	POR	11	588178	4047743	281	11
529-8	POR	11	588130	4047550	264	13
529-9	POR	11	588000	4047319	206	35

Bedding						
Waypoint	Location	Zone	Easting	Northing	Bedding Strike	Bedding Dip
530-11	POR	11	583980	4048237	248	38
530-12	POR	11	583897	4048239	303	24
530-13	POR	11	583983	4048283	238	36
530-14	POR	11	584202	4048569	265	13
530-15	POR	11	584303	4048644	285	18
530-17	POR	11	584459	4048582	318	81
530-19	POR	11	584640	4048732	31	50
530-21	POR	11	584988	4048967	8	36
530-22	POR	11	585109	4048933	193	18
530-26	POR	11	585050	4048612	183	16
530-27	POR	11	585173	4048464	160	3
530-29	POR	11	585012	4048470	322	25
530-3	POR	11	583719	4047860	329	16
530-31	POR	11	584896	4048259	28	35
530-5	POR	11	583842	4047974	332	36
530-6	POR	11	583859	4047985	332	43
530-7	POR	11	583990	4048028	312	31
530-8	POR	11	584080	4048056	319	25
530-9	POR	11	584059	4048230	348	19
531-1	POR	11	587291	4044988	258	8
531-10	POR	11	586937	4042145	346	35
531-11	POR	11	586999	4042133	352	21
531-12	POR	11	586858	4042140	202	40
531-14	POR	11	586843	4041893	308	25
531-2	POR	11	587171	4045015	47	71
531-3	POR	11	587053	4044886	241	18
531-4	POR	11	587148	4044939	211	23
531-8	POR	11	587119	4042134	174	11
601-1	HWSRT	11	569306	4054148	241	35
601-10	HWSRT	11	568540	4054537	254	26
601-12	HWSRT	11	568651	4054625	253	28
601-13	HWSRT	11	568656	4054659	50	59
601-15	HWSRT	11	568690	4054704	78	22
601-16	HWSRT	11	568741	4054829	34	43
601-2	HWSRT	11	569159	4054331	232	66
601-20	HWSRT	11	568835	4054793	246	25
601-23	HWSRT	11	568700	4054999	317	10
601-24	HWSRT	11	568372	4055208	264	21
601-26	HWSRT	11	568299	4055370	221	46
601-27	HWSRT	11	568302	4055471	224	76
601-28	HWSRT	11	568345	4055545	60	61

Bedding						
Waypoint	Location	Zone	Easting	Northing	Bedding Strike	Bedding Dip
601-29	HWSRT	11	568815	4055000	288	18
601-3	HWSRT	11	568962	4054515	228	37
601-30	HWSRT	11	569243	4054478	229	45
601-4	HWSRT	11	568953	4054600	224	44
601-6	HWSRT	11	568911	4054666	254	36
601-9	HWSRT	11	568801	4054623	223	18
602-1	SRT	11	572900	4055137	240	12
602-14	SRT	11	574408	4055408	328	28
602-15	SRT	11	574417	4055457	54	26
602-17	SRT	11	574958	4055226	97	40
602-18	SRT	11	575021	4055421	96	23
602-2	SRT	11	573832	4055616	243	8
602-21	SRT	11	575087	4055546	296	32
602-23	SRT	11	575189	4055543	107	45
602-24	SRT	11	575317	4055435	124	37
602-25	SRT	11	575477	4055377	84	56
602-26	SRT	11	575776	4055458	78	44
602-29	SRT	11	576024	4055608	82	48
602-9	SRT	11	574212	4055640	124	14
603-10	POR	11	582274	4048580	358	16
603-11	POR	11	581652	4048710	353	46
603-12	POR	11	581720	4047792	334	38
603-15	POR	11	581828	4047475	317	46
603-3	POR	11	582456	4048649	33	45
603-4	POR	11	582522	4048713	30	34
603-5	POR	11	582429	4048830	18	15
603-7	POR	11	582347	4048704	49	11
604-10	SRT	11	573717	4054010	74	14
604-11	SRT	11	573898	4053836	73	10
604-16	SRT	11	574541	4053979	99	51
604-2	SRT	11	572824	4054323	144	21
604-5	SRT	11	573229	4054308	94	34
604-7	SRT	11	573423	4054227	101	36
604-8	SRT	11	573605	4054091	149	82
605-10	SRT	11	574157	4055101	144	9
605-11	SRT	11	574423	4055122	212	25
605-2	SRT	11	573603	4054400	68	23
605-3	SRT	11	573655	4054402	203	1
605-4	SRT	11	573659	4054447	69	14
605-5	SRT	11	573729	4054515	144	9
605-7	SRT	11	573908	4054603	128	4

Bedding						
Waypoint	Location	Zone	Easting	Northing	Bedding Strike	Bedding Dip
605-8	SRT	11	574017	4054759	219	26
605-9	SRT	11	574101	4054985	248	4
606-11	CROC	11	576570	4046584	328	28
606-13	CROC	11	576725	4046551	284	26
606-14	POR	11	579543	4044648	18	24
606-21	POR	11	580775	4044877	292	65
606-22	POR	11	580719	4044891	92	54
606-4	CROC	11	576373	4047154	358	18
606-6	CROC	11	576478	4047088	343	16
607-1	POR	11	585563	4047546	184	41
607-11	POR	11	585398	4047343	183	11
607-12	POR	11	585708	4047699	169	75
607-5	POR	11	585564	4047281	178	37
607-7	POR	11	585539	4047238	38	36
607-9	POR	11	585144	4047418	183	48
608-1	POR	11	581624	4047500	358	33
608-3	POR	11	582370	4047701	11	52
608-4	POR	11	582397	4047768	14	63
608-5	POR	11	582395	4047840	23	45
610-10	POR	11	580731	4044316	204	42
610-11	POR	11	581131	4043902	173	29
610-12	POR	11	581280	4043903	187	20
610-13	POR	11	581399	4043893	162	41
610-14	POR	11	581622	4043806	327	36
610-15	POR	11	582037	4043616	350	36
610-16	POR	11	582274	4043255	350	38
610-17	POR	11	582201	4043130	338	44
610-18	POR	11	581988	4043032	173	40
610-19	POR	11	581923	4043008	312	17
610-20	POR	11	581799	4043261	198	30
610-21	POR	11	581778	4043265	228	30
610-23	POR	11	581699	4043271	340	82
610-24	POR	11	581679	4043282	350	75
610-25	POR	11	581621	4043311	355	68
610-26	POR	11	581223	4043279	198	32
610-27	POR	11	581155	4043267	173	40
610-28	POR	11	580808	4043271	192	23
610-8	POR	11	580668	4044406	212	36
610-9	POR	11	580632	4044361	183	48
1214-1	CROC	11	576184	4038676	264	44
1214-11	CROC	11	576430	4038021	341	32

Bedding						
Waypoint	Location	Zone	Easting	Northing	Bedding Strike	Bedding Dip
1214-12	CROC	11	576334	4038092	339	56
1214-2	CROC	11	576329	4038333	340	51
1214-5	CROC	11	576448	4038202	2	29
1214-8	CROC	11	576517	4038093	334	40
1214-9	CROC	11	576521	4038058	3	32
1215-1	SMMSB	11	573460	4028165	359	0
1215-2	SMMSB	11	573132	4028025	44	26
1215-3	SMMSB	11	573093	4028034	350	23
1215-5	SMMSB	11	573033	4027781	13	20
1215-6	SMMSB	11	572859	4027715	344	21
1215-7	SMMSB	11	572664	4027598	10	16
1215-8	SMMSB	11	572474	4027687	299	25
1216-1	POR	11	585717	4042459	8	26
1216-10	POR	11	585696	4042135	9	52
1216-12	POR	11	585755	4042032	334	29
1216-14	POR	11	585757	4041981	329	26
1216-15	POR	11	585727	4041934	273	20
1216-16	POR	11	585701	4041910	323	46
1216-17	POR	11	585693	4041836	332	49
1216-18	POR	11	585785	4041798	344	25
1216-19	POR	11	585816	4041729	314	30
1216-2	POR	11	585690	4042451	14	6
1216-20	POR	11	585844	4041492	329	40
1216-21	POR	11	585790	4041494	332	51
1216-22	POR	11	585758	4041512	333	27
1216-23	POR	11	585639	4041594	344	33
1216-24	POR	11	585590	4041660	340	44
1216-25	POR	11	585558	4041785	335	66
1216-26	POR	11	585543	4041840	340	39
1216-27	POR	11	585563	4041915	314	24
1216-28	POR	11	585511	4042022	337	51
1216-3	POR	11	585668	4042440	104	16
1216-4	POR	11	585649	4042440	130	29
1216-6	POR	11	585602	4042346	155	14
1216-7	POR	11	585622	4042312	90	24
1216-9	POR	11	585667	4042174	98	11
1217-2	POR	11	570823	4048828	243	39
1217-4	POR	11	570807	4048781	208	43
1217-6	POR	11	570942	4048210	226	40
1218-10	SM	11	595379	4039425	235	19
1218-11	SM	11	595239	4039454	264	28

Bedding						
Waypoint	Location	Zone	Easting	Northing	Bedding Strike	Bedding Dip
1218-3	SM	11	594935	4037507	284	21
1218-8	SM	11	595185	4038339	225	30
1218-9	SM	11	595670	4039101	308	44
1220-1	POR	11	583713	4046065	194	65
1220-2	POR	11	583971	4045898	269	7
1220-5	POR	11	583747	4045294	305	23
1220-6	POR	11	583727	4044979	342	52
1221-11	SM	11	594895	4039834	274	24
1221-12	SM	11	594910	4039917	299	34
1221-13	SM	11	595040	4040178	274	30
1221-14	SM	11	595022	4040192	229	32
1221-15	SM	11	595057	4040230	314	35
1221-18	SM	11	595120	4040213	236	49
1221-3	SM	11	594670	4039609	294	30
1221-6	SM	11	594575	4039634	269	17
1222-1	SM	11	594174	4039258	254	22
1222-10	SM	11	593662	4039492	164	23
1222-11	SM	11	593617	4039180	269	11
1222-12	SM	11	593759	4039012	275	23
1222-13	SM	11	593649	4038718	282	33
1222-3	SM	11	594140	4039405	209	25
1222-4	SM	11	594052	4039490	225	25
1222-5	SM	11	593960	4039571	254	16
1222-6	SM	11	593994	4039634	278	30
1222-8	SM	11	593824	4039679	199	46
1222-9	SM	11	593731	4039596	280	22
S-424-1	POR	11	581680	4047533	327	42
S-424-10	POR	11	581920	4049380	255	47
S-424-11	POR	11	581936	4049413	243	62
S-424-12	POR	11	581995	4049473	274	44
S-424-13	POR	11	581965	4049551	244	72
S-424-16	POR	11	581738	4049945	231	17
S-424-2	POR	11	581679	4047584	339	52
S-424-20	POR	11	582066	4050025	235	45
S-424-22	POR	11	582173	4050622	349	23
S-424-24	POR	11	582236	4050196	209	65
S-424-25	POR	11	582249	4050024	241	33
S-424-28	POR	11	582336	4049687	294	15
S-424-29	POR	11	582285	4049713	289	66
S-424-3	POR	11	581673	4047602	7	48
S-424-30	POR	11	582194	4049640	264	34

Bedding						
Waypoint	Location	Zone	Easting	Northing	Bedding Strike	Bedding Dip
S-424-31	POR	11	582182	4049666	249	35
S-424-32	POR	11	582174	4049717	74	79
S-424-34	POR	11	582034	4049762	269	53
S-424-4	POR	11	581683	4047596	356	53
S-424-6	POR	11	581680	4047665	321	31
S-424-7	POR	11	581618	4048769	7	51
S-424-8	POR	11	581873	4049308	259	36
S-424-9	POR	11	581910	4049361	257	43
S-425-10	POR	11	579779	4051642	342	47

APPENDIX C

FRACTURE DATA

Appendix C contains the Waypoint, Location, Zone, Easting, Northing, Fracture Strike, and Fracture Dip. The Waypoint is the unique name for each data collection point. The Location is an acronym allowing for quick sorting of the data by geographic location: (POR) Point of Rocks area, (CROC) Crystal Outcrops, (SMMSB) Southern Mount Schader Basin, (SM) Stirling Mine, (SRT) Specter Range Thrust , and (HWSRT) Hanging Wall of the Specter Range Thrust. Zone, Easting, and Northing are the GPS coordinates for each waypoint, projection UTM and Datum NAD 83. Facture Strike and Fracture Dip were recorded using an azimuthal brunton compass. Planes were measured using the right hand rule and 2006 and 2007 average magnetic declination of 13.5°E.

C.1 PRIMARY FRACTURE

Primary Fracture						
Waypoint	Location	Zone	Easting	Northing	Fracture Strike	Fracture Dip
412-1	POR	11	580532	4046616	218	63

Primary Fracture						
Waypoint	Location	Zone	Easting	Northing	Fracture Strike	Fracture Dip
412-10	POR	11	581306	4047264	252	73
412-12	POR	11	581455	4047467	238	80
412-16	POR	11	581541	4047609	77	85
412-18	POR	11	581415	4047747	106	76
412-19	POR	11	581131	4048302	243	76
412-2	POR	11	580596	4046732	211	45
412-21	POR	11	580891	4048438	90	77
412-22	POR	11	580973	4047749	103	77
412-26	POR	11	580836	4047359	172	84
412-5	POR	11	580968	4046859	274	73
413-6	POR	11	580197	4049597	52	81
414-17	POR	11	582006	4049053	201	87
414-5	POR	11	581786	4047860	18	74
415-1	POR	11	580393	4049238	318	86
417-7	POR	11	582357	4049145	332	75
418-1	HWSRT	11	569414	4054679	319	81
418-13	HWSRT	11	568930	4055430	250	78
418-2	HWSRT	11	569380	4054826	84	84
418-6	HWSRT	11	569223	4055123	309	63
419-7	HWSRT	11	570035	4056775	109	44
420-1	HWSRT	11	569769	4055716	142	78
425-10	POR	11	580541	4048978	207	60
429-1	HWSRT	11	570293	4055560	102	90
429-2	HWSRT	11	570282	4055653	324	73
430-1	POR	11	582118	4047355	98	76
430-13	POR	11	582315	4048010	119	75
430-15	POR	11	582527	4048208	193	75
430-16	POR	11	582528	4048308	92	67
430-2	POR	11	582083	4047417	271	90
430-4	POR	11	582052	4047531	262	86
430-6	POR	11	582014	4047626	248	69
430-7	POR	11	582016	4047671	203	56
502-10	POR	11	582474	4047991	102	63
502-13	POR	11	582620	4048443	154	51
502-16	POR	11	582812	4048465	252	60
502-17	POR	11	582757	4048620	258	60
502-2	POR	11	582233	4047547	242	81
502-21	POR	11	582784	4048799	231	72
502-23	POR	11	582719	4048984	244	77
502-24	POR	11	582892	4049016	284	88
502-26	POR	11	583116	4048855	262	64

Primary Fracture						
Waypoint	Location	Zone	Easting	Northing	Fracture Strike	Fracture Dip
502-3	POR	11	582209	4047679	243	37
502-4	POR	11	582237	4047668	102	85
502-6	POR	11	582366	4047681	204	54
502-7	POR	11	582397	4047764	258	51
504-12	POR	11	583424	4049243	272	75
504-14	POR	11	583541	4049338	308	81
504-15	POR	11	583683	4049474	302	88
504-16	POR	11	584185	4049910	117	73
504-17	POR	11	584267	4050137	289	83
504-19	POR	11	584577	4049874	244	66
504-20	POR	11	584352	4049746	239	59
504-22	POR	11	583759	4049339	127	88
504-25	POR	11	583415	4049064	201	30
504-5	POR	11	583161	4048839	282	84
504-8	POR	11	583351	4049042	308	66
505-1	POR	11	582592	4047514	122	68
505-11	POR	11	582641	4046729	112	64
505-12	POR	11	582745	4046779	52	83
505-15	POR	11	582646	4046615	112	85
505-2	POR	11	582551	4047357	137	65
505-20	POR	11	582473	4046580	144	79
505-21	POR	11	582396	4046554	172	77
505-23	POR	11	582381	4046638	291	86
505-25	POR	11	582337	4046780	62	84
505-4	POR	11	582503	4046964	301	90
505-5	POR	11	582464	4046844	97	83
505-9	POR	11	582544	4046879	72	84
506-10	POR	11	582254	4046412	344	85
506-10A	POR	11	582317	4046328	281	80
506-12	POR	11	582427	4046410	180	56
506-13	POR	11	582417	4046344	117	54
506-15	POR	11	582435	4046290	47	64
506-16	POR	11	582517	4046305	116	80
506-17	POR	11	582587	4046303	299	84
506-19	POR	11	582409	4046055	179	86
506-2	POR	11	582178	4047085	104	58
506-21	POR	11	582186	4045904	122	78
506-23	POR	11	582062	4046037	281	63
506-25	POR	11	582124	4046089	81	84
506-27	POR	11	581688	4046162	94	82
506-27B	POR	11	581665	4046372	235	46

Primary Fracture						
Waypoint	Location	Zone	Easting	Northing	Fracture Strike	Fracture Dip
506-4	POR	11	582102	4046680	136	68
506-5	POR	11	582241	4046676	224	81
506-7	POR	11	582094	4046546	3	56
506-8	POR	11	582151	4046469	29	41
506-9	POR	11	582201	4046411	164	71
507-10	POR	11	583125	4046822	112	84
507-16	POR	11	583377	4046531	268	74
507-19	POR	11	583016	4046528	119	81
507-19A	POR	11	583137	4046620	232	64
507-20	POR	11	583280	4046782	2	84
507-26	POR	11	583298	4046997	360	65
507-3	POR	11	582855	4046778	149	72
507-4	POR	11	582803	4046634	212	74
507-5	POR	11	582769	4046568	63	66
507-6A	POR	11	582856	4046519	297	88
508-12	POR	11	585172	4047987	64	79
508-15	POR	11	585173	4047886	352	68
508-18	POR	11	585244	4047823	308	84
508-2	POR	11	585878	4048154	287	74
508-24	POR	11	585147	4047676	239	65
508-26	POR	11	585009	4047615	314	61
508-30	POR	11	585007	4047810	338	68
508-9	POR	11	585275	4048008	232	88
509-12	POR	11	585253	4047643	259	83
509-14	POR	11	585241	4047574	229	84
509-3	POR	11	585548	4048062	64	75
509-6	POR	11	585672	4047921	77	79
509-7	POR	11	585621	4047723	143	86
512-1	POR	11	585779	4047820	237	77
512-21	POR	11	585063	4047271	342	71
512-4	POR	11	585525	4047472	67	78
512-7	POR	11	585424	4047235	87	73
513-1	POR	11	581987	4045540	217	55
513-13	POR	11	582723	4045834	241	55
513-16	POR	11	582785	4045709	108	82
513-19	POR	11	582669	4045570	234	86
513-20	POR	11	582425	4045830	242	66
513-23	POR	11	581982	4046422	228	72
513-3	POR	11	582267	4045620	37	76
513-4	POR	11	582387	4045653	214	76
513-5	POR	11	582511	4045767	238	85

Primary Fracture						
Waypoint	Location	Zone	Easting	Northing	Fracture Strike	Fracture Dip
514-15B	POR	11	580939	4045470	222	83
515-1	POR	11	587292	4045532	297	86
515-10	POR	11	586575	4045537	352	84
515-11	POR	11	586339	4045567	130	88
515-13	POR	11	586193	4045527	307	83
515-16	POR	11	586056	4045269	283	82
515-17	POR	11	586197	4045225	295	83
515-18	POR	11	586297	4045219	109	70
515-19	POR	11	586423	4045187	23	81
515-22	POR	11	586661	4045066	198	76
515-23	POR	11	586784	4045035	23	70
515-5	POR	11	587073	4045789	18	70
515-8	POR	11	586701	4045450	92	74
516-10	POR	11	583418	4046672	208	80
516-12	POR	11	583902	4046513	250	86
516-16	POR	11	584257	4046550	276	76
516-19	POR	11	584129	4046260	244	86
516-22	POR	11	584135	4046013	10	56
516-23	POR	11	584180	4045974	18	76
516-24	POR	11	584254	4045913	10	72
516-26	POR	11	584323	4045815	62	79
516-29	POR	11	584290	4045473	18	84
516-3	POR	11	583596	4046928	108	78
516-30	POR	11	584139	4045524	14	72
516-4	POR	11	583394	4046857	159	86
516-6	POR	11	583326	4046814	217	79
516-8	POR	11	583318	4046712	203	73
518-1	POR	11	587361	4044703	348	85
518-13	POR	11	585974	4043884	114	81
518-19	POR	11	586175	4044586	291	83
518-2	POR	11	587203	4044553	63	80
518-21	POR	11	586493	4044506	319	64
518-22	POR	11	586861	4044537	84	84
518-7	POR	11	586957	4043907	112	63
519-10	POR	11	588964	4048437	40	76
519-11	POR	11	588962	4048025	66	63
519-12	POR	11	588880	4047977	144	69
519-16	POR	11	588842	4047684	142	75
519-17	POR	11	588741	4047680	24	66
519-20	POR	11	588192	4048429	126	85
519-22	POR	11	586682	4046612	303	88

Primary Fracture						
Waypoint	Location	Zone	Easting	Northing	Fracture Strike	Fracture Dip
519-3	POR	11	588147	4048741	113	84
519-6	POR	11	588338	4048790	212	82
519-8	POR	11	588795	4048974	222	87
521-10	POR	11	580893	4044638	96	61
521-12	POR	11	581307	4044599	188	88
521-13	POR	11	582614	4044451	239	68
521-14	POR	11	583038	4044313	214	70
521-15	POR	11	583402	4044140	64	84
521-16	POR	11	583543	4043777	107	65
521-17	POR	11	583743	4043225	104	79
521-8	POR	11	580764	4044738	90	70
521-9	POR	11	580773	4044665	109	88
523-11	POR	11	588957	4044011	219	78
523-17	POR	11	590077	4043943	97	74
523-19	POR	11	589954	4044500	166	36
523-20	POR	11	589919	4044608	107	76
523-21	POR	11	589523	4044632	336	80
523-22	POR	11	589394	4044872	174	82
523-23	POR	11	588620	4044778	173	81
523-5	POR	11	588220	4043376	113	67
524-1	POR	11	587461	4042753	321	90
524-12	POR	11	586660	4043002	40	75
524-14	POR	11	586343	4043070	96	59
524-16	POR	11	586187	4042533	37	84
524-19	POR	11	586712	4042204	186	88
524-4	POR	11	587409	4042739	310	89
525-1	POR	11	586507	4043600	17	69
525-10	POR	11	585974	4043332	360	76
525-11	POR	11	585910	4043331	352	58
525-15	POR	11	585705	4043488	85	68
525-16	POR	11	585391	4043639	294	81
525-19	POR	11	584953	4043369	114	49
525-20	POR	11	584576	4043113	270	76
525-22	POR	11	583944	4042709	147	61
525-23	POR	11	584100	4042489	90	74
525-28	POR	11	585068	4042944	214	66
525-3	POR	11	586231	4043563	282	75
525-5	POR	11	586124	4043576	307	73
525-7	POR	11	585935	4043564	72	86
525-9	POR	11	586004	4043376	338	71
527-1	POR	11	586623	4043441	56	83

Primary Fracture						
Waypoint	Location	Zone	Easting	Northing	Fracture Strike	Fracture Dip
527-10	POR	11	585500	4042488	278	72
527-12	POR	11	585328	4042199	170	80
527-14	POR	11	585367	4042010	50	76
527-17	POR	11	585689	4041676	273	81
527-18	POR	11	585639	4041599	262	90
527-20	POR	11	586071	4041315	67	62
527-22	POR	11	586140	4041830	262	61
527-4	POR	11	586214	4043103	339	75
527-7	POR	11	585927	4042969	8	82
527-9	POR	11	585533	4042551	9	69
528-14	POR	11	584867	4046355	77	81
528-16	POR	11	585101	4045781	318	73
528-2	POR	11	583591	4047466	193	79
528-21	POR	11	584928	4044782	265	77
528-23	POR	11	584351	4045124	334	80
528-4	POR	11	584043	4047007	309	88
528-6	POR	11	584366	4046976	336	78
528-9	POR	11	584367	4046852	320	88
529-1	POR	11	587997	4048309	23	75
529-15	POR	11	588077	4046469	212	86
529-17	POR	11	588253	4046254	257	86
529-18	POR	11	588599	4045658	142	81
529-19	POR	11	588342	4045086	153	75
529-2	POR	11	588030	4048195	70	53
529-21	POR	11	587592	4047503	149	64
529-4	POR	11	587898	4048076	16	56
529-7	POR	11	588178	4047743	13	76
529-8	POR	11	588130	4047550	174	89
529-9	POR	11	588000	4047319	318	53
530-12	POR	11	583897	4048239	188	81
530-14	POR	11	584202	4048569	4	71
530-17	POR	11	584459	4048582	243	86
530-19	POR	11	584640	4048732	292	76
530-21	POR	11	584988	4048967	101	84
530-22	POR	11	585109	4048933	327	79
530-26	POR	11	585050	4048612	316	78
530-27	POR	11	585173	4048464	66	67
530-3	POR	11	583719	4047860	68	80
530-31	POR	11	584896	4048259	131	68
530-7	POR	11	583990	4048028	36	76
530-8	POR	11	584080	4048056	231	77

Primary Fracture						
Waypoint	**Location**	**Zone**	**Easting**	**Northing**	**Fracture Strike**	**Fracture Dip**
531-11	POR	11	586999	4042133	199	69
531-12	POR	11	586858	4042140	318	83
531-2	POR	11	587171	4045015	114	76
531-3	POR	11	587053	4044886	340	57
531-8	POR	11	587119	4042134	302	78
601-1	HWSRT	11	569306	4054148	332	79
601-12	HWSRT	11	568651	4054625	352	70
601-15	HWSRT	11	568690	4054704	254	76
601-20	HWSRT	11	568835	4054793	98	55
601-23	HWSRT	11	568700	4054999	43	81
601-26	HWSRT	11	568299	4055370	333	65
601-3	HWSRT	11	568962	4054515	345	86
601-30	HWSRT	11	569243	4054478	158	86
601-6	HWSRT	11	568911	4054666	118	56
602-1	SRT	11	572900	4055137	352	81
602-15	SRT	11	574417	4055457	320	83
602-17	SRT	11	574958	4055226	233	63
602-18	SRT	11	575021	4055421	354	73
602-2	SRT	11	573832	4055616	57	85
602-24	SRT	11	575317	4055435	45	76
602-26	SRT	11	575776	4055458	339	55
602-29	SRT	11	576024	4055608	30	58
602-9	SRT	11	574212	4055640	319	90
603-10	POR	11	582274	4048580	103	88
603-11	POR	11	581652	4048710	64	90
603-15	POR	11	581828	4047475	43	86
603-3	POR	11	582456	4048649	223	73
603-5	POR	11	582429	4048830	144	77
603-7	POR	11	582347	4048704	24	86
604-10	SRT	11	573717	4054010	183	71
604-11	SRT	11	573898	4053836	28	80
604-16	SRT	11	574541	4053979	283	82
604-2	SRT	11	572824	4054323	62	89
604-5	SRT	11	573229	4054308	212	73
605-10	SRT	11	574157	4055101	23	77
605-2	SRT	11	573603	4054400	239	75
605-5	SRT	11	573729	4054515	57	74
605-8	SRT	11	574017	4054759	164	75
606-13	CROC	11	576725	4046551	160	78
606-6	CROC	11	576478	4047088	198	69
610-11	POR	11	581131	4043902	353	73

Primary Fracture						
Waypoint	Location	Zone	Easting	Northing	Fracture Strike	Fracture Dip
610-16	POR	11	582274	4043255	251	85
1214-1	CROC	11	576184	4038676	96	66
1214-2	CROC	11	576329	4038333	173	54
1214-5	CROC	11	576448	4038202	75	80
1215-1	SMMSB	11	573460	4028165	58	74
1217-2	POR	11	570823	4048828	120	54
1218-4	SM	11	595051	4037767	252	60

C.2 SECONDARY FRACTURE

Secondary Fracture						
Waypoint	Location	Zone	Easting	Northing	Fracture Strike	Fracture Dip
412-1	POR	11	580532	4046616	358	32
412-19	POR	11	581131	4048302	194	65
412-21	POR	11	580891	4048438	229	73
412-22	POR	11	580973	4047749	228	46
412-5	POR	11	580968	4046859	212	34
414-17	POR	11	582006	4049053	144	76
418-13	HWSRT	11	568930	4055430	169	90
430-13	POR	11	582315	4048010	219	62
430-15	POR	11	582527	4048208	124	76
502-10	POR	11	582474	4047991	242	62
502-13	POR	11	582620	4048443	204	57
502-24	POR	11	582892	4049016	204	58
504-12	POR	11	583424	4049243	132	82
504-19	POR	11	584577	4049874	304	79
504-20	POR	11	584352	4049746	292	75
505-2	POR	11	582551	4047357	73	88
506-12	POR	11	582427	4046410	238	76
506-19	POR	11	582409	4046055	259	85
506-25	POR	11	582124	4046089	115	74
506-27	POR	11	581688	4046162	214	79
506-27B	POR	11	581665	4046372	89	76
506-7	POR	11	582094	4046546	124	83
507-19	POR	11	583016	4046528	218	75

Secondary Fracture						
Waypoint	Location	Zone	Easting	Northing	Fracture Strike	Fracture Dip
507-4	POR	11	582803	4046634	284	86
508-15	POR	11	585173	4047886	78	85
508-18	POR	11	585244	4047823	214	84
508-24	POR	11	585147	4047676	3	83
513-1	POR	11	581987	4045540	311	72
513-23	POR	11	581982	4046422	182	73
513-5	POR	11	582511	4045767	125	70
514-15B	POR	11	580939	4045470	116	66
515-1	POR	11	587292	4045532	5	73
515-18	POR	11	586297	4045219	166	83
515-22	POR	11	586661	4045066	56	77
516-24	POR	11	584254	4045913	110	79
523-11	POR	11	588957	4044011	220	44
525-10	POR	11	585974	4043332	283	84
525-11	POR	11	585910	4043331	279	70
525-5	POR	11	586124	4043576	21	40
529-9	POR	11	588000	4047319	53	52
530-26	POR	11	585050	4048612	48	68
604-11	SRT	11	573898	4053836	284	80
1218-4	SM	11	595051	4037767	28	75

BIBLIOGRAPHY

Abolins, M.J., 1999, I. Stratigraphic constraints on the number of discrete Neoproterozoic glaciations and the relationship between glaciation and Ediacaran evolution; II. The Kwichup Spring Thrust in the northwestern Spring Mountains, Nevada: implications for large-magnitude extension and the structure of the Cordilleran thrust belt: Ph.D. dissertation, California Institute of Technology, Pasadena, California, 347 p.

Albers, J.P., 1967, Belt of sigmoidal bending and right-lateral faulting in the western Great Basin: Geological Society of America Bulletin, v. 78, no. 2, p. 143-156.

Anderson, R.E., 1971, Thin skin distension in Tertiary rocks of southeastern Nevada: Geological Society of America Bulletin, v. 82, no. 1, p. 43-58.

Anderson, R.E., 1973, Large-magnitude late Tertiary strike-slip faulting, north of Lake Mead, Nevada: U. S. Geological Survey Professional Paper, 794, 23 p.

Anderson, R.E., Ekren, E.B., and Wright, L., 1977, Late Cenozoic fault patterns and stress fields in the Great Basin and westward displacement of the Sierra Nevada block: Comment and Reply, Geology (Boulder), v. 5, p. 388-392.

Armstrong, R.L., 1968, Sevier orogenic belt in Nevada and Utah: Geological Society of America Bulletin, v. 79, no. 4, p. 429-458.

Atwater, T., 1970, Implications of plate tectonic for the Cenozoic tectonic evolution of western North America: Geological Society of America Bulletin, v. 81, p. 3513-3536.

Axen, G.J., 2007, Research focus; significance of large-displacement, low-angle normal faults: Geology (Boulder), v. 35, no. 3, p. 287-288.

Barnes, H., Ekren, E.B., Rodgers, C.L., and Hedlund, D.C., 1982, Geologic and tectonic maps of the Mercury quadrangle, Nye and Clark counties, Nevada: U.S. Geological Survey Miscellaneous Investigations Series Map I-1197, scale 1:24,000.

Blakely, R.J., Langenheim, V.E., Ponce, D.A., and Dixon, G.L., 2000, New aeromagnetic survey of the Amargosa Desert: a tool for understanding near surface geology and hydrology figures and captions: U.S. Geological Survey unpublished Administrative Report to Nye and Clark Counties, Nevada, Inyo County, California, 3 p.

Bohannon, R.G., 1979, Strike-slip faults of the Lake Mead region of southern Nevada: Cenozoic paleogeography of the western United States, no. 3, p. 129-139.

Bohannon, R.G., 1984, Nonmarine sedimentary rocks of Tertiary age in the Lake Mead region, southeastern Nevada and northwestern Arizona: U.S. Geological Survey Professional Paper 1259, 72 p.

Bohannon, R.G., and Parsons, T., 1995, Tectonic implications of post-30 Ma Pacific and North American relative plate motions: Geological Society of America Bulletin, v. 107, no. 8, p. 937-959.

Brocher, T.M., Carr, M.D., Fox, K.F., and Hart, P.E., 1993, Seismic reflection profiling across Tertiary extensional structures in the eastern Amargosa Desert, southern Nevada Basin and Range province: Geological Society of America Bulletin, v. 105, p. 30-46.

Burchfiel, B.C., 1964, Precambrian and Paleozoic stratigraphy of the Specter Range Quadrangle, Nye County, Nevada: Bulletin of the American Association of Petroleum Geologists, v. 48, p. 40-56.

Burchfiel, B.C., 1965, Structural Geology of the Specter Range Quadrangle, Nevada, and its Regional Significance: Geological Society of America Bulletin, v. 76, p. 175-192.

Burchfiel, B.C., Fleck, R.J., Secor, D.T., Vincelette, R.R., and Davis, G.A., 1974, Geology of the Spring Mountains, Nevada: Geological Society of America Bulletin, v. 85, p. 1013-1023.

Campagna, D. J. and Aydin, A., 1994, Basin genesis associated with strike-slip faulting in the Basin and Range, southeastern Nevada: Tectonics, no. 2, p. 327-341.

Carr, W.J., 1974, Summary of tectonic and structural evidence for stress orientation at the Nevada Test Site: U.S. Geological Survey Open File Report 74-176, 53 p.

Carr, W.J., 1984, Regional structural setting of Yucca Mountain, southwestern Nevada, and late Cenozoic rates of tectonic activity in part of the southwestern Great Basin, Nevada and California: U. S. Geological Survey, Open-File Report 84-0854, 114 p.

Carr, M.D., Sawyer, D.A., Nimz, K., Maldonado, F., and Swadley, W.C., 1996, Digital bedrock geologic map database of the Beatty 30 X 60-minute quadrangle, Nevada and California: U.S. Geological Survey Open-File Report 96-261, scale 1:100,000, 41 p.

Cladouhos, T.T., 1999, A kinematic model for deformation within brittle shear zones: Journal of Structural Geology, v. 21, no. 4, p. 437-448.

Cole, J.C., and Cashman, P.H., 1999, Structural relationships of pre-Tertiary rocks in the Nevada Test Site Region, southern Nevada: U.S. Geological Survey Professional Paper 1607, 39 p.

Collettini, C., and Sibson, R.H., 2001, Normal faults, normal friction?: Geology (Boulder), v. 29, no. 10, p. 927-930.

Cowan, D.S., Morgan, T.T., and Cladouhos, J.K., 2003, Structural geology and kinematic history of rocks formed along low-angle normal faults, Death Valley, California: Geological Society of America Bulletin, v. 115, no. 10, p. 1230-1248.

Crowe, B.M., Wohletz, K.H., Vaniman, D.T., Gladney, E., and Bower, N., 1986, Status of volcanic hazard studies for the Nevada nuclear waste storage investigations: Los Alamos Scientific Laboratory, LA-9525-MS, 101 p.

DeCelles, P.G., 2004, Late Jurassic to Eocene evolution of the Cordilleran thrust belt and foreland basin system, Western U.S.A.: American Journal of Science, v. 304, p. 105-168.

Deemer, D.L., 2003, Transpressional Deformation at a constraining bend at the northern terminus of the Las Vegas Valley shear zone: Structural history and implications for the formation of the Yucca Mountain region: M.S. Thesis, University of Pittsburgh, Pittsburgh, Pennsylvania, 123 p.

Deemer, D.L., and Anderson, T. H., 2002, Transpressional structures in northern Specter Range and Striped Hills, Nevada; strong contraction within an extensional orogen: Geological Society of America Abstracts with Programs, v. 34, p. 562.

Dettinger, M.D., 1989, Distribution of carbonate-rock aquifers in southern Nevada and the potential for their development; summary of findings, 1985-88: Program for the study and testing of carbonate-rock aquifers in eastern and southern Nevada, Report, 37p.

Dickinson, W.R., Klute, M.A., Hayes, M.J., Janecke, S.U., Lundin, E.R., McKittrick, M.A., and Olivares, M.D., 1988, Paleogeographic and paleotectonic setting of Laramide sedimentary basins in the central Rocky Mountain region: Geological Society of America Bulletin, v. 100, p. 1023-1039.

Dickinson, W.R., 2006, Geotectonic evolution of the Great Basin: Geosphere, v.2, p. 353-368.

Duebendorfer, E.M., and Black, R.A., 1992, Kinematic role of transverse structures in continental extension: an example from the Las Vegas Valley shear zone, Nevada: Geology, v. 20, p. 1107-1110.

Duebendorfer, E.M., and Simpson, D.A., 1994, Kinematics and timing of Tertiary extension in the western Lake Mead region, Nevada: Geological Society of America Bulletin: v. 106, p. 1057–1073.

Eaton, G.P., 1982, The Basin and Range Province; origin and tectonic significance: Annual Review of Earth and Planetary Sciences, v. 10, p. 409-440.

Ekren, E.B., Rogers, C.L., Anderson, R.E., and Orkild, P.P., 1968, Age of basin and range normal faults in Nevada Test Site and Nellis Air Force Range, Nevada: Nevada Test Site, 110, p. 247-250.

Eliassen, A., and Talbot, M.R., 2005, Solution-collapse breccias of the Minkinfjellet and Wordiekammen Formations, Central Spitsbergen, Svalbard; a large gypsum palaeokarst system: Sedimentology, v. 52, no. 4, p. 775-794.

Fenneman and Johnson, 1946, Physical Divisions of the United States: Geological Survey special map series, scale 1:7,000,000.

Fleck, R.J., 1970, Tectonic style, magnitude, and age of deformation in the Sevier orogenic belt in southern Nevada and eastern California: Geological Society of America Bulletin, v. 81, no. 6, p. 1705-1720.

Fleck, R.J., Turrin, B.D., Sawyer, D.A., Warren, R.G., Champion, D.E., Hudson, M.R., and Minor, S.A., 1996, Age and character of basaltic rocks of the Yucca Mountain region, southern Nevada: Journal of Geophysical Research, v. 101, no. B4, p. 8205-8227.

Fridrich, C.J., 1999, Tectonic evolution of the Crater Flat basin, Yucca Mountain region, Nevada, *in* Wright, L.A., and Troxel, B.W., eds., Cenozoic Basins of the Death Valley Region: Boulder, Colorado, Geological Society of America Special Paper 333, p. 169-195.

Fridrich, C.J., Whitney, J.W., Hudson, M.R., and Crowe, B.M., 1999, Space-time patterns of late Cenozoic extension, vertical axis rotation, and volcanism in the Crater Flat basin, southwest Nevada, *in* Wright, L.A., and Troxel, B.W., eds., Cenozoic Basins of the Death Valley Region: Boulder, Colorado, Geological Society of America Special Paper 333, p.197-212.

Hamilton, W.B., 1988, Detachment faulting in the Death Valley region, California and Nevada: Geologic and hydrologic investigations of a potential nuclear waste disposal site at Yucca Mountain, southern Nevada, p. 51-85.

Healey, D.L., and Miller, C.H., 1965, Gravity survey of the Amargosa Desert area of Nevada, Death Valley Sheet: Nevada Bureau of Mines and Geology Map 69, scale 1:250,000.

Hill, M.L., and Troxel, B.W., 1966, Tectonics of death valley region, California: Geological Society of America Bulletin, v. 77, no. 4, p. 435-438.

Hinrichs, E.N., 1968, Geologic map of the Camp Desert Rock quadrangle, Nye County, Nevada: U.S. Geological Survey Quadrangle Map GQ-726, scale 1:24,000.

Holdsworth, R.E., Tavarnelli, E., Clegg, P., Pinheiro, R.V.L., Jones, R.R., and McCaffrey, K.J.W, 2002, Domainal deformation patterns and strain partitioning during transpression; an example from the Southern Uplands terrane, Scotland: Journal of the Geological Society of London, 159, p. 401-415.

Hudson, M.R., Sawyer, D.A., and Warren, R.G., 1994, Paleomagnetism and rotation constraints for the middle Miocene southwestern Nevada volcanic field: Tectonics, v. 13, no. 2, p. 258-277.

Janssen, B., and King, G., 2000, Tectonic modeling of Yucca Mountain, *in* Geologic and geophysical characterization studies of Yucca Mountain, Nevada, A potential high-level radioactive-waste repository: U.S. Geological Survey Digital Data Series 058.

Jayko, A.S., 1990, Shallow crustal deformation in the Pahranagat area, southern Nevada *in* Wernicke ed., Basin and Range extensional tectonics near the latitude of Las Vegas, Nevada: Memoir 176, p. 213-236.

Laczniak, R.J., Cole, J.C., Sawyer, D.A., and Trudeau, D.A., 1996, Summary of hydrologic controls on ground-water flow at the Nevada Test Site, Nye, County, Nevada: U.S. Geological Survey Water-Resources Investigations Report 96-4109, 59 p.

Langenheim, V.E., 2000, Constraints on the structure of Crater Flat, southwest Nevada, derived from gravity and magnetic data, *in* Geologic and geophysical characterization studies of Yucca Mountain, Nevada, A potential high-level radioactive-waste repository: U.S. Geological Survey Digital Data Series 058.

Langenheim, V.E., and Jachens, R.C., 1996, Thickness of Cenozoic deposits and groundwater storage capacity of the westernmost part of the Las Vegas Valley, inferred from gravity data: U.S. Geological Survey Open-File Report 96-0259, 29 p.

Langenheim, V.E., Jachens, R.C., and Schmidt, K.M., 1997, Preliminary location and geometry of the Las Vegas Valley shear zone based on gravity and aeromagnetic data: U.S. Geological Survey Open-File Report 97-441, 25 p.

Langenheim, V.E., Grow, J., Miller, J., Davidson, J.G., and Robison, E., 1998, Thickness of Cenozoic deposits and location and geometry of the Las Vegas Valley shear zone, Nevada, based on gravity, seismic reflection, and aeromagnetic data: U.S. Geological Survey Open-File Report 98-576, 32 p.

Langenheim, V.E., Grow, J.A., Jachens, R.C., Dixon, G.L., and Miller, J.J., 2001, Geophysical constraints on the location and geometry of the Las Vegas Valley shear zone, Nevada: Tectonics, v. 20, no. 2, p. 189-209.

Langenheim V.E.; Page R.J., Lundstrom W.R., Dixon S.C., Jachens G.L., and Blakely R.C., 2005, Geophysical framework of the Las Vegas 30' X 60' quadrangle, Scientific Investigations Map p. 45-55.

Lister, G.S., and Davis, G.A., The origin of metamorphic core complexes and detachment faults formed during Tertiary continental extension in the northern Colorado River region, U.S.A.: Journal of Structural Geology, v. 11, no. 1-2, p. 65-94.

Longwell, C.R., 1960, Possible explanation of diverse structural patterns in southern Nevada: American Journal of Science, v. 258-A, p. 192-203.

Longwell, C.R., 1974, Measure and date of movement on the Las Vegas Valley shear zone, Clark County, Nevada: Geological Society of America Bulletin, v. 85, p. 985-990.

Longwell, C.R., Pampeyan, E.H., Bowyer, Ben, and Roberts, R.J., 1965, Geology and mineral deposits of Clark County, Nevada: Nevada Bureau of Mines and Geology Bulletin 62, 218 p.

Maldonado, F., 1985, Geologic map of the Jackass Flats Area, Nye County, Nevada: U.S. Geological Survey Miscellaneous Investigations Map I-1519, scale 1:48,000.

Marvin, R.F., Byers, F.M. Jr., Mehnert, H.H., Orkild, P.P., and Stern, T.W., 1970, Radiometric ages and stratigraphic sequence of volcanic and plutonic rocks, southern Nye and western Lincoln counties, Nevada: Geological Society of America Bulletin, v. 81, no. 9, p. 2657-2676.

Mckee E.H., Wickham, T.A., and Wheeler, K.L., 1998, Evaluation of faults and their effect on ground-water flow southwest of Frenchman Flat, Nye and Clark Counties, Nevada: U.S. Geological Survey Open File Report 98-580, 17 p.

Mooney, W.D., and Schapper, S.G., 1995, Seismic refraction investigations: U. S. Geological Survey Open-File Report, 95-0074, p. 99-119.

Moore, E.M., and Twiss, R.J., 2000, Tectonics: New York, W.H. Freeman and Company, 415 p.

Nelson, M.R., and Jones, C.H., 1987, Paleomagnetism and crustal rotations along a shear zone, Las Vegas Range, southern Nevada: Tectonics, v. 6, no. 1, p. 13-33.

Nicholson, C., Sorlien, C.C., Atwater, T., Crowell, J.C., and Luyendyk, B.P., 1994, Microplate capture, rotation of the werstern Transverse Ranges, and initiation of the San Andreas transform as a low-angle fault system: Geology, v. 22, p. 491-495.

Nilsen, T.H., and Stewart, J.H., 1980, Penrose conference report; The Antler Orogeny, mid-Paleozoic tectonism in western North America: Geology (Boulder) v. 8, no. 6, p. 298-302.

Nolan, T.B., 1929, Notes on the stratigraphy and structure of the northwest portion of Spring Mountain, Nevada: American Journal of Science, v. 17, no. 101, p. 461-472.

O'Leary, D.W., 2000, Tectonic significance of the Rock Valley fault zone, Nevada Test Site, *in* Whitney, J.W., and Keefer, W.R., eds., Geologic and Geophysical Characterization Study of Yucca Mountain, Nevada, Digital Data Series, DDS-0058, 13 p.

Page, W.R., Lundstrom, S.C., Harris, A.G., Langenheim, V.E., Workman, J.B., Mahan, S.A., Paces, J.B., Dixon, G.L., Rowley, P.D., Burchfiel, B.C., Bell, J.W., and Smith, E.I., 2005, Geologic and Geophysical Maps of the Las Vegas 30’X60’ Quadrangle, Clark and Nye Counties, Nevada, and Inyo County, California: U.S. Geological Survey Scientific Investigations Map 2814, scale 1:100,000.

Petit, J.P., 1987, Criteria for the sense of movement on fault surfaces in brittle rocks: Journal of Structural Geology, v. 9, no. 5-6, p. 597-608.

Plume, R. W., 1989, Ground-water conditions in Las Vegas Valley, Clark County, Nevada; Part 1, Hydrogeologic framework: U. S. Geological Survey Water-Supply Paper, p. A1-A15.

Ponce, D.A., Blakely, R.J., Morin, R.L., and Mankinen, E.A., 2001, Isostatic gravity map of the Death Valley ground-water model area, Nevada and California: Miscellaneous Field Studies Map MF-2381-C, scale 1:250,000.

Potter, C.J., Dickerson, R.P., Sweetkind, D.S., Drake, R.M. II, Taylor, E.M., Fridrich, C.J., San Juan, C.A., and Day, W.C., 2002, Geologic map of the Yucca Mountain region, Nye County, Nevada: U.S. Geological Survey Geologic Investigations Series I-2755, scale 1:50,000.

Potter J, Sweetkind D S, Dickerson R P, and Killgore M L, 2002, Hydrostructural maps of the Death Valley region flow system, Nevada and California: U. S. Geological Survey, Miscellaneous Field Studies Map, MF-2372, scale 1:350,000.

Prothero, D.R., and Dott, R. J., 2004, Evolution of the Earth: New York, McGraw-Hill, 524 p.

Raines, G.L., Sawatsky, D.L., and Connors, K.A., 1996, Great Basin geoscience data base: U. S. Geological Survey Digital Data Series 0041, scale 1:500,000.

Royse, F., Wernicke, B., Spencer, J., and Guth, P.L., 1983, Magnitude of crustal extension in the southern Great Basin; discussion and reply: Geology (Boulder), v. 11, no. 8, p. 495-497.

Sargent, K.A., and Stewart, J.H., 1971, Specter Range NW quadrangle: U.S. Geological Survey Quadrangle Map GQ-884, scale 1:24,000.

Sawyer, David A., R.J. Fleck, M.A. Lanphere, R.G. Warren, D.E. Broxton, and M.R. Hudson, 1994, Episodic caldera volcanism in the Miocene southwestern Nevada Volcanic field: Revised stratigraphic framework, 40Ar/39Ar geochronology, and implications for magmatism and extension: Geological Society of America Bulletin, v. 106, p. 1304-1318.

Sibson, R.H., 1995, Selective fault reactivation during basin inversion: potential for fluid redistribution through fault-valve action, *in* Buchanan, J.G., and Buchanan, P.G., eds., Basin Inversion: Boulder, Colorado, Geological Society of America Special Publication 88 p. 3-19.

Smith, K.D., Brune, J.N., dePolo, D., Savage, M.K., Anooshehpoor, R., and Sheehan, A.F., 2000, The 1992 Little Skull Mountain earthquake sequence, southern Nevada Test Site: Geologic and geophysical characterization studies of Yucca Mountain, Nevada, 16 p.

Snow, J.K., 1992, Large-magnitude Permian shortening and continental margin tectonics in the southern Cordillera: Geological Society of America Bulletin, v. 104, no. 1, p. 80-105.

Snow, J.K., and Wernicke, B., 1989, Uniqueness of geological reconstructions: An example from Death Valley extended terrain: Geological Society of America Bulletin, v. 101, p. 1351-1362.

Snow, J.K., and Lux, D.R., 1999, Tectono-sequence stratigraphy of Tertiary rocks in the Cottonwood Mountains and northern Death Valley area, California and Nevada, *in* Wright, L.A., and Troxel, B.W., eds., Cenozoic Basins of the Death Valley Region: Boulder, Colorado, Geological Society of America Special Paper 333 p. 17-64.

Sonder, L.J., Jones, C.H., Salyards, S.L., and Murphy, K.M., 1994, Vertical axis rotations in the Las Vegas Valley shear zone, southern Nevada: paleomagnetic constraints on kinematics and dynamics of block rotations: Tectonics, v. 13, p. 769-788.

Stewart, J.H., 1967, Possible large right-lateral displacement along fault and shear zones in the Death Valley-Las Vegas area, California and Nevada: Geological Society of America Bulletin, v. 78, p. 131-142.

Stewart, J.H., 1970, Upper Precambrian and Lower Cambrian strata in the southern Great Basin, California and Nevada: U. S. Geological Survey Professional Paper 620, 206 p.

Stewart, J.H., 1980, Geology of Nevada; a discussion to accompany the geologic map of Nevada: Nevada Bureau of Mines and Geology Special Publication 4, 136 p.

Stewart, J.H., 1988, Tectonics of the Walker Lane Belt, western Great Basin; Mesozoic and Cenozoic deformation in a zone of shear: Metamorphism and crustal evolution of the Western United States 7, p. 683-713.

Stewart, J.H., 1992, Walker Lane belt, Nevada and California- an overview, *in* Craig, S.D., ed., Walker Lane Symposium Structure, Tectonics and Mineralization of Walker Lane: Geological Society of Nevada, Proceedings, p. 1-16.

Stewart, J.H., and Carlson, J.E., 1974, Preliminary geologic map of Nevada: U. S. Geological Survey Open-File Report 74-0068.

Tavarnelli, E., Holdsworth, R.E., Clegg, P., Jones, R.R., and McCaffrey, K.J.W, 2004, The anatomy and evolution of a transpressional imbricate zone, Southern Uplands, Scotland: Journal of Structural Geology, v. 26, no. 8, p. 1341-1360.

Trexler, J.H., Jr., Cole., J.C., and Cashman, P.H., 1996, Middle Devonian-Mississippian stratigraphy on and near the Nevada Test Site: Implications for hydrocarbon potential: Bulletin of the American Association of Petroleum Geologist, v. 80, p. 1736-1762.

Trexler, J.H., Jr., and Cashman, P.H., 1997, A southern Antler fore-deep submarine fan: The Mississippian Eleana Formation Nevada Test Site: Journal of Sedimentary Research, v. 67, no. 6, p. 1044-1059.

Turrin, B.D., Champion, D.E., and Fleck, R.J., Measuring the age of the Lathrop Wells volcanic center at Yucca Mountain: Science, v. 257, p. 555-558.

Van Der Pluijm, B.A., and Marshak, S., Earth Structure: New York, W.W. Norton & Company, 656 p.

Wahl, R.R., Sawyer, D.A., Carr, M.D., Minor, S.M., Cole, J.C., Swadley, W.C., Laczniak, R.J., Warren, R.G., Green, K.S., and Engle, C.M., 1997, Digital geologic map database of the Nevada Test Site area, Nevada: U.S. Geologic Survey Open-File Report 97-140, scale 1:100,00.

Wernicke, B.P., 1990, Foreword *in* Wernicke, B.P., ed., Basin and Range extensional tectonics near the latitude of Las Vegas, Nevada: Geological Society of America Memoir 176, 511 p.

Wernicke, B., Spencer, J.E., Burchfiel, B.C., and Guth, P.L., 1982, Magnitude of crustal extension in the southern Great Basin: Geology, v. 10, p. 499-502.

Wernick, B., Axen, G.J, and Snow, J.K, 1988, Basin and Range extensional tectonics at the latitude of Las Vegas, Nevada: Geological Society of America Bulletin, v. 100, p. 1738-1757.

Wernicke, B., Guth, P.L., and Axen, G.J., 1988, Tertiary extensional tectonics in the Sevier thrust belt of southern Nevada, *in* Weide, D.L., and Faber, M.L., eds., This Extended Land; Geological journeys in the southern Basin and Range; Geological Society of America Cordilleran Section Field Trip Guidebook: University of Nevada at Las Vegas Geoscience Department Special Publication, no. 2, p. 473-499.

Wincander, R., and Monroe, J.S., 2000, Historical Geology: Pacific Grove, Brooks/Cole, 580 p.

Winograd, I.J., 1962, Interbasin movement of ground water at the Nevada Test Site: U.S. Geological Survey Technical Report, TEI-807, 12 p.

Winograd, I.J., and Thordarson, W., 1975, Hydrogeologic and hydrochemical framework, south-central great basin, Nevada-California, with special reference to the Nevada Test Site: Geological Survey Professional Paper 712-C, 126 p.

Wright, L.A., and Troxel, B.W., 1966, Limitations on strike-slip displacement along the Death Valley and Furnace Creek fault zones, California: Geological Society of America Special Paper, p. 188-189.

Workman, J.B., Menges, C.M., Page, W.R., Tayor, E.M., Ekron, E.B., Rowley, P.D., Dixon, G.L., Thompson, R.A., and Wright, L.A., 2002, Geologic map of the Death Valley ground-water model area, Nevada and California: Miscellaneous Field Studies Map MF-2381-A, scale 1:250,000.

Zoback, M.L., 1989, State of stress and modern deformation of the northern Basin and Range Province: Journal of Geophysical research, v. 94, p. 7105-7128.